MASTER THESIS

ENERGY TECHNOLOGY FOR SUSTAINABLE DEVELOPENT

"Dynamic Modelling of a Compressed Heat Energy Storage System (CHEST)"

AUTHOR: **SÁNCHEZ CANALES, VIOLETA**

SUPERVISOR: HASSAN, ABDELRAHMAN HUSSEIN

UPV TUTOR: CORBERÁN SALVADOR, JOSÉ MIGUEL

Academic Year: 2018-19

July 2019

ACKNOWLEDGEMENTS

En primer lugar, quería darle las gracias a José Miguel Corberán por darme la oportunidad de formar parte del Instituto universitario de investigación en Ingeniería Energética (IUIIE) y poder realizar este Trabajo Final de Máster, y a Abdel Hassan por todo lo que he aprendido gracias a su apoyo y sus consejos.

Además, quería agradecer a la Fundación Iberdrola por concederme la beca de estudios de posgrado que me permitió realizar este Máster.

También, a los compañeros de trabajo del área térmica. Gracias por hacer más amenas tanto las horas de trabajo como las de ocio.

Finalmente, a mi madre, a mis amigas y a mi pareja. Simplemente, gracias por estar ahí.

The current thesis has been implemented within the framework of the CHESTER project, which has received funding from the European Union's Horizon 2020 research and innovation program under grant agreement No 764042

RESUMEN

Uno de los principales retos en el contexto energético actual es la integración de las energías renovables (EERR) en la red eléctrica. Al contrario que los combustibles fósiles, las EERR dependen de las condiciones meteorológicas, lo que dificulta su predicción y añade incertidumbre a la red. Por tanto, el desarrollo de técnicas de almacenamiento a gran escala es crucial, ya que ayudará a garantizar el suministro y la gestión de las EERR, mejorando su integración en el sistema.

Este Trabajo de Fin de Máster (TFM) propone una solución a través del almacenamiento de energía mediante calor bombeado, tecnología conocida como CHEST por sus siglas en inglés. El sistema CHEST presentado está formado por una bomba de calor de alta temperatura, un sistema de almacenamiento térmico (dividido en latente y sensible) y un ciclo de Rankine orgánico. En periodos de baja demanda eléctrica, el exceso de energía es utilizado en la bomba de calor y la energía es almacenada en forma de calor a alta temperatura. Después, cuando la demanda aumenta, el ciclo Rankine utiliza este calor almacenado para producir electricidad. Este TFM está englobado en el proyecto europeo CHESTER (www.chester-project.eu), el cual propone el desarrollo de una tecnología CHEST con el fin de mejorar la integración de las EERR en la red.

Se ha desarrollado un modelo en TRNSYS para determinar el comportamiento dinámico del sistema CHEST. Dicho modelo permite la evaluación del tamaño del sistema, separando los procesos de carga y descarga y evaluando el comportamiento a carga parcial de los equipos. El modelo ha sido testado bajo diferentes condiciones de contorno y para diferentes opciones de optimización relativas al almacenamiento sensible. Además, se ha propuesto un escenario de integración en la red eléctrica española.

Los resultados muestran que el sistema propuesto puede alcanzar eficiencias de 0.99 para temperaturas de fuente y sumidero de 80 y 10°C respectivamente. Desde un punto de vista técnico-económico, los sistemas CHEST pueden ser viables siempre y cuando puedan conseguirse suficientes contribuciones de energía con periodos de retorno razonables.

Palabras clave: Almacenamiento térmico; bomba de calor de alta temperatura; ciclo Rankine orgánico.

RESUM

Un dels principals reptes en el context energètic actual és la integració de les energies renovables (EERR) a la xarxa elèctrica. Al contrari que els combustibles fòssils, les EERR depenen de les condiciones meteorològiques, fet que dificulta la seua predicció i afegeix incertesa a la xarxa. Per tant, el desenvolupament de tècniques d'emmagatzematge a gran escala és clau, ja que ajudarà a garantir el subministrament la gestió de les ERR, millorant la seua integració al sistema.

Aquest Treball de Fi de Màster (TFM) proposa una solució a través de l'emmagatzematge d'energia mitjançant calor bombejat, tecnologia coneguda com CHEST per les seues sigles en anglès. El sistema CHEST presentat està format per una bomba de calor d'alta temperatura, un sistema d'emmagatzematge tèrmic (dividit entre latent i sensible) i un cicle de Rankine orgànic. En períodes de baixa demanda elèctrica, l'excés d'energia és utilitzat a la bomba de calor i l'energia és emmagatzemada en forma de calor a alta temperatura. Després, quan la demanda augmenta, el cicle Rankine utilitza aquest calor emmagatzemat per a produir electricitat. Aquest TFM està englobat al projecte europeu CHESTER (www.chester-project.eu), el qual proposa el desenvolupament d'una tecnologia CHEST amb l'objectiu de millorar la integració de les EERR a la xarxa.

S'ha desenvolupat un model a TRNSYS per tal de determinar el comportament dinàmic del sistema CHEST. El model en qüestió permet l'avaluació de la grandària del sistema, separant els processos de carga i descàrrega i avaluant el comportament a carga parcial dels equips. El model ha estat testat baix diferent condicions de contorn i per a diferents opcions d'optimització relatives a l'emmagatzematge sensible. A més, s'ha proposat un escenari de integració a la xarxa elèctrica espanyola.

Els resultats mostres que el sistema proposat pot arribar a eficiències de 0.99 per a temperatures de font i embornal de 80 i 10°C respectivament. Des d'un punt de vista tècnic-econòmic, els sistemes CHEST poden ser viables sempre i quan pugues aconseguir-se suficients contribucions d'energia amb períodes de retorn raonables.

Paraules clau: Emmagatzematge tèrmic, bomba de calor d'alta temperatura, cicle Rankine orgànic.

ABSTRACT

One on the main challenges in the current energy context is the suitable integration of the renewable energy sources (RES) in the electrical grid. Unlike fossil fuels, RES are affected by meteorological conditions that affect their predictability and reliability, which adds uncertainty in the electrical grid. Thus, the assessment of large-scale energy storage techniques is an up-to-date subject of study: the improvement of the storage technologies will allow the security of supply and dispatchability of RES, enabling their integration in the system.

The current Master thesis proposes a solution to this issue by means of a **C**ompressed **H**eat **E**nergy **ST**orage (CHEST) technology. The CHEST system proposed is composed of a high temperature heat pump (HT-HP), a thermal energy storage (TES) system (divided into latent and sensible heat storage) and an organic Rankine cycle (ORC). In times of low electric demand, surplus energy is used to drive the HT-HP and store energy in the form of heat in the TES system. Later, when electricity demand is high, ORC utilizes the heat stored to produce electric power. The presented thesis is framed within the European project CHESTER (Compressed Heat Energy STorage for Energy from Renewable sources; www.chester-project.eu), financed by the European Commission, that proposes a large-scale energy storage technology using the CHEST concept.

To evaluate the dynamic behavior of CHEST system a numerical model using TRNSYS was developed and verified. The proposed model considers the scale and size of different equipment, decoupling of charging and discharging cycles (independent behavior), and partial load scenarios. The proposed model was employed to assess different boundary conditions for the CHEST system, available options to optimize of the sensible heat storage system temperature; and, finally, to evaluate a real scenario of integrating the CHEST system in the Spanish electrical grid.

The results indicated that the proposed CHEST system can reach a roundtrip efficiency of 0.99 for source and sink temperatures of 80 and 10°C, respectively. From the techno-economical point of view, the current system shows a promising potential as long as the shares of energy contribution can be achieved at reasonable payback periods.

Keywords: Thermal energy storage; high temperature heat pump; organic Rankine cycle; compressed heat energy storage

TABLE OF CONTENTS

LIST OF FIGURES

LIST OF TABLES

1. INTRODUCTION

1.1 BACKGROUND

Fossil fuels keep playing a major role, regarding consumption, in the current energetic context. The consequences of this, related to CO_2 emissions, resource depletion, or, in the case of Europe, external energy dependency, are already known. For this reason, an energy transition through renewable energy sources (RES), replacing petroleum products, is necessary. However, there are still plenty of challenges that need to be faced in the following years.

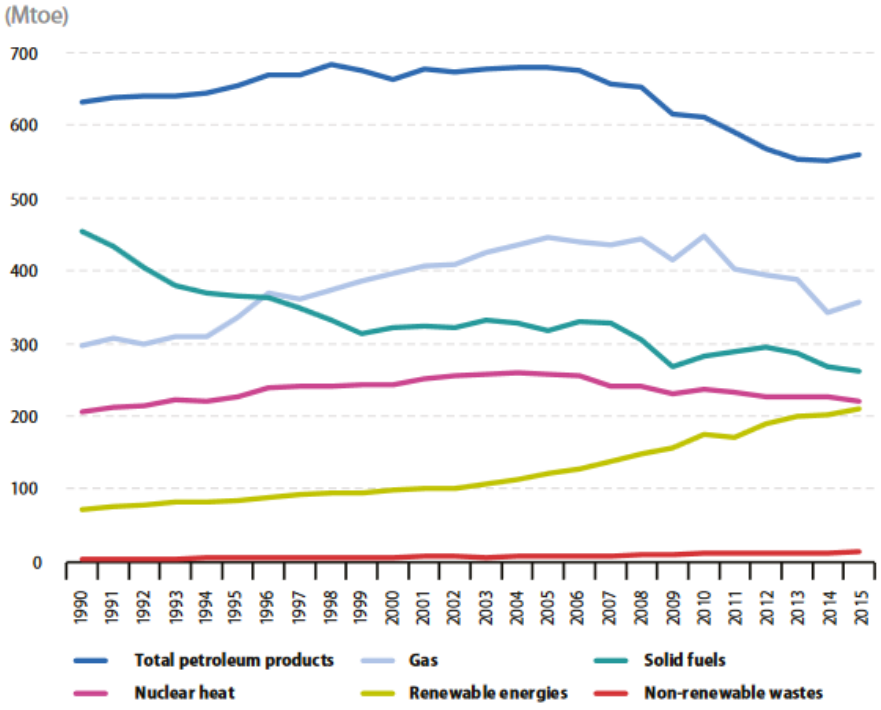

Figure 1. Gross energy consumption in UE-28 between 1990 and 2015 ***[1]***

Figure 1 shows the energy gross consumption in the European Union by their origin. Although the contribution of renewables has had a growing trend since 1990, it is still so far from reaching the consumption figures obtained by the total of the petroleum products. Even though they have suffered a decrease in usage during the last decade, they remain the main source of energy consumption in Europe and, nowadays, a great percentage of the electric energy consumed in Europe comes from non-renewable energy sources.[1]

Unlike fossil fuels, the performance of RES is affected by the meteorological conditions, having intermittency problems and low predictability that may cause imbalance and uncertainty in the electrical grid. This fact hampers the adjustment of the demand and generation profiles along the day, so that in the occasions when the renewable production is higher that the energetic demand, the excess energy is, in many cases, dismissed. [2]

In this context, the improvement of the large-scale energy storage techniques is a crucial matter. Storing of possible energy surplus increases the security of supply and allows a better integration

of the RES in the grid. Thus, the operation of renewable sources can be optimized, reducing the necessary installed capacity to provide the same energy and improving, at the same time, the efficiency of the systems, as storage technologies allow a longer usage periods of them. Moreover, this stored energy could be employed during peak times, contributing to reducing the maximum power demand. [3]

1.1.1. Energy Storage Techniques

As it was mentioned before, energy storage techniques allow the store of energy during high RES production timeframes, or valley periods of the energy demand, in order to have it available in peak demand times or when the current RES production is not enough to cover the demand. [4]

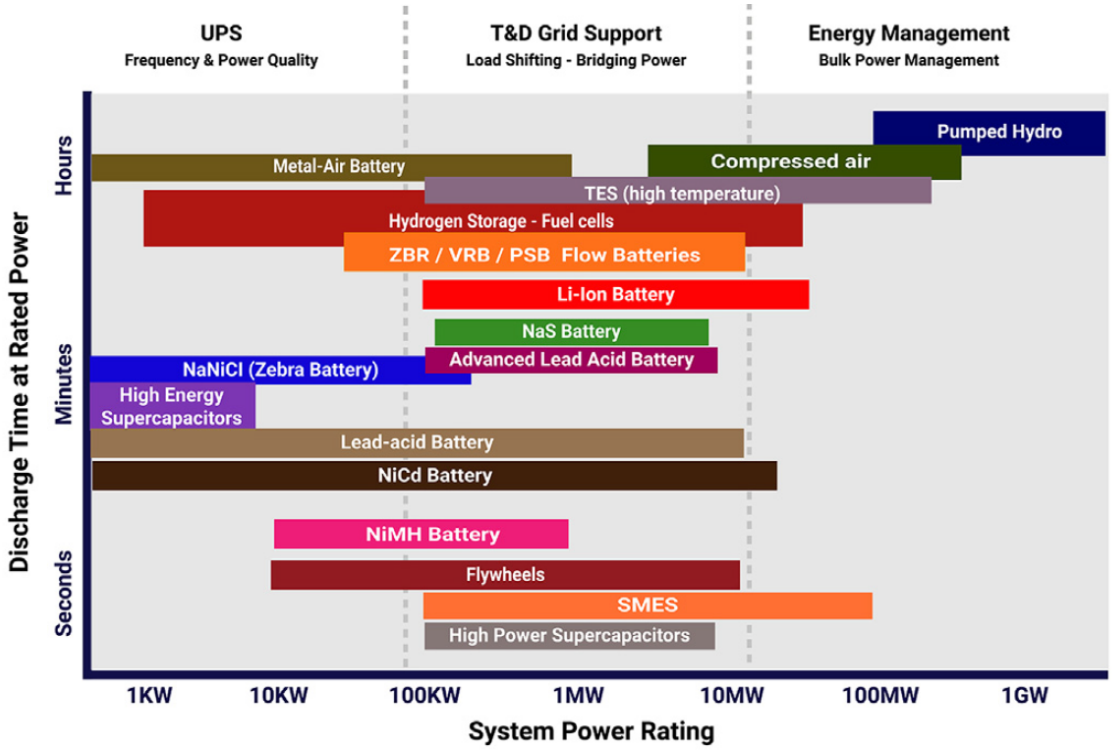

Figure 2. Storage technologies.[4]

The illustration above shows the different available technologies as a function of their storage capacity and discharge time. Within the presented work, we will focus in the storage systems as a helping tool for the integration of RES in the network. To achieve that, different electrical energy storage mechanisms, such as peak saving or load levelling, could be employed. Both of them are based on the storage of energy surplus in valley periods to use it during peak hours, as it is depicted in Figure 3. While peak saving displaces the energy generation from hours of peak demand, load leveling reschedules the loads in order to have less production in period of high demand. Furthermore, the possibility of having seasonal storage system could be interesting. [4]

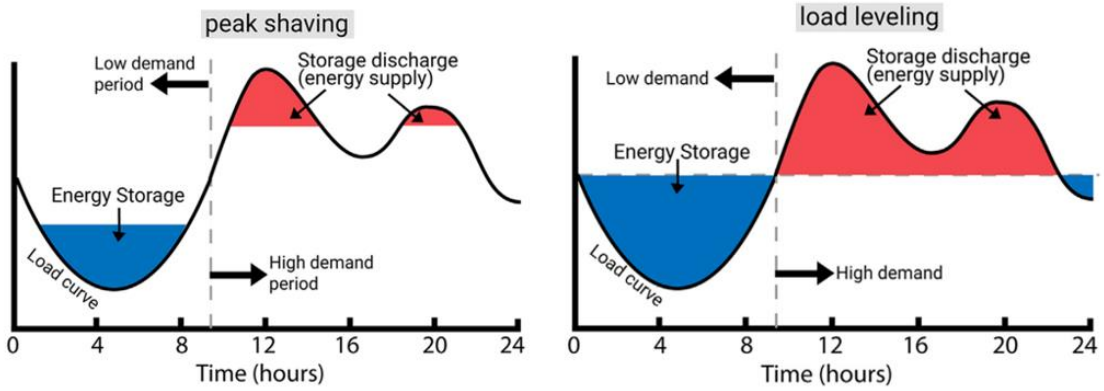

Figure 3. Peak saving and load levelling. [4]

In essence, those systems capable of storing large amounts of energy during long time periods are of particular interest. Among them, Pumped Hydro Storage (PHS), Compressed Air Energy Storage (CAES) and Thermal Energy Storage (TES) are the most relevant ones.[4]

- Pumped Hydro Storage (PHS):
  Currently, this is the most commonly used and mature technology, with a worldwide installed capacity of 169 GW [4]. As it can be seen in Figure 4, its working principle is based on the store of potential energy (E=mgh) by pumping water from a lower reservoir to an upper one –situated at a minimum height[1]- during periods of low energy demand. When the demand increases, water flows from the upper reservoir to the lower one by means of a series of turbines which generate electric energy.
  These systems have a lifetime between 30 and 60 years and efficiencies around 65-85%. Nevertheless, their location requires specific geographical conditions, as they imply the transformation of huge areas of land, resulting in an undoubted environmental impact. [4]

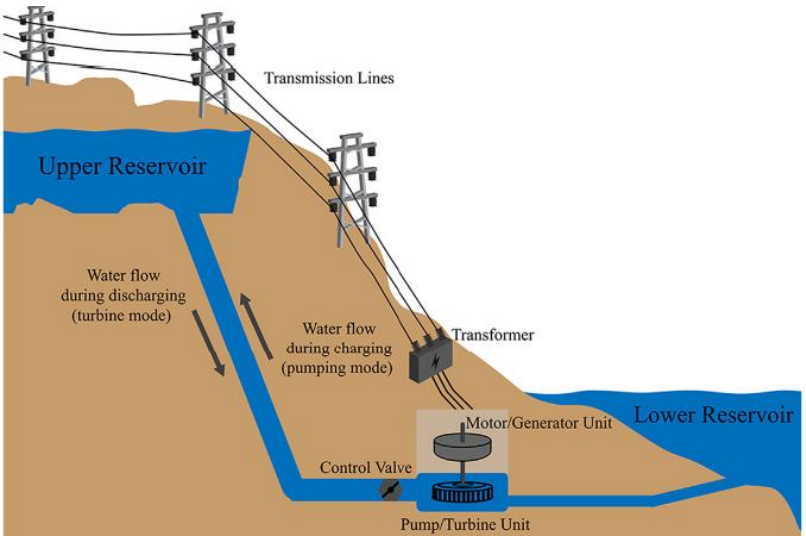

Figure 4. Scheme of pumped hydro storage station (PHS). [4]

[1] As a rule of thumb, the height difference between both reservoirs will be, at least, 300 m.

- Compressed Air Energy Storage (CAES):
  As depicted in Figure 5, these systems use the surplus in the energy production to compress atmospheric air and store it in caverns, which could be natural or artificially excavated. Subsequently, this air is decompressed in a turbine in order to produce electric energy. CAES systems have high storage capacity and efficiencies around 80% and are able to maintain the air reservoirs during long periods of time of almost one year. Moreover, capital costs are relatively low, and their lifetime is of 40 years. The main drawbacks of this technology are lack of maturity compared to others, geographical restrictions, and environmental issues due to the underground storage and the necessity of using fossil fuels during the discharging process (the combustion chamber is used to increase the pressure and temperature of gas before the expansion process). [4, 5]

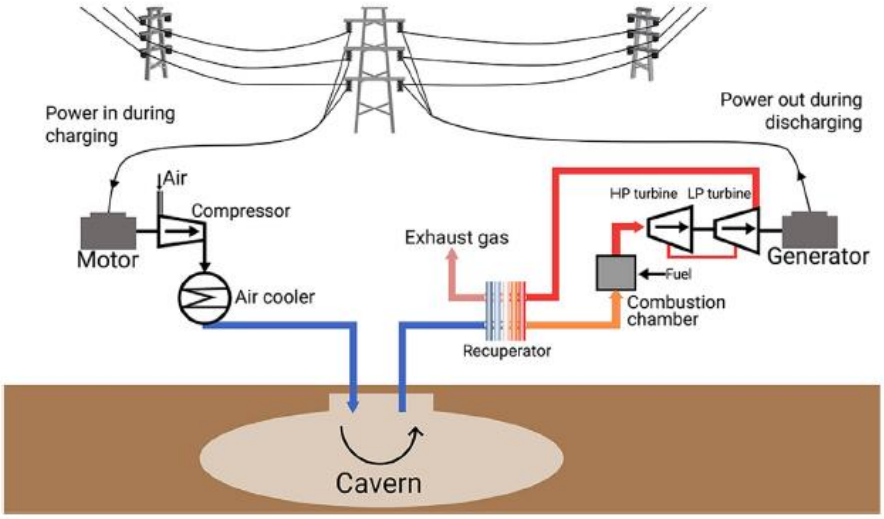

Figure 5. Compressed Air Storage (CAES) diagram. [4]

- Thermal Energy Storage (TES):
  Another possible option to store electrical energy is by means of thermal energy, using the surplus electricity to increase the temperature of a specific material or producing a phase change in it. In this case we can distinguish between low temperature systems, mostly employed for the climate control of industrial and commercial buildings; and high temperature systems, used as storage technique in concentrated solar power plants. For the latter option, there are different possibilities regarding the storage material utilized: concretes and other ceramic materials, phase change materials (PCM) and molten salts. For long term storage, the most interesting option are PCM, as they are capable of storing big quantities of energy, in the form of latent heat, in small volumes with a minimum variation of temperature, resulting in more efficient heat transfer processes. [4]

Analyzing these three technologies, it can be observed that the first and the second one have geographical restrictions that prevent their widespread implementation, as well as environmental impacts related to the modification of the ecosystem, in the case of pumped hydro, or the use of fossil fuels for compressed air technologies. Moreover, the volumetric

capacity of such systems, based on mechanical energy, is lower than the ones based on thermal energy storage, with a difference that could reach one or two orders of magnitude among them. [5]

Hence, thermal storage, without any geological restriction and no major environmental impact and with an expected lifetime of 30-40 years, presents a promising future in this field. [5]

1.1.2. The Pumped Thermal Energy Storage (PTES) Concept

In order to construct successfully a thermal energy storage, several components able to perform all the energy transformations, from electric to thermal and vice-versa, are required. As a first approach, a thermal system could be charged with electric energy by means of electrical heating, and, subsequently, being discharged using a thermodynamic cycle. Nevertheless, the efficiency of this kind of process is limited by Carnot, so, taking into account the exergy losses that may occur, the real values achieved would be around 40%. [5]

In this context, the concept of Pumped Thermal Energy Storage (PTES) is considered to be a promising alternative, in which the excess electricity is used during the charging process to increase the temperature of a heat source. This energy is stored in a thermal system (that could be latent, sensible or both systems) to be used, later, in a thermodynamic cycle to produce electrical power in the periods of high demand (discharging process). Thus, the efficiency of the whole process, so-called roundtrip efficiency, is not restricted anymore by Carnot and, ideally, it can be higher than 100%. [5]

$$\eta_{roundtrip} = \frac{\boldsymbol{Net\ output\ electrical\ energy\ during\ discharge}}{\boldsymbol{Total\ input\ electrical\ energy\ during\ charge}} \qquad \textbf{(1)}$$

As it is shown in the equation above, the roundtrip efficiency is defined as the relationship between the net electrical energy obtained by the thermodynamic cycle during the discharging process of the thermal storage system and the total electrical energy consumed during the charging process. [5]

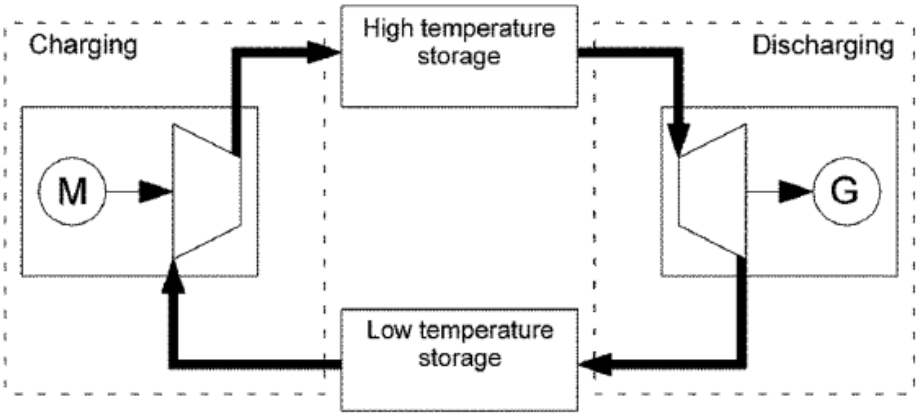

Figure 6. Overview of PTES concept. [5]

Figure 6 depicts the working principle of the PTES concept. It should be noted that, considering the transfer of exergy that takes place, if the temperature difference between the energy

source, in charging process, and the energy sink, in discharging process, is large enough, the irreversibilities produced can be compensated and, then, the generation of energy can exceed the consumption, reaching efficiencies higher than one. [5]

The PTES idea can have multiple applications if it is integrated in current existing technologies. As an example, one attractive option is their implementation in geothermal heat sources, which are currently only employed for district heating (DH) and, as they are used only a few months a year, they have low utilization factors, which usually makes them non-economically feasible. A PTES system would allow the use of that heat source during summer months, this, along with a surplus in electric energy, can be used to charge a storage system, increasing the utilization factor and improving the usage of the resource. [5]

A different possibility is their employment in Smart District Heating (SDH) systems. Nowadays, these are able to use the surplus in electrical energy to drive a heat pump and increase the thermal energy provided. By using a PTES, it would be also possible to convert again the thermal energy to electricity during the high demand peaks. [5]

1.2. OVERVIEW OF THE CHESTER PROJECT

This master thesis is part of the CHESTER (**C**ompressed **H**eat **E**nergy **ST**orage for **E**nergy from **R**enewable sources) project, which is financed by the European Commission and counts with the main participation of twelve organisms such as universities, companies and non-profit organizations. This project proposes the development of a PTES system using a subcritical organic Rankine cycle (ORC) during the discharge process. This concept is also known as CHEST (Compressed Heat Energy STorage). The final goal of the project is to improve the flexibility of the grid, allowing a better integration of the renewable energy sources. [6]

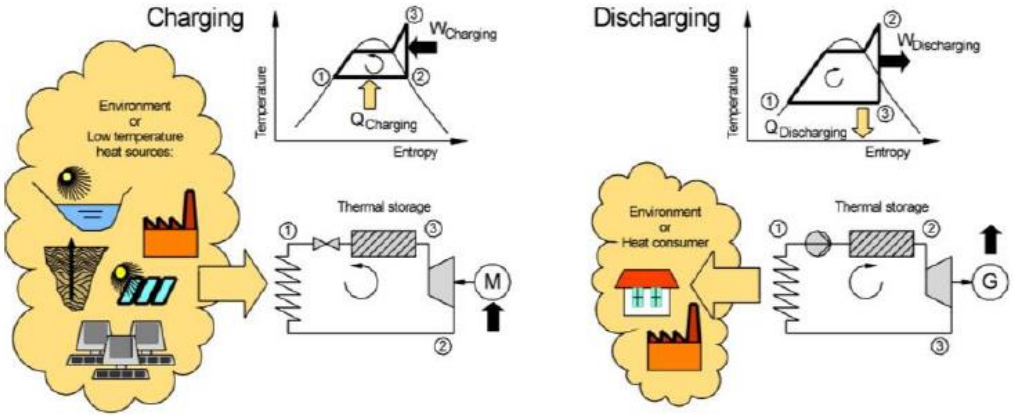

Figure 7. The main components of CHEST system. [6]

Figure 7 represents the overall concept of CHEST system. During charging, the surplus of electricity, coming from RES, is used to drive the compressor of a High Temperature Heat Pump (HT-HP). In this manner, employing a Thermal Storage System (TES), energy is stored in the form of latent and sensible heat at high temperature. Additionally, a low temperature heat source – for example, coming from solar thermal or geothermal installations, or as waste heat from

industrial processes- could be used in the evaporator of HT-HP in order to improve its efficiency. On the other hand, when there is a demand of electricity that cannot be covered by RES production, the previously stored energy is utilized to run an ORC generating the required energy. [6]

Within this project, the combination of the CHEST system and SDH will be analyzed. This will be done using seasonal TES (large volume water reservoir ranges between 10^4 and 10^6 m^3) as the low temperature energy source for the charging cycle. Also, since the size of such reservoir allows for the stratification of stored water, different temperature levels appear so the heat rejected during the functioning of ORC cycle can also be fed to the colder levels of seasonal TES so as to overcome the irreversibilities and increase the system's roundtrip efficiency. Based on this, six different working modes are evaluated regarding the source and sink temperatures and the amount of heat and electricity converted (Figure 8). [6]

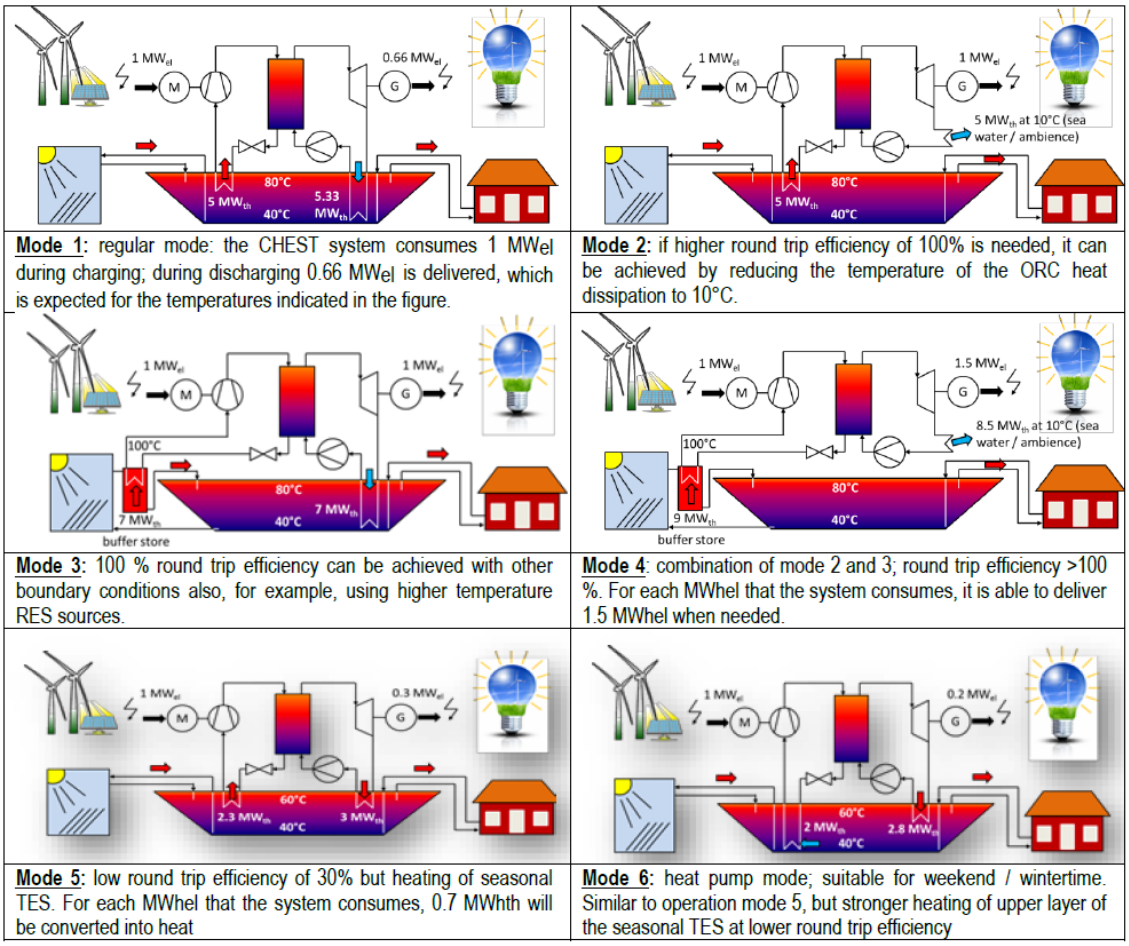

Figure 8 . Working modes of the CHEST system

The different working modes shown in Figure 8 demonstrate the flexibility that the CHEST system can have, which make it a competitive technology able to adapt to the needs of the system. Hence, in winter it can meet the heating demand and provide less electricity – reducing the roundtrip efficiency of the system- and during summer, as the heating demand is almost negligible, it can be used to cover the electrical demand needs. [6]

As it may be seen, the main components of CHEST system are widely known and their individual performance is evaluated and validated. However, the integration of these technologies together in a single system has not been proved yet. So, it is a subject of study how to optimize the whole CHEST system to obtain the desired performance at competitive prices. [6]

1.3. STATE OF THE ART

1.3.1. Thermal Storage Systems: CHEST

As it was mentioned in previous sections, thermo-mechanical systems are a feasible alternative for large scale storage. In Steinmann et al. [7] a comparative among the different possibilities – CAES, PHP[2], PTES and CHEST- was performed, doing an analysis of both the efficiencies and costs. This paper explained the possibility of using not only the electric energy, but also the thermal one, enabling a better adaptation to the costumers needs. What is more, the benefits of using a source of residual heat are highlighted; as well as the importance of minimizing the irreversibilities during the heat transfer processes, making the temperature profiles to be as similar and close as possible by using two different storage systems (latent and sensible). Additionally, other variations within the CHEST system were analyzed, among them, cascade cycles or a system based on cryogenic storage.[3] Conclusions show the benefit of PTES and CHEST systems, as they do not have geological restrictions, do not use fossil fuels to drive their components (unlike CAES systems) and have low environmental impact. Also, their efficiencies are higher, as they are not limited by Carnot like PHP systems; and PTES and CHEST allow the provision of both electricity and heat as well as the integration of sources of waste heat.

With reference to the researches done in the field of thermal energy storage techniques using heat pumps, this, up to date, have only been based on theoretical studies. In Thess [8] simplified models for PTES and pumped cryogenic electricity storage (PCES) were studied, consisting of a heat pump (or refrigerator) and a thermodynamic cycle. Both systems used the ambient as external heat source and a Carnot cycle to perform the study of the roundtrip efficiency as a function of the temperature of the thermal storage system, concluding that the roundtrip efficiency increases with the rise of the temperature of the storage system. However, the level of simplification of the model might be excessive, as it only takes into account the irreversibilities produced as a consequence of the heat transfer due to the temperature difference between the cycles and the ambient and it does not consider, for example, possible losses through the storage system.

In Juncheng et al. [9] a comparison between these same technologies (PTES and PCES), consisted of one Carnot heat pump and one Carnot heat engine, was done. The working temperatures were the ambient and the melting temperature of the PCM of the thermal storage, and it was evaluated both the roundtrip efficiency and power output of the engine. This work includes

[2] Power to Heat to Power. System that makes use of Joule effect to heat up a thermal deposit and, subsequently, discharge it in a thermodynamic cycle. [7]

[3] Known as PCES (Pumped Cryogenic Electricity Storage). This system is analogous to PTES, however, the energy surplus is used to drive a refrigeration cycle, which extracts thermal energy from a cryogenic source [7, 8].

more parameters than the one mentioned above, such as heat losses among the different fluxes or inside the storage tank, as well as the radiation losses that occur in it. Results show that PTES systems have a better overall performance and that heat losses are not negligible and affect the overall efficiency of the system.

A deeper analysis of the CHEST concept was done in Steinmann[10], highlighting its advantages comparing with other PTES systems based on Brayton or CO_2 cycles. This paper presents a CHEST system with a cascade charging cycle, using water and ammonia as working fluids, and the ambient temperature as heat source. For the storage method, a differentiation between latent and sensible storage was proposed in order to improve the temperature profiles and minimize the entropy generation during the heat transfer process. Finally, the benefits of including an external low temperature heat source during the charging phase were remarked, as it allows the compensation of exergy losses produced in the system, improving its efficiency and, thus, eliminating the necessity of introducing the cascade cycle and reducing the technical complexity of the system.

In Frate et al. [11] a numerical model of a PTES system with thermal integration in steady state operation was assessed. The model consisted of a HT-HP with a heat source raging between 80°C and 110°C and an ORC cycle that uses the ambient as sink. The model included the option of using a regenerator in the ORC cycle in case the temperature of the refrigerant after the expansion process is more than 15K higher than the condensation temperature to improve the efficiency and reduce the size of the TES system. In this work several refrigerants were analyzed, bearing in mind their environmental impact to discard those that do not comply with the European legislation. Results show that the efficiency of the PTES system trends to improve with the increase of the source temperature, however, an optimum value is observed, as the efficiency starts to decrease when the source temperature approaches the critical temperature of the fluid. Among the refrigerants under study, R1233zd(E) seems to be the most promising one, reaching high efficiencies (a value of 1.3 is achieved for a source temperature of 110°C) at low operational pressures.

Coupling the CHEST system with a low-temperature heat source was also studied in Jöckenhofer et al. [5]. The model simulates a coupled[4] CHEST-ORC system of an input power of 1MW working in steady conditions. Firstly, the different kinds of refrigerants that could be used were analyzed, focusing on the effect of saturated vapor slope in the system performance. The results showed that isentropic fluids, with an almost vertical saturation line, achieve the best performance as they minimize the subcooling or superheating needed. Finally, butene was selected as refrigerant for both the heat pump and the Rankine cycle; and separated heat source and sink, working at different temperatures, were used. In this analysis pressure losses and pinch temperatures, as well as isentropic, mechanical and electrical efficiencies of the equipment, were considered; and the influence of the different source and sink temperatures in the net

[4] The coupled model is an initial approach of the CHEST system where there is an ideal heat transfer in the TES system and all the heat produced by the HT-HP is immediately discharged in the ORC, assuming steady state conditions. This implies that the ratio between latent and sensible heat should be always the same for both charging and discharging processes.

power ratio[5] and exergetic efficiency was assessed. It should be noted that, having saturated liquid at the outlet of the preheater in the discharge side, there is an imbalance between latent and sensible storage systems which makes the latent storage system became empty before the sensible one for some operating points. To solve this issue sensible excess heat is rejected by means of an extra heat exchanger located in the heat pump side.

To the best of our knowledge, there is no experimental research regarding CHEST system so far. However, one of the objectives of the CHESTER project is to build a lab scale prototype for validating the simulations.

1.3.2. EES-CHEST Model from the UPV: Previous Work

This thesis is an extension of the previous work presented in Lindeman [12], in which a preliminary study of the thermodynamic cycles of the HT-HP and ORC that compose the CHEST system was done using the program Engineering Equation Software (EES)[13]. A coupled CHEST model was simulated and several PCMs with different melting temperatures, as well as three groups of refrigerants (isentropic, wet and dry)[6] and different configurations for the thermodynamic cycles were assessed. Lindeman presented two types of analysis. Firstly, refrigerant selection analysis, then, system configuration analysis. These can be summarized as follows:

a) <u>Refrigerant selection analysis:</u>

The first analysis carried out was the selection of refrigerants for each type of PCM. The PCMs and refrigerant selected can be seen in Table 1:

Table 1. PCM and refrigerant selection for Cases 1,2 and 3 [12]

Case	PCM	$T_{melt,PCM}$ (°C)	Wet fluid selected	Isentropic fluid selected	Dry fluid selected
Case 1	$LiNO_3$-KNO_3	133	Acetone	R1233zd(E)	HFO1336mzz(Z)
Case 2	KNO_2-$NaNO_3$	149	Acetone	R1233zd(E)	HFO1336mzz(Z)
Case 3	LiOH-$LiNO_3$	183	Acetone	R141b	Cyclopentane

Different performance indicators were studied as a function of source's inlet water temperature (T_{source}) varying from 40 to 100°C and for a fixed value of 25°C for the sink's inlet water temperature (T_{sink}). Results indicated that, for the three cases studied, isentropic fluids are the most suitable for a CHEST system. Dry fluids require high degrees of superheat inside the HT-HP's evaporator to avoid wet compression, so the roundtrip efficiency of the CHEST system is reduced. On the other hand, wet fluids have high discharge temperature at the outlet of HT-

[5] The net power ratio is the net power output produced during the discharge divided by the net power input provided in the charge, that is, taking into account parasitical power consumptions produced by the pumps. [5]

[6] The difference between the three kind of fluids is the slope of the saturated vapor line in the T-s diagram. For wet fluid it is negative, for dry it is positive and for isentropic fluid this line is semi-vertical. [12]

HP's compressor which can damage the equipment and degrade the efficiency of lubricating oil. Figure 9 shows an example of simulations of EES-CHEST model using R1233zd(E) as refrigerant, where electrical power input to the HT-HP ($P_{input,HP}$)= 1 MW, T_{source}= 70 °C, T_{sink}= 25 °C, and $T_{melt,PCM}$= 133 °C (no pressure drops inside heat exchangers were assumed).

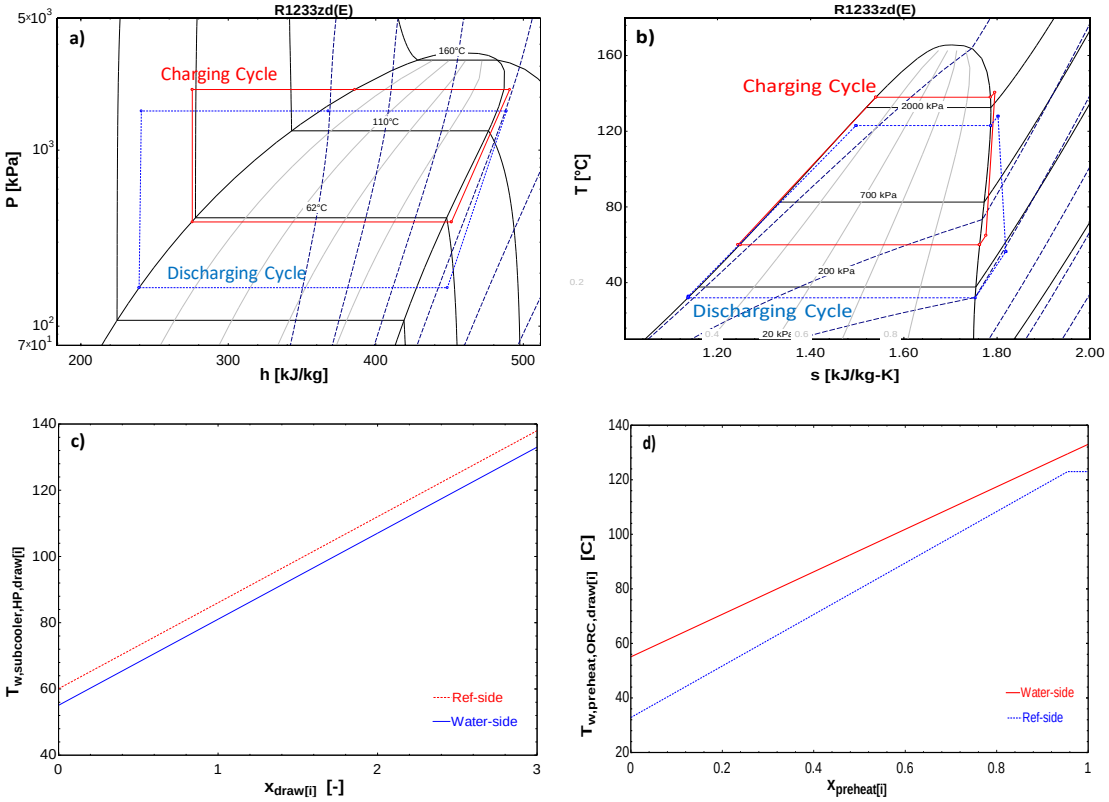

Figure 9. EES-CHEST model simulations for R1233zd(E), where $P_{input,HP}$= 1Mw, T_{source}= 70 °C, T_{sink}=25 °C, and $T_{melt,PCM}$= 133 °C (no pressure drops inside heat exchangers): a) P-h diagram, b) T-s diagram, c) temperature profiles inside HT-HP's subcooler, and d) temperature profiles inside ORC's preheater.

For these reasons, isentropic fluids are the best option, as they do not require high superheat and do not have high discharge temperatures. In case 1, a roundtrip efficiency of 1 is reached for a T_{source} of 74°C. Accordingly, so far, the competitiveness of the system was demonstrated.

b) <u>System configuration analysis:</u>

The second study was focused on the analysis of different configurations for the HT-HP and ORC cycles.

In the HT-HP the possibility of including several stages of compression was assessed. This option permits to solve the problem of having high discharge temperatures when using wet fluids mentioned above. However, the increase in complexity of the system does not compensate the improvements made.

For the ORC cycle the influence of including recuperation and/or regeneration processes were studied. For both cases the thermal efficiency of the ORC is improved slightly while the COP of the HT-HP is reduced, thus, the total roundtrip efficiency of the CHEST system nearly remains the same.

1.4. AIMS AND OBJECTIVES

So far, the previous studies were based on the coupled CHEST model working under steady state conditions: a fixed input power is used in the HT-HP and the energy charged in the TES systems (LHS and SHS) is immediately used to drive the ORC, having a different net output power depending on the boundary conditions of the system (T_{source} and T_{sink}). No analysis of requirements or evolution of the TES systems have been done.

In this thesis, previous studies of CHEST steady behavior done in UPV are taken as a starting point to go beyond within the project and assess the transient evolution of a decoupled CHEST system composed of HT-HP, ORC and a TES system consisting of LHS and SHS units. All the components of the CHEST system, including energy storage, have been implemented bearing in mind the previous work done: isentropic fluids and simple configurations of thermodynamic cycles are used. To achieve this main goal, different objectives have been set:

- To decouple the CHEST model in order to have a more accurate representation of the reality: power input for the HT-HP will come from the surplus of electricity generation and net power output from the ORC will be demanded in case there is a deficit of electricity. So, the logical idea would be that CHEST system tries to use as much surplus power as possible and, in the same way, to cover as much deficit as it can. Thus, heat stored in, or demanded from the TES systems may be different for the HT-HP and ORC: not all the heat charged will necessary be used for the discharging process as the boundary conditions for each process, at first, are unknown.
- To implement performance maps for HT-HP and ORC, using Butene as refrigerant, for a given nominal power of 1 MWe. The independent parameters for these maps are the water-side temperatures in the HT-HP's evaporator and ORC's condenser and the temperature of the water contained in the cold tank of the sensible heat storage system
- To develop a dynamic model for the CHEST system (TRNSYS-CHEST model), this model takes into account the working conditions of HT-HP and ORC, the state of charge of the TES system and the overall performance of the system.
- To perform parametric studies. These studies include the study of the different working modes proposed by the CHESTER project; the assessment of three different optimization strategies proposed along the Thesis; and the study of a possible application of a CHEST system in the current Spanish energy market.

2. METHODOLOGY

2.1. TRANSIENT STUDY OF A CHEST SYSTEM

This master thesis presents a model of the CHEST system using TRNSYS (**TR**a**N**sient **SY**stem **S**imulation) [14] for the transient study of the complete system. Thermodynamic cycles employed for the development of the model were previously decoupled using EES.

TRNSYS has been selected as the software employed for this work as it performs transient simulation of energy systems with a given timestep and for a defined period of time. It is composed of a series of basic components (Types) that are connected with each other. Types are seen as black boxes by the user but, internally, are formed by a system of equations that determine the behavior of the component at each timestep. In each Type three kind of variables are distinguished: [14]

- **Inputs:** independent variables of the type that are expected to change during the time of the simulation (temperatures, flow rates, etc.)
- **Parameters:** independent variables that define the type and are not expected to change during the simulation (area, volume, fluid properties, etc.)
- **Outputs:** dependent variables obtained once the internal system of equations is solved.

While the simulation is performed, inputs of each type are checked and outputs are calculated every timestep. In case an input value changes during one timestep, the type is called again and outputs are recalculated. [14]

The model proposed in this work aims to be a template of the CHEST system that can be integrated into a complete energy system to study the interaction among CHEST and other systems such as RES production or seasonal storage units. This can be done by connecting the inputs (explained in Section 2.5) with the data coming from the complete system. Three different options to optimize the model are given, depending on the optimization of the temperature of the low-temperature water tank (T_{LTWT}) that is related to the sensible heat storage (SHS) system (see Section 2.6.1). The proposed model adapts to the different sizes of the equipment and working modes assessed in the project (Figure 8), modifying the boundary conditions (sink and source temperatures).[6]

To do so, the following steps were proposed to develop the TRNSYS-CHEST model:

- Classification of modeling variables and parameters (independent, dependent, and fixed).
- Definition of performance maps for HT-HP and ORC.
- Modelling and sizing of TES system (latent and sensible heat storage sub-systems).
- Development of a control strategy to study the evolution of the system during the time of the simulation.
- Display of the results obtained per simulation.

The current model permits analyzing the evolution of the TES system during the required simulation period, controlling the state of charge of the thermal storage tanks, as well as,

studying the global performance of the system. This is done by evaluating some system parameters during the simulations such as the seasonal roundtrip efficiency[7], electrical energy bypassed, thermal energy charged or discharged, etc.

2.2. OVERALL CHEST SYSTEM

As mentioned before, the CHEST system comprises a high temperature heat pump (HT-HP), organic Rankine cycle (ORC), and a thermal energy storage (TES) system divided into latent (LHS) and sensible (SHS) heat storage systems. The phase change material (PCM) used in the LHS system is $LiNO_3$-KNO_3, which has a melting temperature (T_{melt}) of 133 °C. According to this melting temperature, Butene is selected to be the working fluid for both HT-HP and ORC, as it is an isentropic refrigerant with suitable working temperatures and pressures.

Table 2 . Properties of Butene. [5]

Property	Value	Unit
Normal Boiling Point (NBP)	-6	°C
Critical Temperature	146.14	°C
Critical Pressure	40.05	bar

Complete outline of the CHEST system and T-s diagram can be seen, respectively, in Figure 9 and Figure 10.

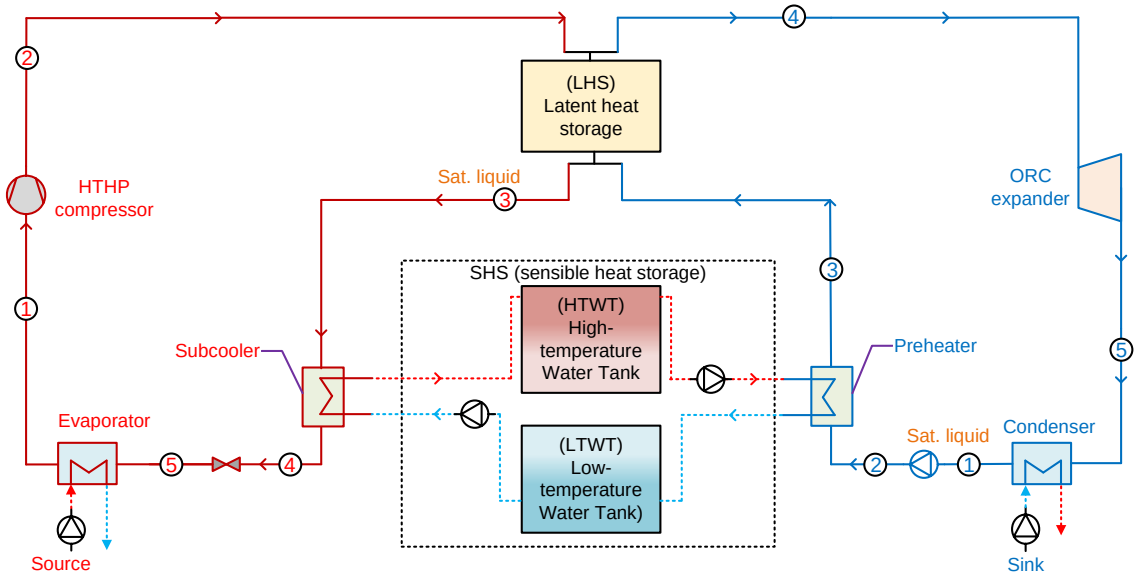

Figure 9. CHEST system layout

[7] A seasonal roundtrip efficiency is defined for the simulation period, and it is calculated as the sum of the net energy produced by the ORC divided by the total input energy used by the HT-HP

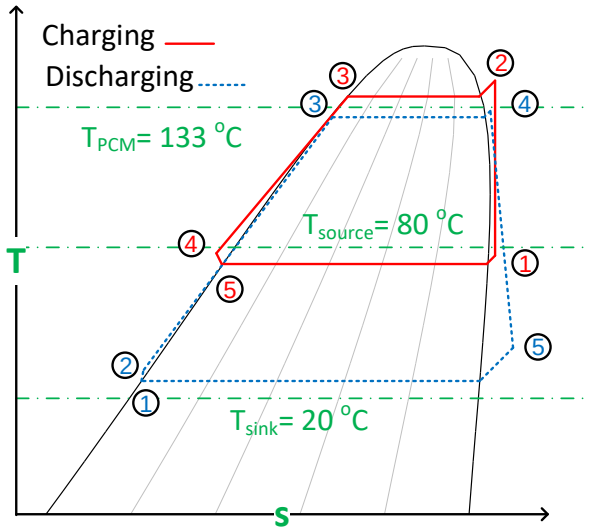

Figure 10. Schematic of T-s diagram for charging and discharging cycles in CHEST system for Butene, where the T_{source} = 80 °C and T_{sink} = 20 °C (no pressure drops inside heat exchangers)

During the charging cycle (left-hand side of Figure 9 and red solid line in Figure 10) surplus electricity from RES generation is used to drive the compressor of the HT-HP (process 1-2). Then, the butene is condensed in the LHS unit (2-3), subcooled by means of the SHS system (3-4), expanded (4-5) and evaporated using an external heat source (5-1).

In the other hand, if there is a deficit in the electricity demand, ORC (right-hand side of Figure 9 and blue dotted line of Figure 10) is activated to cover the maximum possible amount of that deficit. So, refrigerant is compressed (1-2) and preheated using the energy previously stored in SHS (2-3). Then, it is evaporated exchanging heat with the LHS (3-4), expanded (4-5) and condensed (5-1).

TES system is depicted in Figure 9. Latent heat storage (LHS) system consist of a tank filled with PCM. During charging, heat rejected during condensation is used to melt the PCM and store energy in form of latent heat. In the discharging this stored heat is utilized in the evaporator of the ORC and the PCM turns into solid again.

Sensible heat storage (SHS) is composed of two tanks filled with water at different temperature levels. In the charging process water from low temperature water tank (LTWT) goes through the subcooler of the HT-HP, where is heated up, and, later, it is stored in the high temperature water tank (HTWT). During the discharging, hot water in HTWT is used to drive the preheater of the ORC and, then, it is stored in the LTWT.

2.3. CLASSIFICATION OF VARIABLES FOR TRNSYS-CHEST MODEL

In order to design the model in TRNSYS, the CHEST system was implemented previously in EES (EES-CHEST model) giving detailed information about every parameter of the cycle. In order to structure this information and decide which of these variables could be implemented in TRNSYS-CHEST model and which ones will be given by the EES-CHEST model, an analysis of all of them was carried out.

To obtain the independent variables that will be modified in TRNSYS, a classification of all the parameters of the system has been done. The variables and parameters considered were:

- Melting temperature of PCM in latent heat storage.
- HT-HP's compressor overall and isentropic efficiencies.
- ORC's expander overall and isentropic efficiencies.
- ORC's main pump overall and isentropic efficiencies.
- Electrical power input/output for compressor, expander, and pump.
- Secondary fluid (source) inlet temperature and temperature difference for HT-HP's evaporator.
- Secondary fluid (sink) inlet temperature and temperature difference for ORC's condenser.
- Superheat in HT-HP's evaporator and ORC's LHS.
- Pinch point inside heat exchangers.
- Temperature of the Low-temperature water tank and high-temperature water tank.
- Secondary fluid mass flow rates in subcooler, preheater, HT-HP's evaporator, and ORC's condenser.
- Refrigerant mass flow rates in HT-HP and ORC.
- Pressure drop in heat exchangers.
- Heat capacities of heat exchangers.

These variables have been classified into three different categories, depending on their values throughout the simulations:

- **Fixed variables:** Their values have previously been predefined in the EES-CHEST model, so it is constant for the whole simulations and cannot be changed in the TRNSYS-CHEST model. If one of them needs to be changed, new performance maps should be generated. These variables are:

  - Efficiencies of compressor ($\boldsymbol{\eta_{com}}$), expander ($\boldsymbol{\eta_{exp}}$), and pump ($\boldsymbol{\eta_{pump}}$).
  - Pinch point ($\boldsymbol{\Delta T_{pinch}}$) and pressure drop ($\boldsymbol{\Delta P}$) values inside heat exchangers.
  - Superheat values inside the HT-HP's ($\boldsymbol{SH_{evap}}$), evaporator and ORC's LHS ($\boldsymbol{SH_{ORC-LHS}}$).

- **Independent variables:** Variables that determine the performance of the system. They can be modified by the user or, in the case of the temperatures of the tanks, depend on the initial state of the system and its evolution in the TRNSYS-CHEST model:

  - Input electrical power for the HT-HP: $\boldsymbol{P_{input,HP}}$
  - Water-side (source) temperature difference and inlet temperature for the HT-HP's evaporator: $\boldsymbol{\Delta T_{w,evap}}$ and $\boldsymbol{T_{w,inlet,evap}}$
  - Net output power from the ORC: $\boldsymbol{P_{output,ORC}}$
  - Water-side (sink) temperature difference and inlet temperature for the ORC's condenser: $\boldsymbol{\Delta T_{w,cond}}$ and $\boldsymbol{T_{w,inlet,cond}}$
  - Temperatures of the low-temperature and high-temperature water tanks: $\boldsymbol{T_{LTWT}}$ and $\boldsymbol{T_{HTWT}}$

- **Dependent variables:** Obtained as a function of the other variables:

- Mass flow rates for refrigerants ($\dot{m}_{ref,HTHP}$, $\dot{m}_{ref,ORC}$) and water ($\dot{m}_{w,subc-HTHP}$, $\dot{m}_{w,preh-ORC}$).
- Heat capacities of the heat exchangers ($\dot{Q}_{LHS,HTHP}$, $\dot{Q}_{SHS,HTHP}$, $\dot{Q}_{evap,HTHP}$, $\dot{Q}_{LHS,ORC}$, $\dot{Q}_{SHS,ORC}$, $\dot{Q}_{cond,ORC}$).

The classification of the variables in the diagram is depicted in Figure 11. The fixed, independent, and dependent variables are marked in red, blue, and black, respectively.

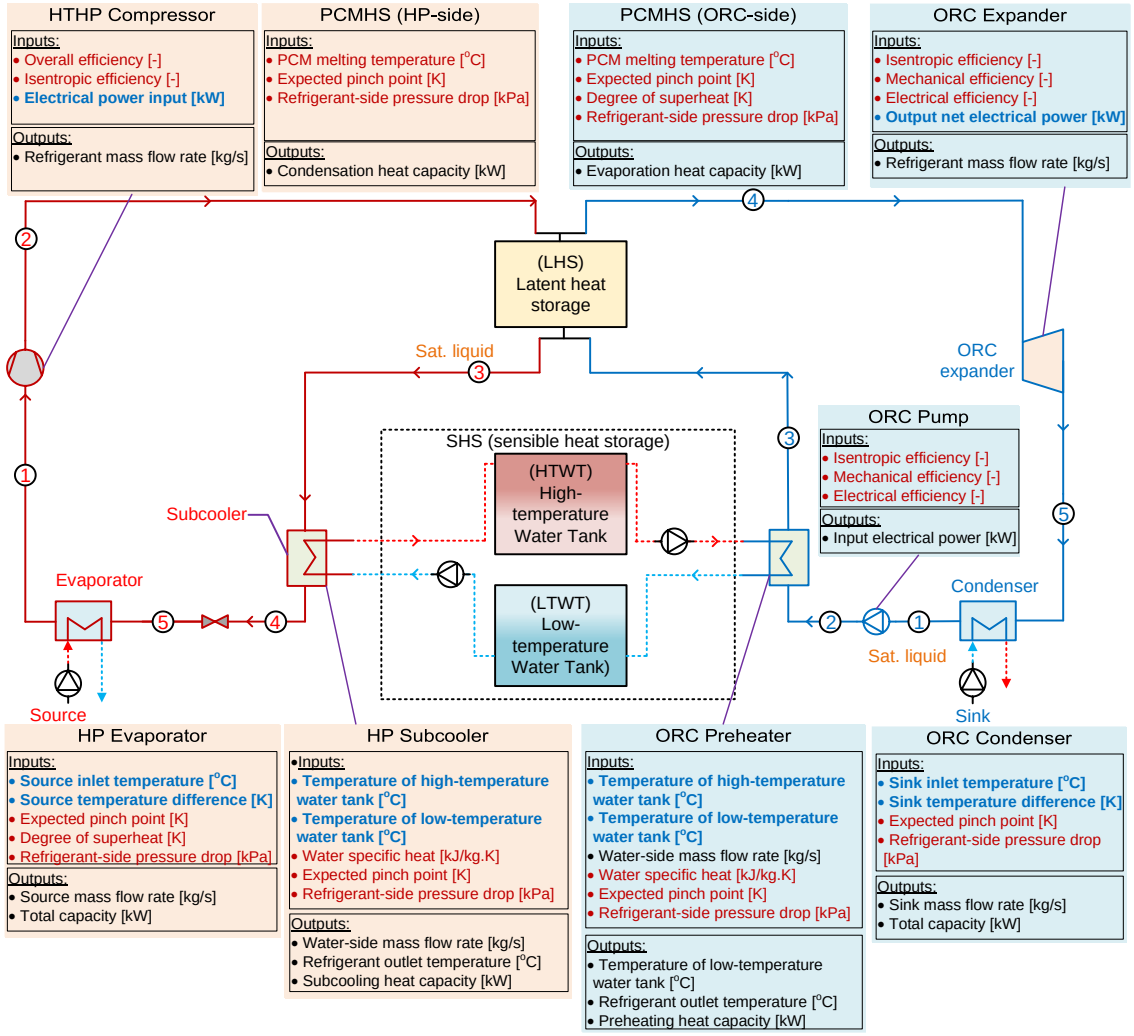

Figure 11 . Classification of variables of the CHEST system: fixed (red), independent (blue), and dependent (black)

The complete variables with the final classification are listed in Annex I.

Following this decision, there are now five independent variables per equipment:

- HT-HP: $P_{input,HP}$, $T_{w\_inlet,evap}$, $\Delta T_{w,evap}$, T_{LTWT} and T_{HTWT}
- ORC: $P_{output,ORC}$, $T_{w\_inlet,cond}$, $\Delta T_{w,cond}$, T_{LTWT} and T_{HTWT}

2.4. TRNSYS-CHEST MODEL OVERVIEW

Once the independent variables, that define the behavior of the system, are specified, the TRNSYS-CHEST model is defined. In this section, a general scheme of the proposed model, with the different sub-systems, is presented.

The complete TRNSYS-CHEST model is depicted in Figure 12.

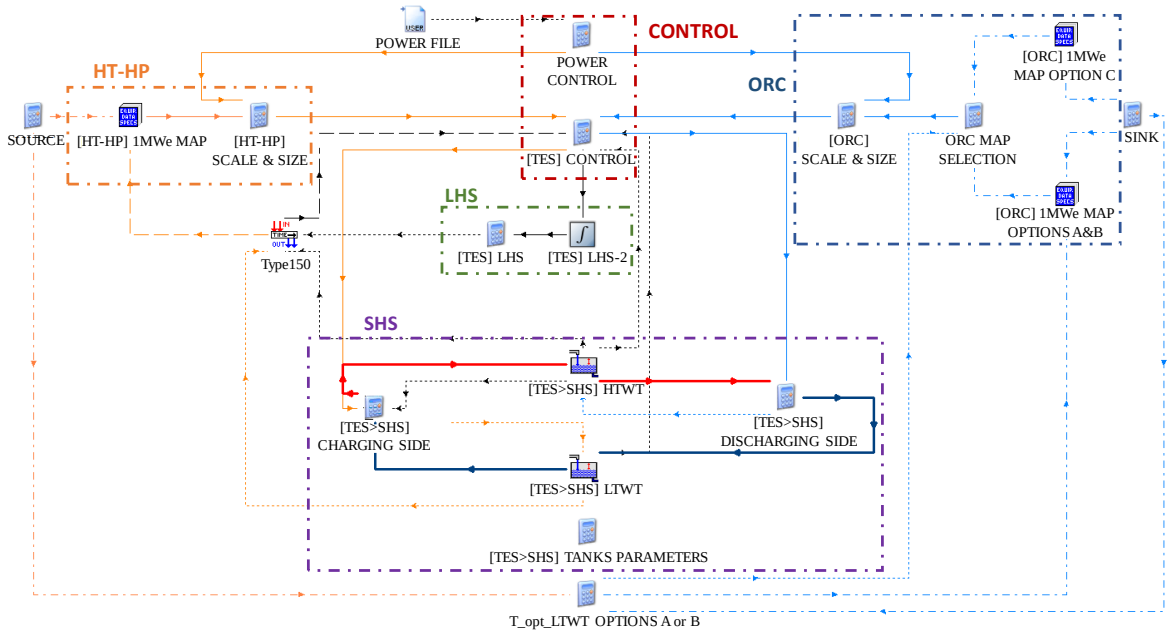

Figure 12 . TRNSYS-CHEST model

As it can be seen, there are five differentiated blocks that interact with each other:

- **CONTROL:** different control strategies are implemented in this block considering the different cases that may take place for power and heat variables.
- **HT-HP:** in this block the HT-HP performance is calculated using the performance maps, generated at the nominal conditions, and scaling factors to adapt the outputs of the map to the conditions of the simulations.
- **ORC:** the performance of the ORC is also obtained by the performance maps generated at the nominal conditions and scaling factors. In this case, two different maps can be employed depending on the option selected (see Section 2.6.1).
- **LHS:** a simplified model of the latent heat storage system is implemented to calculate the energy stored and the state of charge of the LHS tank.
- **SHS:** the sensible heat storage system is simulated using two variable volume storage tanks containing water at two different temperature levels.

Apart from that, other types that are excluded from the previous classification can be sorted in:

- **INPUTS:** *POWER FILE*, *SOURCE* and *SINK* are values to be changed by the user in order to adapt the model to the case of study.
- **INTERNAL CALCULATIONS:** [TES>SHS] *TANKS PARAMETERS*, *T_LTWT OPTIONS A or B* and *ORC MAP SELECTION* are implemented to calculate parameters required internally in the model.

The functioning and interaction of all these components will be explained in detail in the following sections. As a general idea, the "INPUTS" define the performance of the equipment (HT-HP and ORC) which determines the state of the storage system TES. The "CONTROL" system is responsible for controlling the amount of power provided to the HT-HP or produced by the ORC and stopping the system or bypassing the excess energy.

2.5. INPUTS TO THE TRNSYS-CHEST MODEL[8]

Once selected the independent variables of the system (Section 2.3), these can easily be changed, along with other basic parameters such as sizing of the equipment and TES system, in order to adapt the simulation to the corresponding case study. These inputs can be found either in external data readers (Type 9c) or as fixed values in *CONTROL CARDS*; and are related to the power generated or demanded, with the sizing of equipment and TES tanks or working temperatures of the system.

2.5.1. Power File

The power data is introduced from a data reader type as it is expected to change during the simulation. So, an external ".txt" file, that contains the following information in columns, is needed:

- **Column 1 (Time information):** This column must include the timestep (in hours) in which the data has been read. It starts from zero in order to have an initial value in the beginning of the simulations.
- **Column 2 (P_el_out_RES_MW):** In this column, the amount of total power generated by the RES is collected for each timestep defined before (in MW).
- **Column 3 (P_el_dem_MW):** The demand of electrical power, in MW, is presented per timestep.

The data is expected to be the gross input or output power, calculations about deficit or surplus power will be done inside the TRNSYS-CHEST model.

2.5.2. Control Cards

In *CONTROL CARDS* information about the size of the equipment, the storage capacity of the tanks, the properties of water or source and sink temperatures can be modified. Additionally, the working criteria of the ORC is chosen here[9].

These variables are:

- **Option_A, B, C**: Variable used to define the way of identifying T_{LTWT}. For more details see Sub-section 2.6.1.
- **P_el_in_nom_HP_MW**: The nominal input power to the HT-HP's compressor, in MW.

[8]The data of this section is expected to be given in the units mentioned in each case; otherwise, conversion factors should be applied either in the input file or in the TRNSYS-CHEST model.

[9] Two options A, B or C cannot be selected at the same time. Only one option can be chosen (equals to 1) and the rest should be equal to 0.

- **P_el_net_nom_ORC_MW**: The net output power from the ORC, in MW
- **Cp_w_kJ_kgK:** Specific heat of water in kJ/kg·K.
- **Rho_w_kg_m3**: Density of water in kg/m^3
- **V_w_SHS_m3:** Volume of each water tank of the SHS system in m^3. The size of the tanks is the same for both the cold and hot tanks.
- **E_q_max_LHS_MWh**: Maximum storage capacity of the LHS tank in MWh.
- **T_w_in_evap_HP_C**: Inlet water temperature, in °C, for the HT-HP's evaporator. This temperature represents the source for the HT-HP and it should be inside the working range of the equipment, that is, between 40 and 100 °C.[10,11]
- **DT_w_evap_HP_K**: water-side temperature difference for the HT-HP's evaporator. This temperature is used as an input for the HT-HP performance map so its value should be inside the working range of the equipment, that is, between 2 and 6 K.
- **T_w_in_cond_ORC_C**: Inlet water temperature, in °C, for the ORC's condenser. This temperature represents the sink for ORC and it is used as an input for the ORC performance map, so its value should be inside the working range of the equipment, that is, between 10 and 60 °C.
- **DT_w_cond_ORC_K**: Water-side temperature difference for the ORC's condenser. This temperature is used as an input for the ORC performance map so its value should be inside the working range of the equipment, that is, between 2 and 10 K.
- **T_opt_LTWT_user_option_B:** Optimum temperature at the outlet of the preheater (T_opt_LTWT) selected by the user when Option B is chosen.
- **DT_cond_LTWT_option_B:** minimum temperature difference between T_opt_LTWT_user_option_B and T_w_in_cond_ORC_C to ensure always the validity of second law of thermodynamics during the simulations.

2.6. PERFORMANCE MAPS FOR HT-HP AND ORC

EES-CHEST model was initially coupled with the TRNSYS-CHEST model, but the simulation time was too long and, for this reason, the best option which was found was to model the HT-HP and the ORC independently in EES and generate the corresponding performance maps. Such maps can be integrated in TRNSYS-CHEST model by using linear interpolation types. The main drawback of this choice is that maps are created for one specific fluid and certain fixed parameters. So, for any change in refrigerant or parameters, new individual maps have to be created. For the proposed model, Butene has been chosen as the heat transfer fluid for both HT-HP and ORC cycles.

To introduce the maps in TRNSYS-CHEST model, Type 42 was used. This type allows integration of maps that accept up to three independent variables as inputs with a maximum of five

[10] For further information about working modes of the CHEST system, see Section 2.6.1

[11] The data related to the working temperatures for the evaporator and condenser are to be inside the range used for the corresponding performance map. If the data introduced is outside this range, the accuracy of the results obtained cannot be guaranteed.

different values for each one; and up to five dependent variables as outputs. To calculate the outputs, it interpolates linearly within the values of the range.

Thus, the maximum number of points per map is 5^3= 125.

As explained earlier, the classification of variables in Section 2.3 leads to five independent variables per equipment. In order to reduce these variables to the maximum allowed by TRNSYS's types, some assumptions were made.

2.6.1. Selection of Independent Variables for the Performance Maps

To reduce the number of independent variables, the HT-HP and ORC performance maps were done for an electrical nominal power of 1 MWe. Subsequently, sizing and scale factors were applied in the TRNSYS-CHEST model (Section 2.7.2) to compensate the fluctuations of the power demanded or produced. Thus, the variables considered to do the maps are:

- $\text{HT-HP}|_{1\text{ MWe}} = f\left(T_{w,inlet,evap}, \Delta T_{w,evap}, T_{LTWT} \text{ and } T_{HTWT}\right)$
- $\text{ORC}|_{1\text{ MWe}} = f\left(T_{w,inlet,cond}, \Delta T_{w,cond}, T_{LTWT} \text{ and } T_{HTWT}\right)$

While the temperatures in the evaporator and the condenser are values that can be introduced by the user, the tank temperatures are obtained either from the corresponding type in the TRNSYS-CHEST model (inlet temperatures for subcooler and preheater) or by the optimum outlet water temperature from subcooler and preheater.

The results from the EES-CHEST models show that the optimum value of T_{HTWT} is always equal to the melting temperature of the PCM (assuming fixed pinch point of 5 K inside the subcooler), in this case it equals to 133°C. Thus, T_{HTWT} has been eliminated as independent variable and is fixed to 133°C for the elaboration of the performance maps.

The way to proceed with T_{LTWT} is different for the HT-HP and ORC map. During charging, the value of T_{LTWT} is estimated by the model as a boundary condition and corresponds to the actual temperature of the tank in each timestep. However, during discharging, the T_{LTWT} corresponds to the optimum outlet water temperature from the ORC's preheater. Accordingly, three different options have been implemented to estimate the optimum value for the lower tank (**T_opt_LTWT**):

- **Option A:** The T_opt_LTWT value is obtained from Eq. (2) based on the results of the coupled model of the CHEST system. The TRNSYS-CHEST system is dynamic but this helps as a first control strategy.
- **Option B:** Predefined value of the T_opt_LTWT by the user (defined in the CONTROL CARDS as T_opt_LTWT_user_option_B).
- **Option C:** T_opt_LTWT is obtained as an output from the ORC performance map when fixing the condition of having saturated liquid at the outlet of the preheater. This option might be interesting to simulate laboratory conditions.

Based on this, the independent variables for each one of the maps are:

- HT-HP's map= $f\left(T_{w,inlet,evap}, \Delta T_{w,evap}, T_{LTWT}\right)$

- ORC's map for Options A and B= $f(T_{w,inlet,cond}, \Delta T_{w,cond}, T_{LTWT})$
- ORC's map for Option C= $f(T_{w,inlet,cond}, \Delta T_{w,cond})$

The range of each variable has been selected to cover the six different operating modes of the CHEST system (seen in Figure 8). In the case of $\Delta T_{w,cond}$, it has a wider range than $\Delta T_{w,evap}$ in order to allow the integration with a district heating system. Average values of the sink and source temperatures for each working mode of Figure 8 can be seen in Table 3.

Table 3. Source and sink temperatures in the different working modes

Variable	Mode 1	Mode 2	Mode 3	Mode 4	Mode 5	Mode 6
$T_{w,inlet,evap}$	80	80	100	100	60	40
$T_{w,inlet,cond}$	40	10	40	10	60	60

2.6.2. HT-HP Performance Map[12]

The independent variables used for the HT-HP map are, as aforementioned, $T_{w,inlet,evap}$, $\Delta T_{w,evap}$ and T_{LTWT}. While the range of the temperatures in the evaporator is selected according to the working modes of the CHEST system, the range of T_{LTWT} is the temperature of the tank in the timestep that is being evaluated, and is in the range from the ambient temperature (assumed to be 25 °C in the current study) to the maximum value that it is expected to reach (based on the coupled EES-CHEST model simulations).

Table 4. Temperature ranges for HT-HP performance map

Variable	Values (°C)				
$T_{w,inlet,evap}$	40	55	70	85	100
$\Delta T_{w,evap}$	2	4	6	-	-
T_{LTWT}	25	55	70	85	100

Thus, the total number of points of this map is 5^2*3= 75.

The TRNSYS-CHEST model has the following inputs for the performance map:

- **T_w_in_evap_HP_C**: Variable located in *CONTROL CARDS* that can be modified by the user according to the working mode to define the source inlet temperature.
- **DT_w_evap_HP_K**: Also modified by the user, in *CONTROL CARDS,* to define the water-side temperature difference inside the HT-HP's evaporator.
- **T_w_LTWT_SHS_C:** Temperature of the cold tank at that time step. The map will use this temperature to provide the heat needed to reach the optimum output temperature from the subcooler, which equals the T_{HTWT}= 133 °C.

The outputs obtained from the map that are employed in the TRNSYS-CHEST model are:

- **P_q_sen_nom_HP_MW:** Nominal sensible heat delivered by the HT-HP to be stored in the SHS storage tanks, in MW.

[12] Complete HT-HP performance map can be consulted in Annex II.

- **P_q_lat_nom_HP_MW:** Nominal latent heat delivered by the HT-HP to be stored in the LHS storage tank, in MW.
- **COP_nom_HP:** Nominal COP for the HP.

These outputs are calculated for a nominal input total electrical power to the HT-HP's compressor of 1 MWe working at full load. Later on, these values are adjusted in case the input power differs from 1 MWe (see Section 2.7.2).

2.6.3. ORC Performance Map

As mentioned before, three options are given to the user to select the optimum outlet temperature for the preheater of the ORC (T_opt_LTWT). For Options A and B the same ORC map is used, as the difference between them is the way to obtain T_opt_LTWT (by means of a correlation or introduced by the user). However, for option C, an extra condition has been set in the EES-CHEST model (saturated state at the preheater outlet), so a different performance map is needed.

To ensure that only one of the options is selected, the variable **SF_option_selection** has been included. In the case of more than one option (or none of them) is chosen, this variable will try to make a division by zero, leading to an error and stopping the simulation.

a) ORC's map for options A and B[13]

To create this ORC map $T_{,inlet,cond}$, $\Delta T_{w,cond}$ and T_{LTWT} were used. In this case, the range of temperatures is also selected considering the working modes, but for the T_{LTWT} the optimum value for these conditions is the input introduced to the map, so the range does not have to cover until the ambient temperature.

Table 5. Temperature ranges for ORC performance map

Variable	Values (°C)				
$\boldsymbol{T_{w\_inlet\_cond}}$	10	20	35	40	60
$\boldsymbol{\Delta T_{w\_cond}}$	2	5	10	-	-
$\boldsymbol{T_{LTWT}}$	40	55	70	85	100

Thus, the total number of points of this map is 5^2*3= 75.

The inputs to the map are as follows:

- **T_w_in_cond_ORC_C**: Variable located in *CONTROL CARDS* that can be modified by the user according to the working mode to define the sink inlet temperature.
- **DT_w_cond_ORC_K:** Also modified by the user, in *CONTROL CARDS,* to define the water-side temperature difference inside the ORC's condenser.

[13] Complete ORC performance map for Options A and B can be consulted in Annex III.

- **T_opt_LTWT_C:** Optimum temperature that the outlet flow from the preheater has to reach. This value is estimated using Eq. (2) (Option A) or introduced directly by the user in *CONTROL CARDS* (Option B)

The outputs from this map are:

- **P_q_sen_nom_ORC_MW**: Nominal sensible heat delivered to the ORC by the SHS to have a nominal electrical net power of 1 MW.
- **P_q_lat_nom_ORC_MW:** Nominal latent heat delivered to the ORC by the LHS to have a nominal electrical net power of 1 MW.
- **P_q_cond_ORC_MW:** Nominal heat capacity of the ORC's condenser when having a nominal electrical net power of 1 MW.

In this map there are some combination of points that cannot be calculated in the EES-ORC model because the second law of thermodynamics would be violated, as the temperature of the refrigerant entering the preheater is higher than the outlet temperature of the water, T_{LTWT}. However, as TRNSYS's type 42a needs a complete input file, these combinations have been included writing a zero for all the outputs. This does not affect the performance of the model when using Option A, as it has been proved that these conditions are impossible to reach in the simulation. However, for option B, an adequate value of **T_opt_LTWT_user_option_B** should be selected so as to have a correct interpolation.

The correlation employed for the OPTION A was obtained using results from the coupled model of the EES-CHEST system. T_opt_LTWT_C is calculated as a function of the variables T_w_in_evap_HP, DT_w_evap_HP, T_w_in_cond_ORC and DT_w_cond_ORC. To find the appropriate correlation, the software R was used.

Results show that the most influential variable is T_w_in_cond_ORC and that the value of T_opt_LTWT_C increases with the increase of the other variables. The most suitable option found was a quadratic correlation with a maximum error of ±1.3%:

$$
\begin{aligned}
\boldsymbol{T\_opt\_LTWT\_C} &= 31.55 + 0.8614 \times T\_w\_in\_cond\_ORC \\
&+ 0.2117 \times T\_w\_in\_evap\_HP \\
&+ 0.8314 \times DT\_w\_cond\_ORC \\
&- 0.2228 \times DT\_w\_evap\_HP \\
&- 4.716 \times 10^{-4} \times T\_w\_in\_cond\_ORC^2 \\
&- 1.241 \times 10^{-3} \times T\_w\_in\_evap\_HP^2 \\
&- 4.548 \times 10^{-4} \times T\_w\_in\_cond\_ORC \\
&\times T\_w\_in\_evap\_HP \\
&- 1.101 \times 10^{-3} \times T\_w\_in\_cond\_ORC \\
&\times DT\_w\_cond\_ORC \\
&+ 2.567 \times 10^{-3} \times T\_w\_in\_evap\_HP \times DT\_w\_evap\_HP
\end{aligned}
\qquad \textbf{(2)}
$$

b) ORC's Map for Option C[14]

To create the ORC map for option C, $T_{w\_in_{cond}}$ and ΔT_{w_cond} have been used. In this case, the range of the temperatures is also selected considering the different working modes:

Table 6. Temperature ranges of the ORC performance map

Variable	Values (°C)				
$T_{w\_in_{cond}}$	10	20	35	40	60
ΔT_{w_cond}	2	5	10	-	-

Thus, the total number of points of this map is 5*3=15.

The inputs of the TRNSYS-CHEST model are similar to the HT-HP case:

- **T_w_in_cond_ORC_C**: Variable located in *CONTROL CARDS* that can be modified by the user according to the working mode.
- **DT_w_cond_ORC_K:** Also modified by the user, in *CONTROL CARDS*.

The outputs from this map used in the TRNSYS-CHEST model are:

- **P_q_sen_nom_ORC_MW**: Nominal sensible heat consumed from SHS by the ORC to have a nominal output power of 1 MWe.
- **P_q_lat_nom_ORC_MW:** Nominal latent heat consumed from LHS by the ORC to have a nominal output power of 1 MWe.
- **P_q_cond_ORC_MW:** Nominal heat capacity of the ORC's condenser when having a nominal output power of 1MWe.
- **T_opt_LTWT_C:** Optimum temperature for the LTWT. In Option C, this value is obtained assuming that the outlet of the ORC's preheater is always saturated liquid.

These outputs are obtained for an ORC providing 1 MWe of nominal net power. If this is not the actual case, the outputs are scaled according to the real state of the system (see Section 2.7.2).

2.7. TRNSYS-CHEST MODEL CONTROL STRATEGY

A control strategy for the model has been developed in order to check that the behavior of the system is consistent. The following steps were followed:

a) Control of the power entering the HT-HP or to be produced by the ORC.
b) Control of the load conditions for both the HT-HP and ORC.
c) Control of the charging levels for SHS and LHS tanks.
d) Control of temperatures of the SHS tanks for the correct functioning of the equipment.

[14] Complete ORC performance map for Option C can be consulted in Annex IV.

These different variables are used to limit either the entering power that drives the HT-HP or ORC or the heat that is stored or removed from the tanks.

2.7.1. Power control

The first check is to ensure that the HT-HP and ORC are not working during the same timestep, as that means that there is electricity production from renewable energy sources available to cover the demand, or at least part of it, so there is no need to use it to drive the HT-HP and store energy in the TES system. To do so, the power can be directly bypassed from one side to another, without using the storage system, this is defined by the variable P_el_bypass_RES_MW:[15]

$$\begin{aligned} \boldsymbol{P\_el\_bypass\_RES} \\ &= (P\_el\_out\_RES > P\_el\_dem) * P\_el\_dem \\ &+ (P\_el\_out\_RES < P\_el\_dem) * P\_el\_out\_RES \\ &+ (P\_el\_out\_RES = P\_el\_dem) * P\_el\_dem \end{aligned} \quad \textbf{(3)}$$

According to equation (3), the bypassed power is equal to the lower value between the P_el_out_RES and P_el_dem, at each timestep. Then, the surplus power available to drive the HT-HP or the deficit power, to be supplied by the ORC, are defined as:

$$\boldsymbol{P\_el\_surplus\_RES\_MW} = P\_el\_out\_RES - P\_el\_bypass\_RES \quad \textbf{(4)}$$

$$\boldsymbol{P\_el\_def\_pass\_dem\_MW} = P\_el\_dem - P\_el\_bypass\_RES \quad \textbf{(5)}$$

Once the surplus and the deficit power are defined, it should be considered that their values can be higher than the maximum that the equipment can work with. Thus, to ensure that the actual power, useful for HT-HP or that the ORC can supply does not exceed the maximum capacity, the following control variables have been defined:

$$\boldsymbol{SF\_P\_el\_in\_HP} = (P\_el\_surplus\_RES > P\_el\_in\_nom\_HP) \quad \textbf{(6)}$$

$$\boldsymbol{SF\_P\_el\_net\_ORC} = (P\_el\_def\_pass\_dem > P\_el\_net\_nom\_ORC) \quad \textbf{(7)}$$

These variables will be 0 if the available power is lower than the size and 1 otherwise. The real available power (estimated electrical power) will take values between zero and the size of the equipment:

$$\begin{aligned} \boldsymbol{P\_el\_in\_est\_HP\_MW} \\ &= P\_el\_surplus\_RES * (1 - SF\_P\_el\_in\_HP) \\ &+ P\_el\_in\_nom\_HP * SF\_P\_el\_in\_HP \end{aligned} \quad \textbf{(8)}$$

[15] In the following equations, expressions such as (P_el_dem > P_el_out_RES) are employed. They actually are control variables which have a value of 1 if the condition written in brackets is true and 0 if it is false. In TRNSYS this is programmed using the commands GT (Greater Than), LT (Lower Than) or EQL (Equal).

$$P\_el\_net\_est\_ORC\_MW = P\_el\_def\_pass\_dem * (1 - SF\_P\_el\_net\_ORC) + P\_el\_net\_nom\_ORC * SF\_P\_el\_net\_ORC \quad \textbf{(9)}$$

These terms calculated in Eqs. (8) and (9) are the ones connected to the performance maps, since they can be employed to drive the HT-HP or the ORC at each timestep.

2.7.2. Control of the Load Conditions

As the performance maps are done for a size of the systems of 1 MWe working at full load, scale and size factors are applied in the case that the load or the size differs from this value.

In the performance maps generated by the EES-CHEST model, the following values are obtained:

- P_q_sen_nom: nominal sensible heat in MW
- P_q_lat_nom: nominal latent heat in MW

In the TRNSYS-CHEST model these parameters are scaled according to the actual size of the equipment and its current load.

a) Relevant Parameters

In the maps introduced in TRNSYS-CHEST model the parameters are introduced for a heat pump or an ORC of 1 MWe of nominal power working at full capacity. These output parameters have to be sized (if the nominal power is different) and scaled (for partial load conditions). There are two different variables per system to pay attention to:

1. The nominal (maximum) capacity of the HP or ORC (P_el_in_nom_HP_MW or P_el_net_nom_ORC_MW).
2. Power input/output at each timestep (P_el_in_est_HP_MW or P_el_net_est_ORC_MW): these correspond to the actual estimated power provided to the HT-HP or demanded to be supplied by the ORC in every timestep. In this case, there are two different situations per component:
   - <u>For the HT-HP</u>
     a. P_el_in_est_HP = P_el_in_nom_HP → HP is working at full load
     b. P_el_in_est_HP < P_el_in_nom_HP →HP is working at partial loads, scale factor (**F_q_capacity_PLR_HP**) is employed.

   - <u>For the ORC:</u> This is analogous to the heat pump.
     a. P_el_net_est_ORC = P_el_net_nom_ORC_MW → ORC is working at full load
     b. P_el_net_est_ORC < P_el_net_nom_ORC_MW →ORC is working at partial load, scale factor (**F_capacity_PLR_ORC**) is used.

b) HT-HP Scaling and Sizing Factors

I. COP vs load capacity: state of the art

References show that for heat pumps with variable speed compressor there is an increase in the COP when working at a partial load (between 30-50%). This is due to the fact that the mass flow rate also decreases, leading to a reduction in the temperature difference in the evaporator and condenser, which lowers the pressure ratio [15, 16]. Below, several examples from literature illustrating this behavior are discussed.

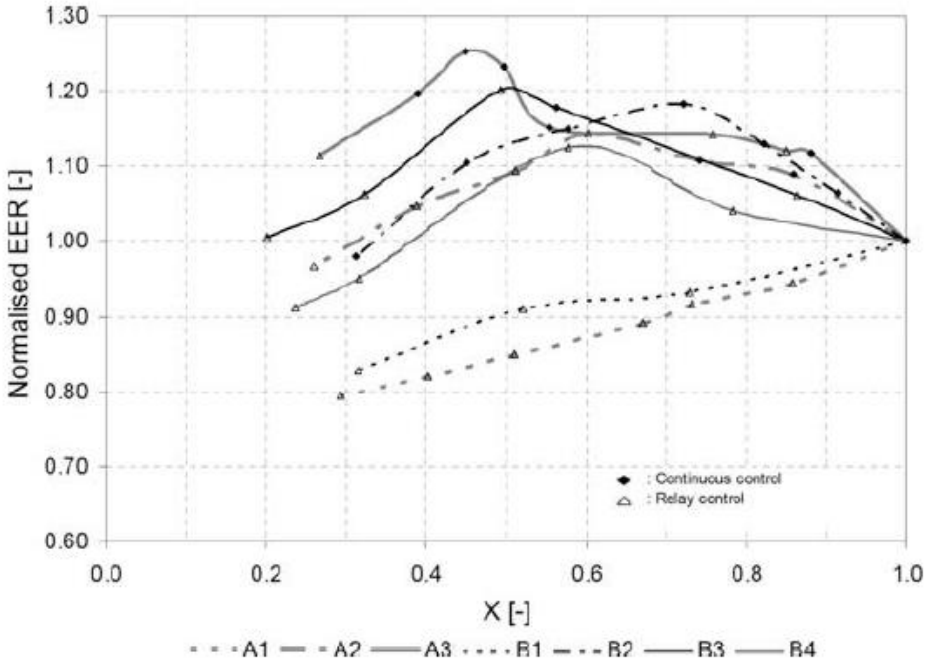

Figure 13. Normalized EER vs Load of compressor [15]

In Figure 13 the normalized Energy Efficiency Ratio (EER), defined as the ratio between the cooling capacity and the total power input is plotted as a function of the load of the compressor for different configurations: A1 and B1 represent cases without an inverter; A2 and B2 are single inverter compressors; and A3, B3 and B4 are cases with two compressors in tandem configuration, one of them driven by an inverter. As can be seen, in cases with an inverter there is an improvement of the efficiency when working at partial load, reaching their maximum value at 50% of the load.

In the report [16], the improvement of using an inverter to operate at partial load instead of an ON-OFF controller is highlighted, as it allows to reduce the temperature lift between the condenser and evaporator, decreasing the compression ratio and improving the efficiency for loads around 50%.

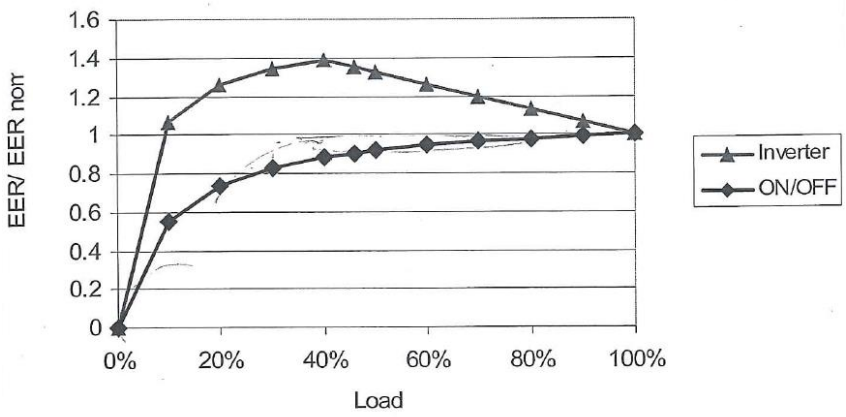

Figure 14. EER/EER_nom in inverter and ON/OFF compressors at different working loads[16]

Figure 15 shows some experimental results carried out by CETITAT illustrating the same behavior for different air temperatures. On it, the Partial Load Factor (PLF), which is the ratio between the actual COP and the nominal one, is plotted with the Partial Load Ratio (PLR), which corresponds with the equipment's load divided by its total capacity [17].

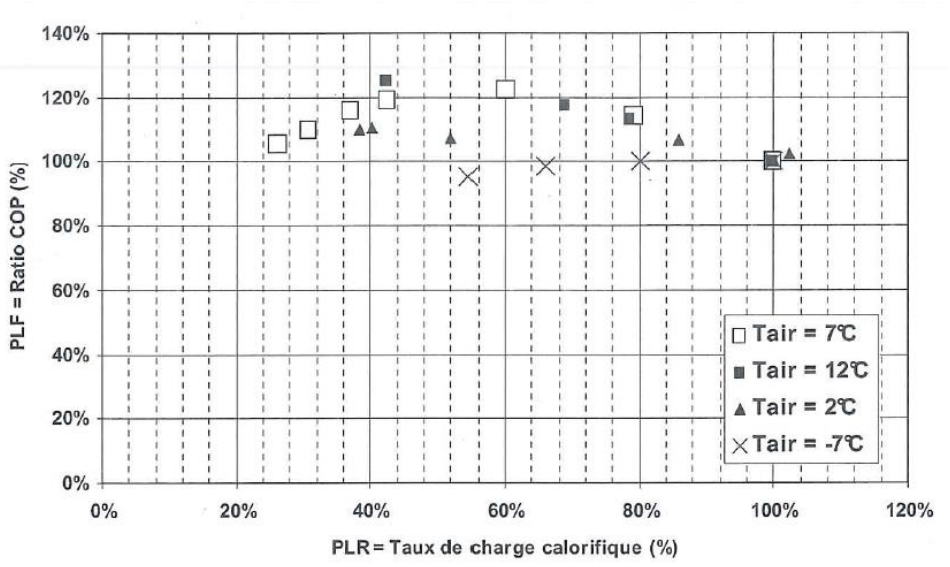

Figure 15. PLF vs PLR [17]

The same pattern is presented in other compressors that can be found in the market. For example, Figure 16 illustrates the performance of Turbocor TT500 compressor [18].

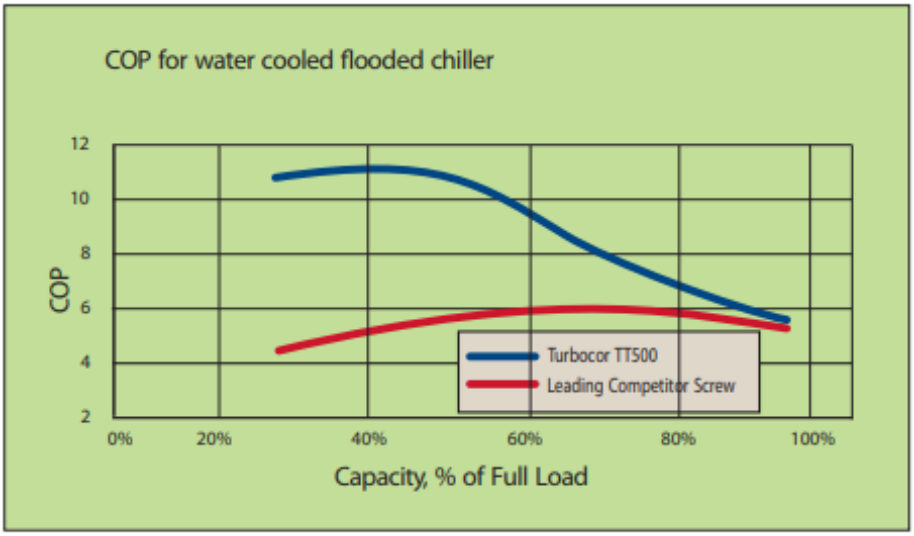

Figure 16. COP vs capacity in TURBOCOR compressors [18]**.**

The relationship between the fractional capacity and COP was also studied in [19] for three different motors (b=basic, m=modern, and n=new design). The results indicate an increase in the COP when the load is lower than 100%.

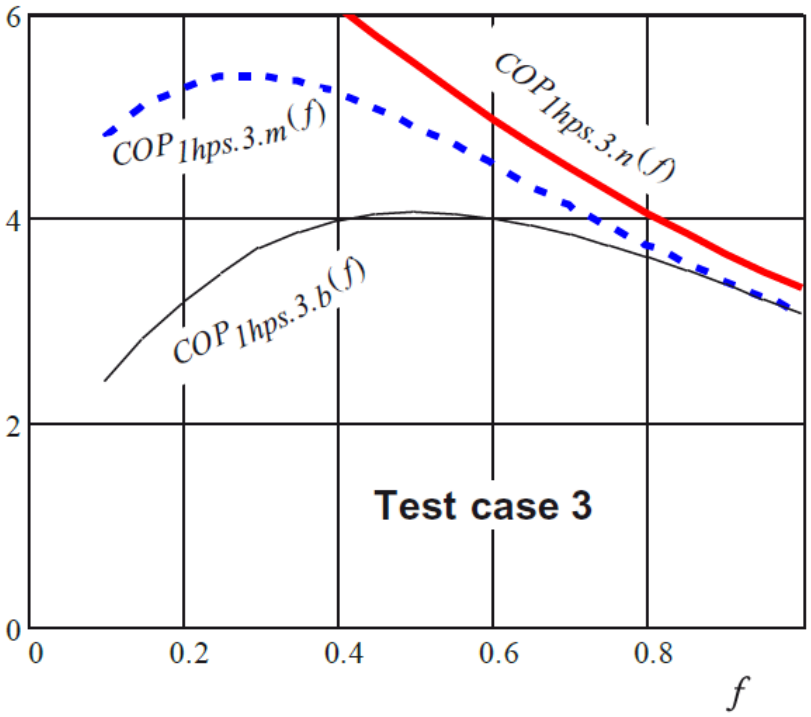

Figure 17. COP vs fractional capacity [19]**.**

Figure 17 and Table 7 resume the values of COP for different loads. As can be observed in case 3 (adapted flow) for a modern motor, the maximum values of COP range between 20% and 40% of the maximum load.

Table 7. COP at different load fractions[19].

Alternative	COP	$f=1.0$	$f=0.5$	$f=0.2$
1. Constant evaporating and condensing temperature.	$COP_{1hps.1.b}$	3.1	2.4	1.4
	$COP_{1hps.1.m}$	3.1	2.8	2.2
	$COP_{1hps.1.n}$	3.3	3.2	2.8
2. Constant flow rates, constant fan powers. Decreasing temperature lift.	$COP_{1hps.2.b}$	3.1	3.5	2.8
	$COP_{1hps.2.m}$	3.1	4.1	4.0
	$COP_{1hps.2.n}$	3.3	4.5	4.7
3. Adapted flow rates, decreasing fan powers. Decreasing temperature lift.	$COP_{1hps.3.b}$	3.1	4.1	3.2
	$COP_{1hps.3.m}$	3.1	4.9	5.3
	$COP_{1hps.3.n}$	3.3	5.5	7.1

II. HT-HP scale factors in the TRNSYS-CHEST model: [HT-HP] SCALE & SIZE

The scale factors are employed in the case that the HT-HP is working under partial load conditions. They have been evaluated following the approach discussed in the previous point. To do this, values from case 3m (Figure 17 and Table 7) have been used.

Table 8. Values of COP and ratios between actual and nominal COP (COP_100) at different Partial Load Ratios (PLR)

PLR	**1**	**0.8**	**0.6**	**0.5**	**0.3**	**0.2**	**0.1**
COP	3.1	3.6	4.5	4.9	5.5	5.3	4.9
COP/COP_100	1.000	1.161	1.452	1.581	1.774	1.710	1.581

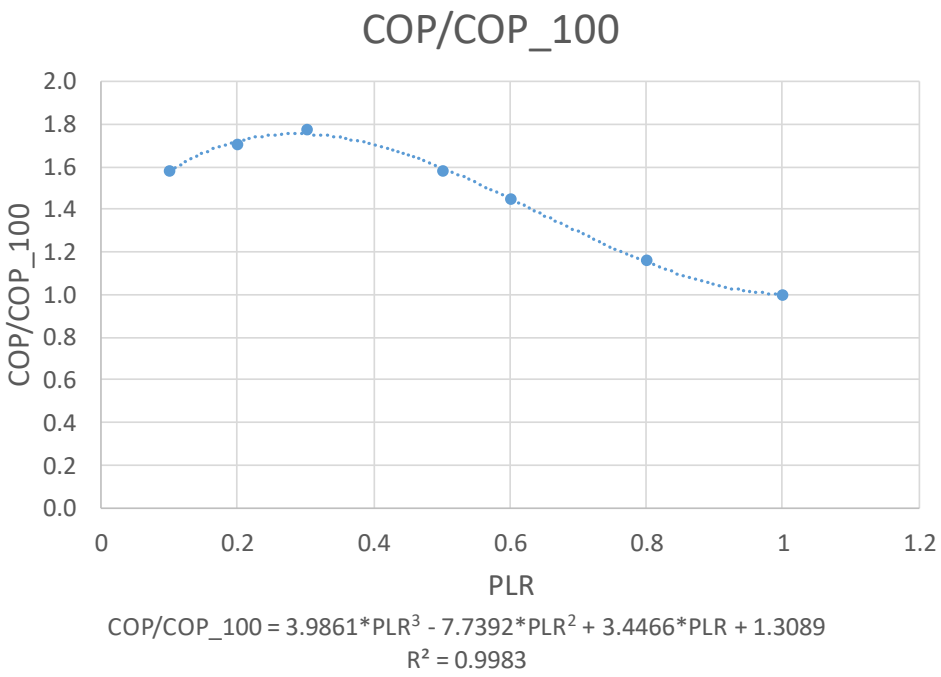

Figure 18. Ratio between actual and nominal COP at different PLR values

In TRNSYS-CHEST model, the Partial Load Ratio (F_PLR_HP) of the HT-HP is calculated as follows:

$$\boldsymbol{F\_PLR\_HP} = \frac{P\_el\_in\_est\_HP}{P\_el\_in\_nom\_HP} \quad \textbf{(10)}$$

The estimated COP of the HT-HP (COP_HP) is obtained as a function of the PLR and the nominal COP:

$$\begin{aligned} \boldsymbol{COP\_HP} &= COP\_nom\_HP * \left[\frac{COP}{COP\_nom\_HP}(PLR)\right] \\ &= COP\_nom\_HP * (3.9861 * F\_PLR\_HP^3 - 7.7392 \\ &* F\_PLR\_HP^2 + 3.4466 * F\_PLR\_HP + 1.3089) \end{aligned} \quad \textbf{(11)}$$

Based on the actual and nominal COP values, the estimated and nominal total heat that should be delivered by the HT-HP are expressed as follows:

$$\boldsymbol{P\_q\_tot\_est\_HP\_MW} = COP\_HP * P\_el\_in\_est\_HP \quad \textbf{(12)}$$

$$\boldsymbol{P\_q\_tot\_nom\_HP\_MW} = COP\_nom\_HP * P\_el\_in\_nom\_HP \quad \textbf{(13)}$$

The scale factor F_q_capacity_PLR_HP is calculated as:

$$\boldsymbol{F\_q\_capacity\_PLR\_HP} = \frac{P\_q\_tot\_est\_HP\_MW}{P\_q\_tot\_nom\_HP\_MW} \quad \textbf{(14)}$$

This is used to scale the other outputs of the HT-HP's performance map.

II. Heat pump sizing factor in the TRNSYS-CHEST model: [HT-HP] SCALE & SIZE

In case the nominal input power of the equipment differs from 1 MWe, a sizing factor (F_size_nom_HP) is applied. As a first approach, this sizing factor will be linearly proportional to the nominal input power of 1 MW.

$$\boldsymbol{F\_size\_nom\_HP} = \frac{P\_el\_in\_nom\_HP}{1\ MW} \quad \textbf{(15)}$$

Thus, considering all the parameters mentioned before, the estimated thermal capacities are:

$$\boldsymbol{P\_q\_lat\_est\_HP\_MW} = F\_size\_nom\_HP * F\_q\_capacity\_PLR\_HP * P\_q\_lat\_nom\_HP \quad \textbf{(16)}$$

$$\boldsymbol{P\_q\_sen\_est\_HP\_MW} = F\_size\_nom\_HP * F\_q\_capacity\_PLR\_HP * P\_q\_sen\_nom\_HP \quad \textbf{(17)}$$

Also, the actual evaporator capacity, considering the mechanical and electrical compressor efficiencies (eta_mech_comp_HP and eta_el_comp_HP) introduced in EES-CHEST model, is calculated in *[HT-HP] SCALE & SIZE,* taking into account the scale and sizing factors explained in this section and also TES control factors that will be explained in Section 2.7.3:

$$\boldsymbol{P\_q\_evap\_HP\_MW} = (P\_q\_sen\_est\_HP + P\_q\_lat\_est\_HP - (P\_el\_in\_est\_HP * eta\_mech\_comp\_HP * eta\_el\_comp\_HP)) * F\_ctrl\_char\_TES \quad \textbf{(18)}$$

c) Organic Rankine Cycle Scaling and Sizing Factors: [ORC] SCALE & SIZE

For the ORC, proportional sizing and scale factors are employed as follows:

$$\boldsymbol{F\_capacity\_PLR\_ORC} = \frac{P\_el\_net\_est\_ORC\_MW}{P\_el\_net\_nom\_ORC} \quad \textbf{(19)}$$

$$\boldsymbol{F\_size\_nom\_ORC} = \frac{P\_el\_net\_nom\_ORC}{1\ MW} \quad \textbf{(20)}$$

$$\boldsymbol{P\_q\_lat\_est\_ORC\_MW} = F\_size\_nom\_ORC * F\_capacity\_PLR\_ORC * P\_q\_lat\_nom\_ORC \quad \textbf{(21)}$$

$$\boldsymbol{P\_q\_sen\_est\_ORC\_MW} = F\_size\_nom\_ORC * F\_capacity\_PLR\_ORC * P\_q\_sen\_nom\_ORC \quad \textbf{(22)}$$

2.7.3. Thermal Energy Storage: [TES] CONTROL

Estimated latent and sensible heats for both the HT-HP and ORC are previously obtained from the scaling and sizing factors mentioned above. However, it is necessary to check the actual state of charge, in each timestep, of the thermal storage system, and also, if the heat demanded by the ORC can be provided by the thermal system. Otherwise, the CHEST system has to either reject the excess heat produced or stop.

In the case of the latent heat storage, the control is done by ensuring that the energy entering the tank at each timestep of the simulation (*step*) is less than the remaining space for energy storage in the tank during the charging (*char*) process; and that the energy leaving the tank at each timestep is less than the total energy stored in it in the discharge (*dchar*). To ensure this the following factors are introduced:

$$\boldsymbol{F\_char\_LHS} = (P\_q\_lat\_est\_HP * step) < (E\_q\_max\_LHS\_MWh - E\_q\_lat\_TES\_MWh) \quad \textbf{(23)}$$

$$\boldsymbol{F\_dchar\_LHS} = (P\_q\_lat\_est\_ORC * step) < E\_q\_lat\_TES\_MWh \quad \textbf{(24)}$$

The variable E_q_lat_TES_MWh is defined in Section 2.8 , and corresponds to the total energy stored in the LHS tank till the current timestep.

To control the sensible heat storage, the level of water of the tanks is checked every timestep. Therefore, in the charge process the cold tank has to have enough available water to provide the demanded mass flow rate during the specified interval of time; and for the discharge, the hot tank has to be full enough to cover the mass flow demand.

$$\boldsymbol{F\_char\_V\_SHS} = (V\_w\_LTWT\_SHS - V\_w\_min\_SHS) > \frac{m\_est\_subc\_HP * step}{Rho\_w} \quad \textbf{(25)}$$

$$\boldsymbol{F\_dchar\_V\_SHS} = (V\_w\_HTWT\_SHS - V\_w\_min\_SHS) > \frac{m\_est\_preh\_ORC * step}{Rho\_w} \quad \textbf{(26)}$$

V_w_LTWT_SHS-V_w_min_SHS corresponds to the total amount of water available in the LTWT till the current time step.

The mass flow rates used for the calculation of these control variables have been obtained using the sensible estimated heats calculated before (P_q_sen_est_HP and P_q_sen_est_ORC), the temperatures of SHS tanks (**T_w_LTWT_SHS_C** and **T_w_HTWT_SHS_C**) and the optimum outlet temperatures from the subcooler and the preheater (**T_w_out_subc_HP_C** and **T_w_out_preh_ORC_C**):

$$\boldsymbol{m\_est\_subc\_HP\_kg\_s} = \frac{P\_q\_sen\_est\_HP}{Cp\_w * (T\_w\_out\_subc\_HP - T\_w\_LTWT\_SHS)} \quad \textbf{(27)}$$

$$\boldsymbol{m\_est\_preh\_ORC\_kg\_s} = \frac{P\_q\_sen\_est\_ORC}{Cp\_w * (T\_w\_HTWT\_SHS - T\_w\_out\_preh\_ORC)} \quad \textbf{(28)}$$

T_w_out_subc_HP_C is always equal to 133 °C, as it corresponds to the water entering in the HTWT and that is the optimum obtained in the EES-CHEST coupled model; and the value of T_w_out_preh_ORC_C, which corresponds with the water entering the LTWT, varies depending on the option (A, B or C) selected.

As E_q_lat_TES_MWh, V_w_LTWT_SHS and V_w_HTWT_SHS change for each timestep, the control variables cannot use the instantaneous value of them but the values from the previous timestep. To achieve that, Type150 (Delayed Inputs Controller) has been used to save the last value of the previous time step during the next one. This approach avoids convergence problems during the simulation.

2.7.4. Control of Temperatures in the SHS Tanks

As the ORC performance map is done for a constant T_w_HTWT_SHS of 133 °C, the temperature of the hot tank cannot be below this value during the discharge process. Otherwise the output obtained in the ORC Map would be incorrect. Hereby, the following control has been made:

$$\boldsymbol{SF\_T\_dchar\_HTWT} = (T\_w\_HTWT\_SHS > 130) \quad \textbf{(29)}$$

2.7.5. Outputs Obtained from Control Variables

The control strategy allows the functioning of the HT-HP as long as one of the storage systems (LHS or SHS) is not full yet and is able to store more energy, rejecting extra sensible or latent heat when one system is filled before the other. On the other hand, the ORC will stop when one of the storage systems is empty.

Depending on the temperature conditions in the source and the sink, an imbalance may appear between the ratios of sensible and latent heat for charge and discharge, meaning that, if the system is stopped when one of the storage tanks is full or empty, after a certain number of cycles, one of the TES tanks may be full and the other be empty[16]. If this happens, the CHEST system would be blocked, as it would not be capable of charging or discharging energy. This is the reason why the control strategy allows the charging of the CHEST system until both the LHS and SHS are full and, in case one system charges before the other, an extra heat exchanger is activated to reject the excess heat.

The latent heat entering or leaving the LHS system is calculated as the summation of latent heat inlet during the charging process (positive) and the latent heat leaving the LHS during discharging (negative):

[16] The systems may not be completely full or empty, but they do not have sufficient capacity to charge or discharge during the next timestep.

$$\boldsymbol{P\_q\_lat\_TES\_MW} = P\_q\_lat\_est\_HP * F\_char\_LHS - P\_q\_lat\_est\_ORC * F\_dchar\_V\_SHS * F\_dchar\_LHS * SF\_T\_dchar\_HTWT \quad \textbf{(30)}$$

As explained above, the charging process will allow both TES systems to charge completely, so the charging is only controlled by the variable F_char_LHS. However, the discharging has more constraints, as it not only has to have remaining energy in the LHS (F_dchar_LHS), it also needs the SHS to keep functioning (F_dchar_V_SHS) at a proper temperature for the HTWT (SF_T_dchar_HTWT).

Following the same criteria, the sensible heat charged or discharged is calculated as follows:

$$\boldsymbol{P\_q\_sen\_char\_TES\_MW} = P\_q\_sen\_est\_HP * F\_char\_V\_SHS \quad \textbf{(31)}$$

$$\boldsymbol{P\_q\_sen\_dchar\_TES\_MW} = P\_q\_sen\_est\_ORC * F\_dchar\_V\_SHS * F\_dchar\_LHS * SF\_T\_dchar\_HTWT \quad \textbf{(32)}$$

Finally, as the power employed to drive the different components of the CHEST system is not limited by the volume and temperature control variables, a calculation of the actual useful power is done in order to evaluate the performance of the system.

$$\boldsymbol{P\_el\_in\_HP\_MW} = P\_el\_in\_est\_HP * F\_ctrl\_char\_TES \quad \textbf{(33)}$$

$$\boldsymbol{P\_el\_net\_ORC} = P\_el\_net\_est\_ORC * F\_dchar\_V\_SHS * F\_dchar\_LHS * SF\_T\_dchar\_HTWT \quad \textbf{(34)}$$

To control the input power to the HT-HP, the variable F_ctrl_char_TES is used:

$$\boldsymbol{F\_ctrl\_char\_TES} = (F\_char\_LHS + F\_char\_V\_SHS) > 0 \quad \textbf{(35)}$$

This variable is 1 when at least one of the storage systems can be charged and 0 if both are full.

2.8. LATENT HEAT STORAGE SYSTEM (LHS)

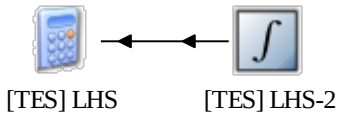

Figure 19. LHS module in the TRNSYS-CHEST model

The Latent Heat Storage (LHS) system consists of a tank filled with a Phase Change Material (PCM) able to store energy in the form of latent heat. The PCM chosen for this model is $LiNO_3$-KNO_3 with a melting temperature (**T_melt_PCM_C**) of 133 °C.

During the charge the tank is heated up and the PCM changes from solid to liquid state and, in the discharge, it is cooled down and is solidified. Depending on the input and output heats, the percentage of PCM in liquid state inside the tank varies.

In order to simplify the implementation of the LHS in the TRNSYS-CHEST model, the following assumptions have been made:

- Solidification and melting temperatures are always constant and equal to 133 °C.
- No temperature glide during the phase change.
- The PCM is constantly in phase change. That is, once 100% of it is in liquid state, the system cannot store more energy. So, any latent heat delivered from the HT-HP will be rejected, preventing the PCM from increasing its temperature. On the other hand, if the tank is 100% solid (no energy is stored in it), the ORC will stop, preventing it from decreasing its temperature.

Thus, as can be seen in Figure 19, the implementation of the LHS in the model will be done using an integrator and the calculator *[TES] LHS*. The input of the LHS system will be the variable **P_q_lat_TES_MW** (Eq. (30)), previously calculated in *[TES] CONTROL*, which includes the heat delivered by the HT-HP and rejected to the ORC and the control variables for the tank volumes and temperatures.

P_q_lat_TES_MW is integrated to obtain the energy stored in the PCM tank at each timestep (**E_q_lat_TES_MWh**)**.** This energy is measured in MWh and will go from zero to the maximum tank capacity (**E_q_max_LHS_MWh**), whose value can be set in *CONTROL CARDS*.

The Level of Charge (LoC) of the LHS is calculated as:

$$\boldsymbol{F\_LoC\_LHS} = \frac{E\_q\_lat\_TES\_MWh}{E\_q\_max\_LHS\_MWh} \quad \textbf{(36)}$$

The physical meaning of **F_LoC_LHS** is the quantity of PCM which is in liquid state. When **F_LoC_LHS**=0, the PCM is in solid state and energy cannot be withdrawn from it; and when it equals 1, the PCM is completely liquid and it cannot store more energy, so any further heat entering the system is rejected (excess heat). This amount of latent excess heat is calculated as:

$$P\_q\_lat\_excess\_HP\_MW = P\_q\_lat\_est\_HP * F\_char\_V\_SHS * (1 - F\_char\_LHS) \quad \textbf{(37)}$$

This variable activates when the LHS system is full but the SHS is not, so it allows the HT-HP to work until both storage systems are full. Then, in the final results, the value of the total latent excess heat is represented.

2.9. SENSIBLE HEAT STORAGE SYSTEM (SHS)

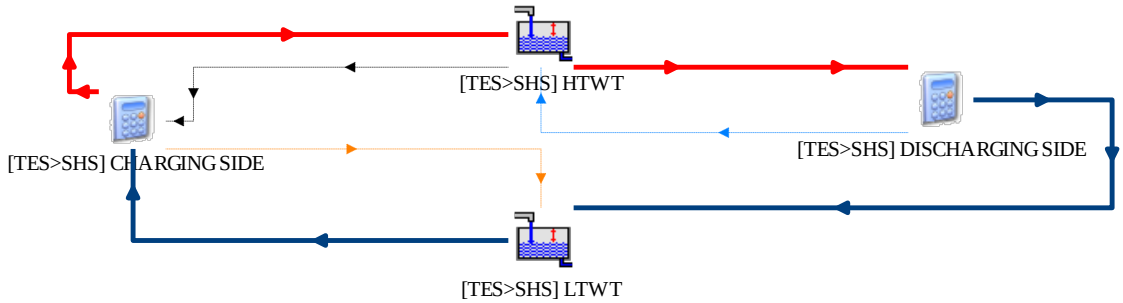

Figure 20. SHS system of the TRNSYS-CHEST model

In order to simulate the sensible heat storage system two variable volume tanks (Type 39) are used along with two calculators (simulating the subcooler in the HT-HP and the preheater in the ORC). During the charging, the water goes from the cold tank (LTWT) through the subcooler (*[TES>SHS] CHARGING SIDE* calculator) to the hot one (HTWT) and it is heated up using the sensible heat obtained from the HT-HP map. In the discharge, hot water goes to the preheater (*[TES>SHS] DISCHARGING SIDE* calculator) where it is cooled down and stored in the cold tank.

The inputs introduced to the SHS system are the ones calculated in *SCALE & SIZE* and *[TES] CONTROL*:

- **P_q_sen_char_TES_MW**: Heat entering the system considering the control variables related to tank volumes and temperatures (Eq. (31)).
- **P_q_sen_dchar_TES_MW**: Heat leaving the system considering the control variables related to the tank volumes and temperatures (Eq. (32)).

2.9.1. Variable Volume Water Tank (Type 39): Tanks Parameters

Variable volume tanks have been employed to simulate the state of the tanks in each timestep. Type 39 has been selected for this task, as it allows different mass flow rates entering and exiting the tank. In this model the user can introduce the desired volume of the tank, and the other required parameters are calculated as a function of this input and the ratio between the diameter and height of the tank (currently set to 1/1.5) in the calculator *[TES>SHS] TANKS PARAMETERS*. Thus, the parameters required by the type are [7][8]:

Table 9. Parameters of Type 39 (variable volume storage tank)

Parameter	Description
V_w_SHS_m3	Total volume of the water tank. Same for both hot and cold
Circ_SHS_m	Circumference of the tank
A_cross_SHS_m2	Cross sectional area of the tanks
V_w_max_SHS_m3	Maximum volume of water that the tanks can store
V_w_min_SHS_m3	Minimum volume of water that the tanks can store
V_w_init_HTWT_SHS_m3	Initial volume of the hot tank at the beginning of the simulation
V_w_init_LTWT_SHS_m3	Initial volume of the cold tank at the beginning of the simulation
T_init_SHS_C	Initial temperature of the water contained in the tanks at the beginning of the simulation
U_wetted _kJ_hm2K	Loss coefficient for the part of the tank in contact with the fluid
U_dry_kJ_hm2K	Loss coefficient for the part of the tank in contact with the air

To calculate the minimum and maximum volumes of water contained in the tank, it is important to notice that Type 39 does not allow the tank to be completely empty, so the minimum volume is set to the 0.1% of the total volume of the tank. The maximum volume allowed is the total volume of the tank.

The initial volumes of the tanks are calculated to have the minimum level of water in the hot tank and the maximum in the cold one. At the beginning of the simulation, the CHEST system will not start working until there is a surplus electricity that drives the HT-HP, so the hot tank of the SHS and the PCM tank of the LHS need to be nearly empty to have enough storage capacity.

The inputs and outputs of Type 39 employed in this model are listed below [20]:

Table 10. Inputs and outputs of Type 39 (variable volume storage tank)

	Type 39 variable	TRNSYS variable name[17]	Units	Description
INPUTS	Inlet Temperatures	**T_w_out_subc_HP / T_w_out_preh_ORC**	C	Temperature of the flow entering the tanks
	Inlet flow rates	**m_w_subc_HP / m_w_preh_ORC**	kg/h	Mass flow rate entering the tanks
	Flow rate to load	**m_w_dem_preh_ORC/ m_w_dem_subc_HP**	kg/h	Mass flow rate that exits the tank
OUTPUTS	Fluid temperatures	**T_w_HTWT_SHS/ T_w_LTWT_SHS**	C	Temperature of the liquid contained inside the tank
	Load flow rate	**m_w_out_HTWT_SHS/ m_w_out_LTWT_SHS**	kg/h	Mass flow rate exiting the tanks. Usually is the same as the input "flow rate to load" but may differ from it if as a consequence of the current volume of water in the tank
	Fluid volume	**V_w_HTWT_SHS/ V_w_LTWT_SHS**	m^3	Amount of water in the tanks

[17] The first variable corresponds to inputs or outputs of the HTWT and the second one with inputs or outputs of LTWT.

Type 39 does not consider the thermal stratification inside the tank, so the whole volume is at the same temperature.

2.9.2. Heat Losses to the Environment

In the current study, as no losses have been considered in LHS system, the SHS tanks have also been considered to be adiabatic. So, the parameters **U_wetted _kJ_hm2K** and **U_dry _kJ_hm2K** from Table 9 are set to 0.

2.9.3. Charging Process of SHS

When there is an excess of electricity, the heat pump is activated to store energy in the tanks. For the SHS, the sensible heat **P_q_sen_char_TES_MW** (Eq. (31)), previously scaled and controlled, the optimum outlet temperature the water has to reach in the subcooler (**T_w_out_subc_HP_C**) and the current temperature of the cold tank (**T_w_LTWT_SHS_C**) are used to calculate the demanded mass flow rate in the subcooler (**m_w_dem_subc_HP**).

$$\boldsymbol{m\_w\_dem\_subc\_HP} = \frac{P\_q\_sen\_char\_TES}{Cp\_w * (T\_w\_out\_subc\_HP - T\_w\_LTWT\_SHS)} \quad \textbf{(38)}$$

In the charging process the value of **T_w_out_subc_HP_C** is always equal to 133°C.

The variable **m_w_dem_subc_HP** is connected to the input "Flow rate to load" of the cold tank, as it is the desired mass flow to exit that tank. After that, the output "Load flow rate" of the cold tank is connected to the variable **m_w_subc_HP_kg_h** and this variable is the one employed for the rest of the calculations. This is done as a control strategy, because, as it was mentioned before, if there is not enough water in the tank to cover the mass flow rate demand, the outlet flow rate may be lower than that the demanded one. The, m_w_subc_HP_kg_h and T_w_out_subc_HP_C are connected as inputs to the hot tank.

Finally, the sensible excess heat is obtained as:

$$\boldsymbol{P\_q\_sen\_excess\_HP\_MW} = P\_q\_sen\_est\_HP * F\_char\_LHS * (1 - F\_char\_V\_SHS) \quad \textbf{(39)}$$

This variable activates when the SHS system is full and it allows the system to keep working to fill the LHS. By doing this, a complete charge of both the LHS and SHS can be achieved. Then, in the final results, the value of the total excess sensible energy is presented.

2.9.4. Discharging Process of SHS

The discharge process is similar to the charge one. When there is a demand of electricity, the ORC starts to work and the water contained in the hot tank is circulated inside the preheater to give energy to the refrigerant. The inputs in this case are the sensible heat **P_q_sen_dchar_TES_MW**, the optimum outlet temperature from the preheater

(**T_w_out_preh_ORC_C**) and the current temperature in the hot tank (**T_w_HTWT_SHS_C**). Thus, **m_w_dem_preh_HP** is calculated as follows:

$$\boldsymbol{m\_w\_dem\_preh\_HP} = \frac{P\_q\_sen\_dchar\_TES}{Cp\_w * (T\_w\_HTWT\_SHS - T\_w\_out\_preh\_ORC)} \quad \textbf{(40)}$$

In this case the value of **T_w_out_preh_ORC_C** will vary depending on the Option A, B or C that has been selected:

- Option A: Optimum temperature is obtained by means of the correlation in the coupled model
- Option B: Optimum temperature is set by the user
- Option C: Optimum temperature obtained from the ORC's performance map based on the assumption of saturated liquid at the outlet of preheater.

Similarly to the charging case, the demanded mass flow rate (**m_w_dem_preh_ORC**) is connected to the input "Flow rate to load" of the hot tank because that is the flow rate that has to leave the tank. Then, the output "Load flow rate" of the hot tank is connected to the variable **m_w_preh_ORC_kg_h** and this variable is the one used for calculations.

2.9.5. State of Sensible Heat Storage

The **F_LoC_SHS** variable has been introduced to calculate the state of charge of the SHS system. Actually, it refers to the state of the hot tank, as it is the one which is actually storing the energy, in terms of sensible heat.

F_LoC_SHS is defined as the level of charge of the HTWT, that is, the ratio the total amount of water available in the current timestep and the maximum amount of water that can be stored in the hot tank and used for the discharge. Thus, its value is between 0 and 1:

$$\boldsymbol{F\_LoC\_SHS} = \frac{V\_w\_HTWT\_SHS - V\_w\_min\_SHS}{V\_w\_max\_SHS - 2 * V\_w\_min\_SHS} \quad \textbf{(41)}$$

V_w_max_SHS-2*V_w_min_SHS corresponds with the total useful amount of water the SHS tanks can store, as both tanks always require a minimum level of water.

3. RESULTS AND DISCUSSION

In this section first studies carried out with the TRNSYS-CHEST model are presented. So far, no facility with the characteristics of this CHEST system has been developed, so the experimental validation of this model remains to be done. However, a preliminary verification of it is done so as to verify the fulfillment of the energy balances and the evolution of the different variables of the system.

Then, a comparison of the working modes suggested along the project (Figure 8) is performed to study their suitability for electricity production.

Later, Options A, B and C for the optimization of T_LTWT are analyzed to determine their efficiency and technical feasibility. For Option B, a parametric study varying the temperature among the values obtained in A and C is done.

Finally, a possibility for the implementation of a CHEST system in the Spanish electrical grid is presented along with a techno-economic analysis for two different possibilities.

3.1. MODEL VERIFICATION: ONE WEEK SIMULATION

In order to make a first verification to ensure that the results obtained in the model are consistent, a period of one week (168 h) is simulated using a timestep of one hour. The option selected for the optimization of the water preheater's outlet temperature is A (correlation using the coupled model, Eq. (2)) and the evaporator and condenser temperatures correspond to the working Mode 1 (T_w_in_evap_HP= 80 °C and T_w_in_cond_ORC= 40 °C) with a water temperature difference for both heat exchangers of 4 K.

3.1.1. Inputs and Sizing Data

a) Sizing Data for the Equipment

The nominal power of the equipment (HT-HP and ORC) was set to 1 MW for this first simulation, so no sizing factors will be needed. On the other hand, the capacities of the TES systems are fixed to values of 23 MWh for LHS system and 400 m^3 for SHS in order to allow a discharge time of 6h. The discharge time was set to 6h as it is in the range of the discharge times used in TES systems of concentrated solar power plants, which use similar storage techniques [21].The sizing criterion chosen is "discharge time" because during charge the state of charge of the TES systems is balanced thanks to the excess heat produced, so both systems can be completely full at the end of the charging process, however, for discharge, state of charge cannot be compensated in case the systems do not empty at the same time. To size the LHS and SHS systems, the values of latent heat and mass flow rate in the preheater during discharge are assessed.

b) Data for Generated and Demanded Power

In this first verification, an artificial power profile with a surplus-deficit day cycle is utilized for the analysis of the performance of the system (Figure 21). The goal of this profile is to recreate

a series of complete charge and discharge cycles to ensure that the TRNSYS-CHEST model behaves as expected. The details of this input profile are as follows:

- **Surplus cycle:** 12 hours with 3 MW of power generated by RES (P_el_out_RES_MW) and 1 MW of demanded power (P_el_dem_MW). During this period the demand is covered by the bypassed power from RES generation and 2 MW of surplus are available to be used to charge the CHEST system.

- **Deficit cycle:** the charging cycle is followed by another 12 hours with 1 MW of power generation (P_el_out_RES_MW) and 3 MW of demanded power (P_el_dem_MW). In this occasion the power generated is completely bypassed and there is no power left for storage. The 2 MW that cannot be covered by the RES generation should be provided to the CHEST system.

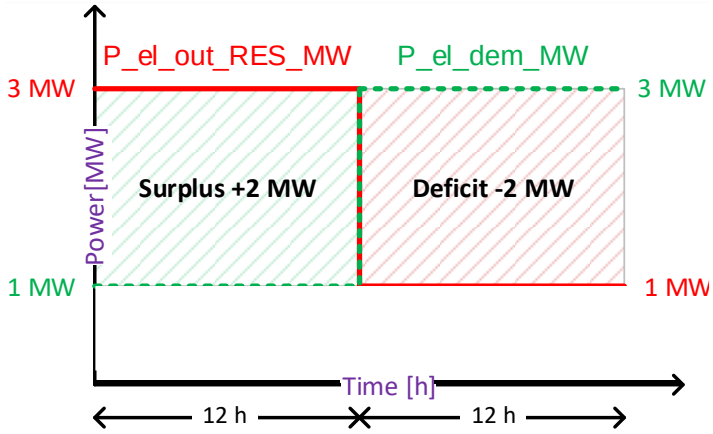

Figure 21. Daily pattern of the power profile

3.1.2. Power and Temperature Analysis

Two plots are implemented in the TRNSYS-CHEST model to see the evolution of the power entering and leaving the system and the temperatures along the time of the simulation. In Figure 22 the RES generation (P_el_out_RES) is plotted along with the estimated power entering the HT-HP (P_el_in_est_HP) and the actual power useful for the HT-HP (P_el_in_HP). Bypassed power is also plotted, but, as it always equals to 1, it is not clear enough in the figure. It can be seen that, even if the remaining power (after bypass) is 2 MW, the estimated power to be used by the HT-HP is only 1 MW, as that is the nominal power for the equipment, so it cannot use more than that. While the signal of the estimated power has the same duration as the RES generation power, actual power employed by the system lasts less. This is due to the fact that this variable (P_el_in_HP) is the one that takes into account the control factors related to TES state of charge and temperatures. Then, as the charging process is to stop when both storage systems are full, its duration is limited by their size. It should be noted that the first charging process is of 11 hours and the others are of 9 hours.

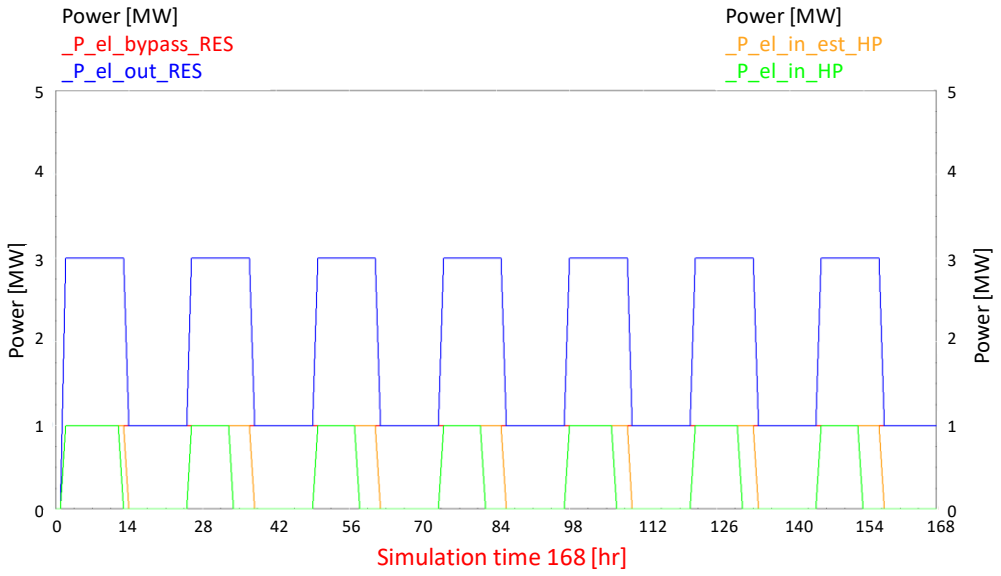

Figure 22 . Power generated by RES and consumed by the HT-HP during charging processes (within one week of simulation)

Figure 23 illustrates the power demanded (P_el_dem), the estimated (P_el_est_ORC) and actual net power that is provided by the ORC cycle (P_el_net_ORC) of the CHEST system. As for the charging case, bypassed power is equal to 1 MW. Regarding the 2 MW deficit, only a maximum of 1 MW could be covered by the CHEST system, as its nominal net output power is 1 MW. As it was mentioned before, the estimated power is the one that the equipment could potentially give; while, the actual one considers the TES sizing and temperature restriction. So, the discharging cycle comes into action until one of the storage systems becomes empty. In this occasion all the discharge cycles have the same duration (6 hours).

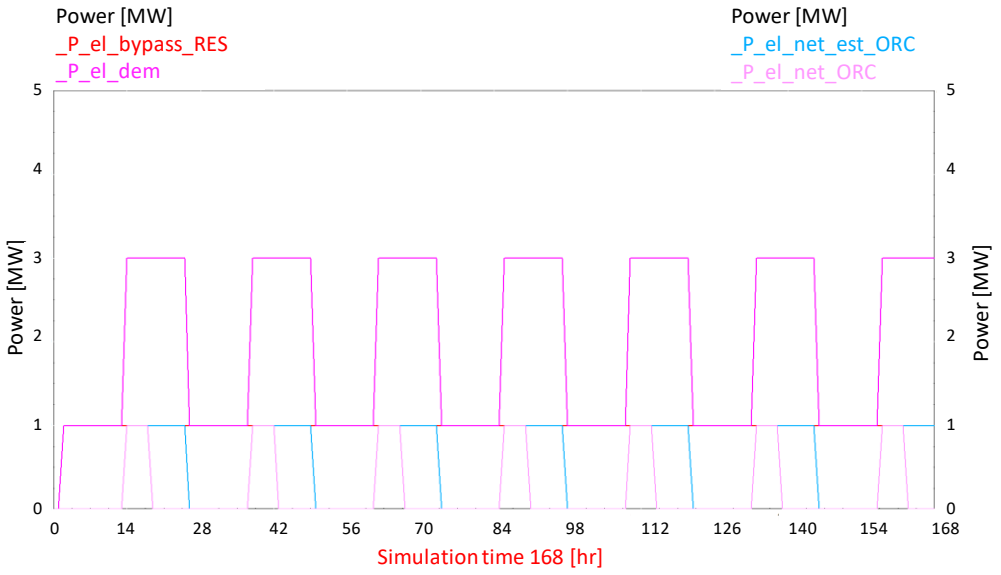

Figure 23 . Power demanded and provided by the ORC during discharging process (within one week of simulation)

Figure 24 depicts the evolution of different temperature profiles during simulation. As evaporator (T_w_in_evap) and condenser (T_w_in_cond) inlet water temperatures were set in *CONTROL CARDS*, their values remain the same during the simulation. The melting temperature

of the PCM is also plotted and, according to the assumptions made for the model, it has to be constant and equal to 133°C. Moreover, the temperatures of the water contained in the hot (T_HTWT) and cold (T_LTWT) tanks are also represented. The water contained in SHS tanks is initially at ambient temperature (25 °C). In the first charge the hot tank is nearly empty, as it is filled with water coming from the hot tank. However, the water enters the hot tank is firstly heated up to 133 °C in the subcooler of the HT-HP. It reaches this optimum temperature in 6h, when the first charging cycle is completed. Then, in the first discharging cycle, the cold tank is filled with water coming from the hot tank passing through the ORC's preheater. The water enters the cold tank at the optimum outlet temperature (specified according to the option selected for calculating the T_LTWT). It reaches that value at the end of the cycle, after 18 hours. For Option A and Mode 1 the value of the optimum outlet temperature from the preheater is 75.98 °C. As the SHS is considered to be adiabatic, no heat loss to the ambient, the temperatures of the cold and hot tanks remain constant during the rest of the simulation.

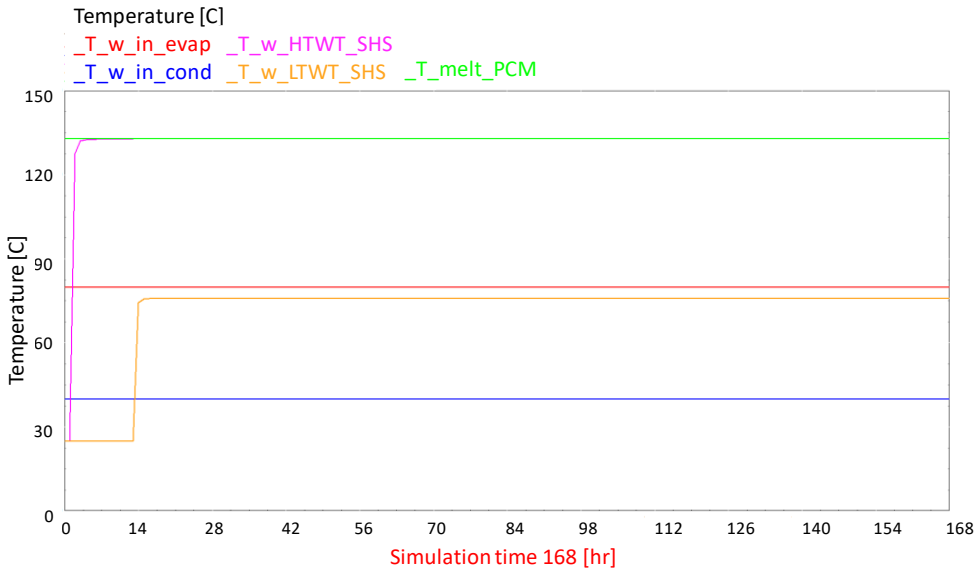

Figure 24 . Different temperature profiles for one week simulation

3.1.3. Thermal Energy Storage Systems Analysis

Three plots are introduced to evaluate the state of the thermal storage system at every timestep. In the first plot (Figure 25), the latent (P_q_lat_TES) and sensible (P_q_sen_TES) heat stored (positive values), during charging, or extracted (negative values), in the discharging, are represented along with the level of charge (LoC) of the systems. It can be observed that the ratio between sensible and latent heat is different in the first charging cycle compared with the successive cycles. This occurs because the relationship between these two factors (P_q_sen_TES and P_q_lat_TES) is influenced by the working conditions of the equipment (in this case, the HT-HP). Thus, the sensible and latent heat produced depend on the working point selected from the HT-HP's map, which, in turn, depends on the values of the independent variables. In this case, as the temperature of the cold tank is an input of the map, the value of this variable for the first charge is 25°C, as the tank is initially at ambient temperature. Then, for the rest of the charges that take place, the water of the cold tank is at the optimum temperature obtained in

the discharge process (≈76°C in this case), so the working point selected in the HT-HP map is different compared with the initial one. Also, it can be noticed that in the initial of the charging process the LHS became full before the SHS, then, latent excess heat is expected to be found. In the rest of charges, the difference between sensible and latent systems is less visible. The reason for this is that in option A the coupled model is taken as a reference, so, all the energy charged is expected to be discharged, so the ratios of sensible and latent heat for charge and discharge are similar. However, small amounts of excess heat may appear during the simulation for example due to the interpolation processes within the performance maps or the unproper sizing of the TES systems.

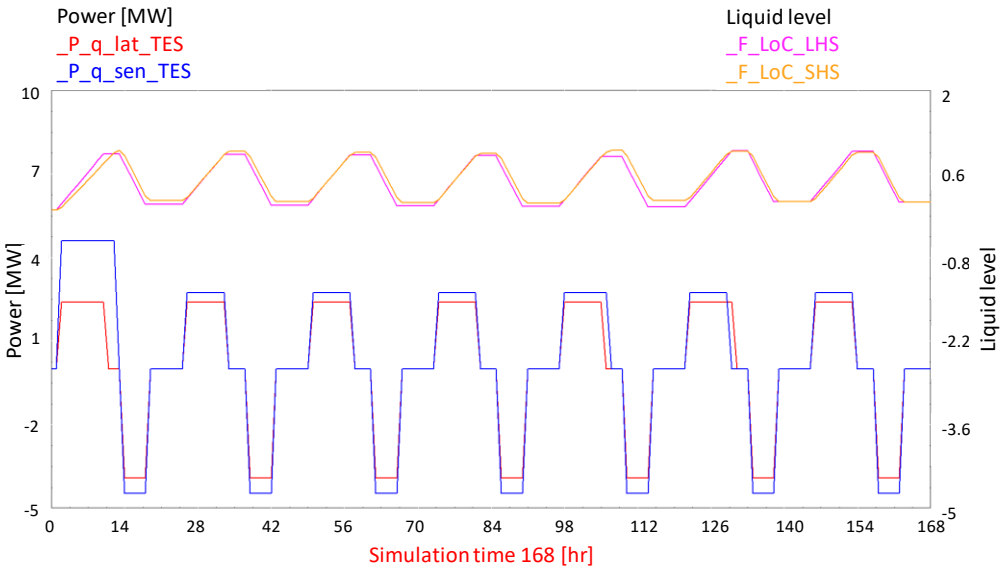

Figure 25 . Latent and sensible heat transferred to or extracted from the TES systems and level of charge (within one week of simulation)

The second plot (Figure 26) represents the latent thermal energy exchanged with the PCM tank (E_q_lat_TES) and the energy stored in it at each timestep. It is worth noting that the control variables make the maximum value of energy stored lower than the specified maximum capacity of the LHS tank (23 MWh), so the maximum energy stored during this simulation is 22.81 MWh. In this manner it can be ensured that the PCM is not changing its temperature and that the assumptions made in Section 2.8 are fulfilled. Also, it can be observed that during the first charging cycle, the variable P_q_lat_TES shows that the LHS tank is full by hour 9 even though the charging cycle lasts 11 hours. This implies that the excess latent heat (after hour 9) is rejected from the CHEST system to allow the proper operating of the HT-HP to continue charging the SHS system.

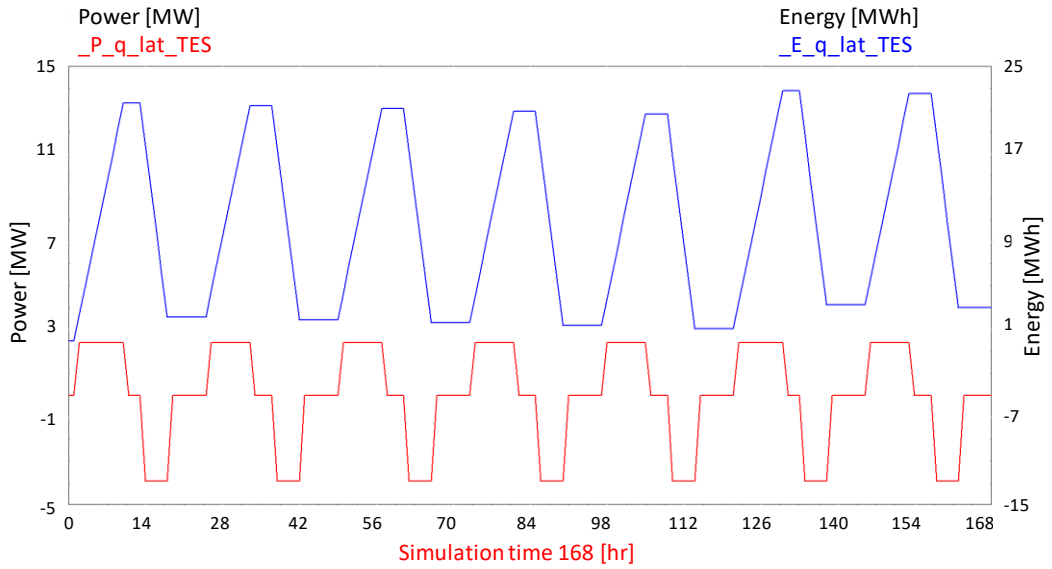

Figure 26 . Latent heat and energy stored in LHS system (within one week of simulation)

The final plot (Figure 27) depicts the evolution and behavior of SHS system. At the beginning of the simulation the hot tank (HTWT) is empty and the cold one (LTWT) is full. So, in each charging cycle the water level rises in the HTWT tank and declines in the LTWT tank in an oscillating curve; and, for the discharging cycles is the other way around. Mass flow rates were checked to ensure that the time of charge/discharge mentioned above (Figure 22 and Figure 23) match with the time needed to fill or empty the tanks (Table 11).

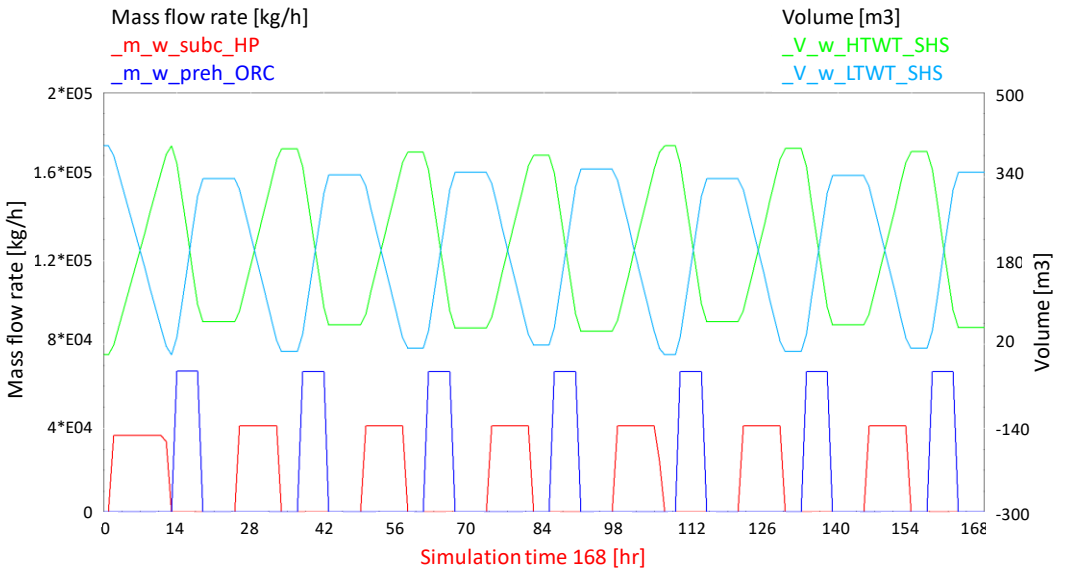

Figure 27 . Mass flow rates and water volumes inside the SHS system (within one week of simulation)

Table 11 . Charging and discharging times for SHS system (within one week of simulation)

	Mass Flow Rate [kg/h]	Volume [m^3]	Time [h]
First Charging cycle	36537	400	11
Next Charging cycles	41213	400	9
Discharging cycles	69139	400	6

3.1.4. Excess Energy Analysis

Excess sensible and latent heat is plotted alongside the level of charge of the systems in Figure 28. As it was expected, the working conditions of the first charging cycle resulted to an excess of latent heat. In Figure 26 it can be seen that the LHS fills in 9 hours, however, the complete charging process lasts 11 hours. Figure 28 shows that there is excess latent heat (P_q_lat_excess) from the 9^{th} hour of the simulation to the 11^{th} hour. Then, in the following cycles both LHS and SHS systems charge at the same time and there is no excess heat produced; but when the system is a bit unbalanced, excess sensible or latent heat is likely to appear, like in the charging cycles 5 and 6.

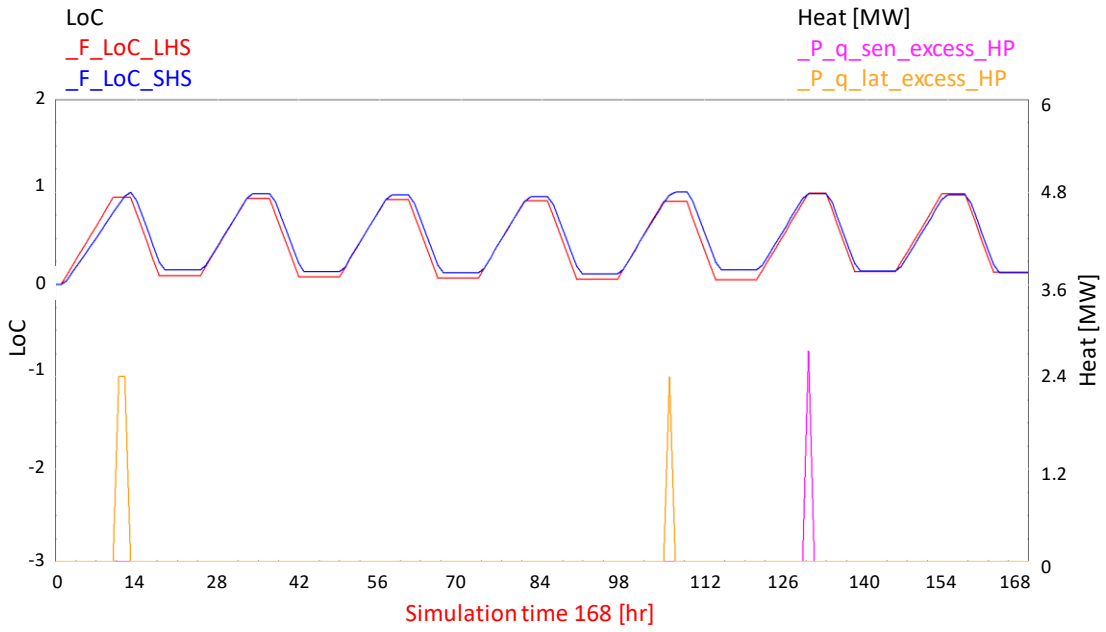

Figure 28 . Excess sensible and latent heat of TES systems (within one week of simulation)

3.1.5. Energy Balance Analysis

Results for the complete simulation are obtained in order to check the performance of the system. In Figure 29 the RES energy production is divided into different terms. First, when there is electricity demand and RES production at the same time, the energy is bypassed, and the surplus energy is the remaining one for the functioning of the HT-HP. However, not all this surplus is finally used by the HT-HP: some of it cannot be used due to the size of the equipment (for example, if the surplus is of 2MW and the nominal power of the HT-HP is 1MW, there is 1MW that cannot be used because the capacity of the HT-HP is not large enough). This is

represented by the variable E_el_ex_RES_size_HP. On the other hand, when the TES system is full, HT-HP cannot work anymore even if there is still surplus of energy. This non-used energy is expressed by the variable E_el_ex_RES_size_TES. In this case 50% of the RES production is directly bypassed, 18% is employed to drive the HT-HP and 32% cannot be used for the CHEST system (sum of variables E_el_ex_RES_size_HP and E_el_exRES_size_TES).

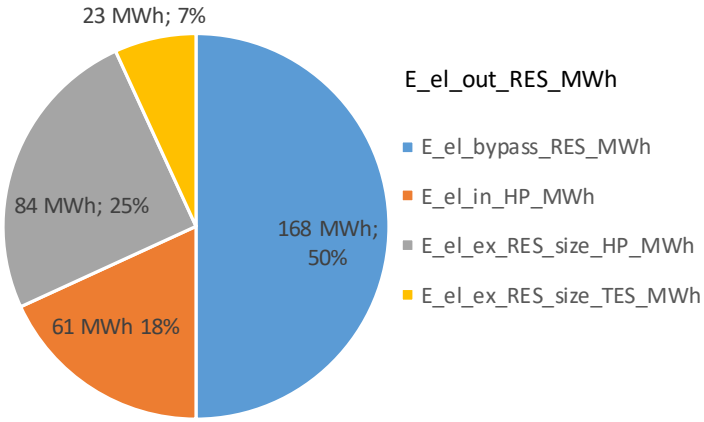

Figure 29. Energy balance of RES generation for one-week simulation.

In Figure 30 the total electrical demand (E_el_dem) is split into the part of it covered by bypassed energy (E_el_bypass_RES), the energy produced by means of the ORC (E_el_net_ORC) and the part of the demand that cannot be covered by the systems aforementioned and that will have to be supplied by the grid or some other external system (E_el_def_tot_dem). In this simulation 50% of the demand is covered using bypassed energy, 10% is covered by the ORC and 40% of it remains uncovered.

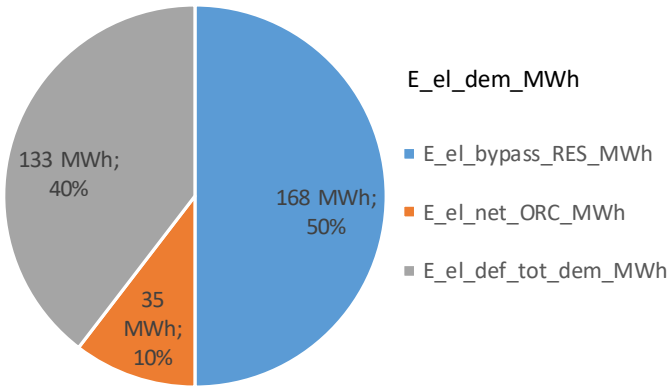

Figure 30. Energy balance of demanded energy for one-week simulation.

Last results obtained are presented in Table 12, which collects the seasonal roundtrip efficiency obtained for the whole time of the simulation (Eta_roundtrip_CHEST) and the amount of latent (E_q_lat_excess_HP) and sensible (E_q_sen_excess_HP) excess heat that is produced.

Table 12 . Seasonal roundtrip efficiency and excess latent and sensible heats (in MWh) for one-week simulation

Eta_roundtrip_CHEST	E_q_lat_excess_HP_MWh	E_q_sen_excess_HP_MWh
0.57	7.23	2.74

3.2. COMPARATIVE OF THE DIFFERENT WORKING MODES

After the model verification, the next step carried out is to study different working modes proposed within the CHESTER project (depicted in Figure 8). To do so, the CHEST system is simulated for a period of one year using a timestep of one hour. Option A is selected for the optimization of the parameter T_LTWT, the water temperature differences for source and sink (DT_w_evap_HP and DT_w_cond_ORC) are set to 4 K, the nominal power of both HT-HP and ORC are set to 1 MW and the power profile explained in Sub-section 3.1.1 was used. Regarding the sizes of the LHS and SHS systems, they are chosen so as to adjust the state of charge of both latent and sensible system as much as possible and to allow the discharge of both systems in a period of 6h, except for Modes 5 and 6. These two modes have, respectively, discharge times of 3h and 2.5h because the difference in sensible to latent heat produced during charge and needed for discharge is really large and, to be able to discharge during 6h, they need charging periods larger than 12 h, which is the maximum time available in the file used.

The objective of this section is to determine which one of the six proposed working modes is the most suitable one for a scenario of electricity production. The main parameters for this assessment are the roundtrip efficiency and the working temperatures of the CHEST system.

Table 13 shows the inputs introduced and the results obtained for each working mode. It can be observed that the best performance (Eta_roundtrip) is achieved by Modes 2, 3 and 4. So, these options are the ones with more capacity of providing electrical energy to the system. The other modes are more suitable for heating purposes (for instance, if there is integration of the CHEST system with a DH network) or for a mix of electricity and heat delivery.

Among Modes 2, 3 and 4, Mode 2 is the one that allows for more electricity production by means of the ORC (1882 MWh) followed by Mode 3 (1869 MWh). Moreover, Mode 2 is the one that requires lower amount of heat source (E_q_evap_HP), as its temperature (T_w_in_evap) is 20 K lower than in Modes 3 and 4. Also, the optimum temperature of the LTWT is lower for Modes 2 and 4 than for Mode 3, which, in reality, will lead to lower energy losses to the environment. For these reasons Mode 2 is seen as the most suitable one for electricity purposes, as it is the most efficient with an energy source temperature lower than the other options available.

Finally, it should be mentioned the behavior of the excess heat for each one of the modes. As this simulation is done using Option A for the optimization of T_LTWT, which is the alternative that makes use of the coupled model of the CHEST system, the ratios obtained of sensible and latent heat in the performance maps for HT-HP and ORC are supposed to be very similar. However, due to the interpolation made inside the maps, unbalances may be produced with respect to the level of charge of the storage tanks and, subsequently, excess heat appears.

Table 13. Simulation results after one year for different working modes.

		Mode 1	Mode 2	Mode 3	Mode 4	Mode 5	Mode 6
INPUTS	T_w_in_evap (°C)	80.0	80.0	100.0	100.0	60.0	40.0
	T_w_in_cond (°C)	40.0	10.0	40.0	10.0	60.0	60.0
	Capacity LHS (MWh)	23.5	15.0	24.0	15.0	18	15.0
	Capacity SHS (m^3)	400.0	230.0	400.0	230.0	325.0	260.0
OUTPUTS	T_opt_LTWT (°C)	76.0	52.0	75.6	51.9	91.1	89.7
	E_el_in_HP (MWh)	3058.0	1893.0	2103.0	1212	2660.0	3461.0
	E_el_net_ORC (MWh)	1835.0	1882.0	1869.0	1807	763.0	730.0
	Eta_roundtrip (-)	0.6	0.99	0.9	1.5	0.3	0.2
	E_q_lat_excess (MWh)	197.6	2.4	353.4	36.4	22.4	130.0
	E_q_sen_excess (MWh)	76.8	32.8	216.4	0.0	0.0	57.2
	E_q_evap_HP (MWh)	12898.3	9692.7	14456.5	9961.9	6129.0	5223.6

3.3. COMPARATIVE OF THE OPTIONS FOR T_OPT_LTWT FOR WORKING MODE 2

In this section a comparative analysis of the three different options to optimize the variable T_LTWT is done. As it was previously explained, this variable determines the outlet water temperature of the preheater of the ORC cycle, which can be obtained from the optimum value of the coupled model (Option A), introduced by the user (Option B) or derived from the extra condition, fixed in the EES model, of having saturated liquid at the outlet of the preheater (Option C).

To perform this analysis the system is simulated under the same conditions as in the previous section, besides, using the power profile indicated in Sub-section 3.1.1. Regarding the size of the TES systems, this is done allowing 6 hours of discharge time.

In this study only Mode 2 (T_w_in_evap_HP= 80 °C and T_w_in_cond_ORC= 10 °C) is adopted, as the main objective of this section is to focus on the differences among the T_LTWT options.

Mode 2 is selected because it is the most promising one compared with others, based on the conclusions from the previous section.

3.3.1. Parametric study for Option B

Firstly, a parametric study was developed in order to determine which is the best temperature that can be set by the user in Option B. This option uses, as in Option A, the ORC map with no restriction at the outlet of the preheater so, the optimum value of T_LTWT is expected to be closed to the one obtained by means of the correlation from the coupled model (Eq. (2)). The values introduced for this variable (T_opt_LTWT_user_option_B) are started from 30°C, which is closed to the value obtain in Option C (see Table 15 in next Sub-section), to 60°C, to cover the temperature obtained in Option A (52°C, according to Table 13). The sizing parameter of the TES systems are scaled for each case so as to have discharge times of 6h and be able to compare under similar conditions. Input data introduced for each simulation is showed in Table 14.

Table 14.Input data for the parametric study of Option B

Case	Capacity LHS MWh	Capacity SHS m^3	T_opt_LTWT_user_option_B °C
B.1	15	190	30
B.2	15	200	35
B.3	15	200	40
B.4	15	215	43
B.5	15	215	45
B.6	15	230	50
B.7	15	230	50.5
B.8	15	230	51
B.9	15	230	51.25
B.10	15	230	51.5
B.11	15	230	51.75
B.12	15	230	51.8
B.13	15	230	51.99
B.14	15	245	55
B.15	15	265	60

In Figure 31 the roundtrip efficiency is plotted along the amount of excess latent and sensible heat obtained during the simulation for different values of T_opt_LTWT_user_option_B. It can be observed that for all the cases the efficiency is above 0.9, but the highest values are reached when the excess heat is minimum. At low temperatures (from 30°C to 45°C) excess sensible heat appears and roundtrip efficiency decreases by approximately 2%, compared to the best case (Case B.13). On the other hand, when temperatures are above 52°C, the excess latent heat appears and the roundtrip efficiency starts to decrease substantially up to 10% for Case B.15, compared with Case B.13. Although Case B.1 produces the maximum quantity of excess sensible heat (1660 MWh), which is three times higher than the maximum excess latent heat produced in Case B.15 (554 MWh), the roundtrip efficiency is more sensitive to the amount of excess latent heat than the amount of excess sensible heat. Then, it is recommended to avoid the appearance of latent excess heat in any case.

Finally, it is observed that the highest roundtrip efficiency (0.9942) is reached at the same temperature obtained in the correlation used for Option A (51.99°C), so it has been proved that the optimum, regarding efficiency, when the outlet of the preheater is not fixed to saturated liquid is the one obtained in the coupled model. Nevertheless, it should be bared in mind that depending on the application of the system in a real case, excess heat may not be wasted heat, as it might be re-used, for example, in a DH network.

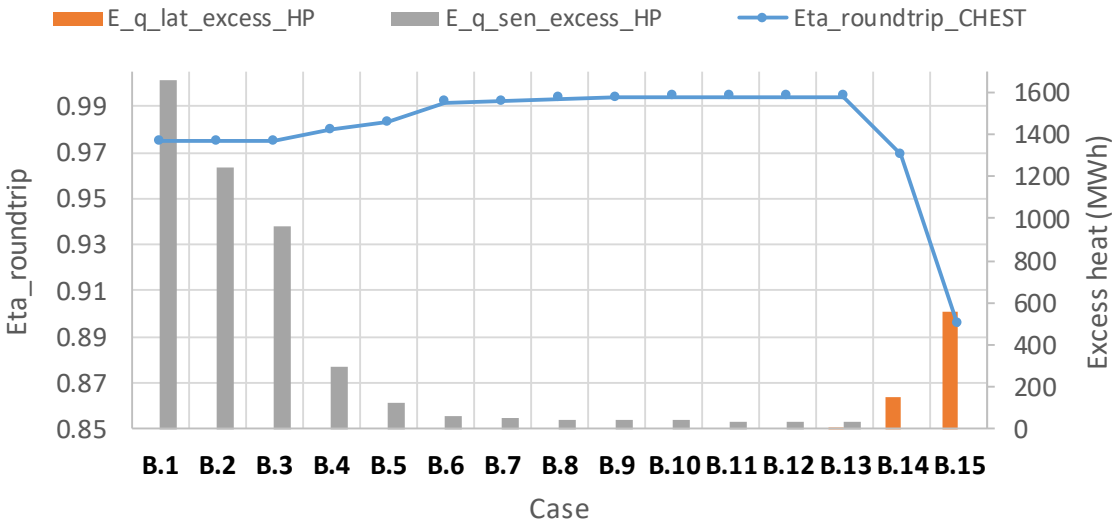

Figure 31. Seasonal roundtrip efficiency, latent and sensible excess heat for different T_LTWT

In order to understand the differences seen in the excess heat for each case, Figure 32 shows the ratios of sensible to latent heat (Q_sen/Q_lat) for charging and discharging processes. As expected, the closer the ratio the most efficient the system. Then, for the cases with temperatures lower than the optimum value this ratio is larger for charging than for discharging, and vice versa for the cases with temperatures above the optimum one.

As for this study TES systems are sized to fulfill the discharging heat ratio, if the charging ratio differs from the discharging one excess heat appears. For low temperatures, the amount of sensible heat needed for charge is higher than for discharge, then, there is sensible excess heat. For high temperatures, less share of sensible heat is required during charge, so that there is latent excess heat in these cases.

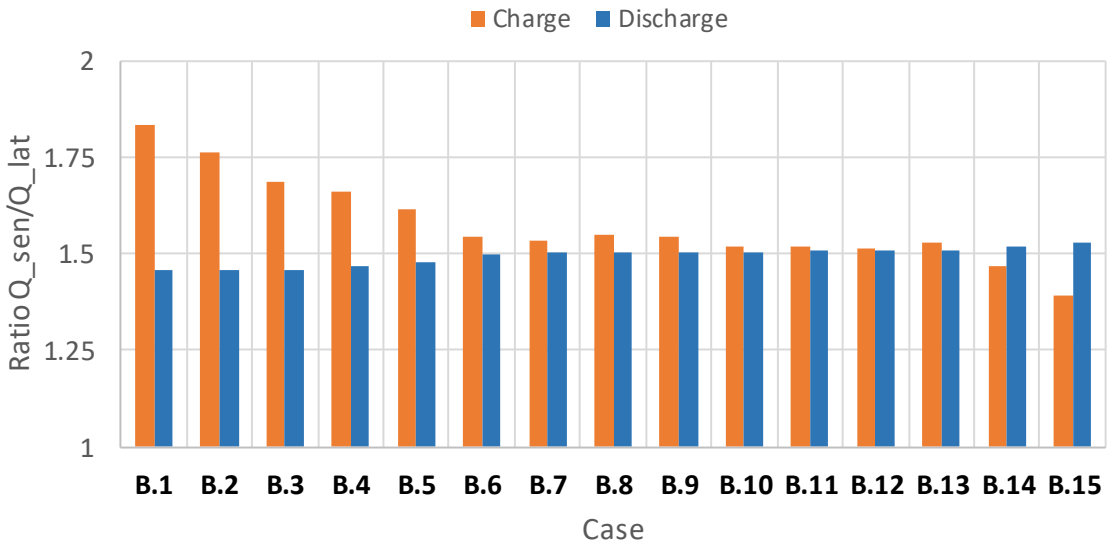

Figure 32. Ratio Q_sen/Q_lat for charge and discharge for different T_LTWT

3.3.2. Comparison of Options A and C

In this section a comparison among Options A and C is done. Option B is eliminated from this analysis as in the previous section it was proved that the most optimum temperature that can be chosen for it (T_opt_LTWT_user_option_B) coincides with the value obtained in the correlation used in Option A, then, results for Option A and best-case of Option B are equal.

Simulations are performed under the conditions explained in 3.3. Sizing parameters and results for each case are presented in Table 15. Firstly, it can be seen that the temperature of the LTWT in the SHS is 20 K lower for Option C, which will lead to lower losses to the environment. Also, TES capacities needed to allow 6h of discharge are lower in Option C, which can potentially reduce the construction cost of the installation. On the other hand, Option A allows for more energy production by means of the ORC, has a better roundtrip efficiency, needs less heat source for the same temperature (T_w_in_evap_HP=80 °C) and produces less sensible excess heat.

Table 15. Simulation results for options A and C

	Option A	Option C
Capacity LHS (MWh)	**15**	**14.5**
Capacity SHS (m3)	**230**	**180**
T_opt_LTWT (°C)	51.99	29.77
E_el_in_HP (MWh)	1893	1817
E_el_net_ORC (MWh)	1882	1733
Eta_roundtrip_CHEST (-)	0.994	0.954
E_q_lat_excess_HP (MWh)	2.41	0
E_q_sen_excess_HP (MWh)	32.828	1853.836
E_q_evap_HP (MWh)	9692.681	10728.972

Regarding the excess heat obtained for the two cases, sensible excess heat is fifty times higher for Option C, however, a small amount of latent excess heat is observed in Option A. This quantity (2.41 MWh) is a consequence of the different working conditions that take place during the first charge of the system, as the LTWT is at ambient temperature (25°C) and has not reached yet its optimum value (51.99°C), then, while the energy input in LHS remains the same, the mass flow rate in the subcooler is lower than for the rest of the charges, so the SHS systems needs more time to fill in and latent excess heat appears.

In Figure 33 charge and discharge ratios as well as temperatures of LTWT are presented for Options A and C. It is observed that while in Option A ratios are virtually equal, in Option C the charging ratio is 30% higher than the discharging one, which results in the production of excess sensible heat.

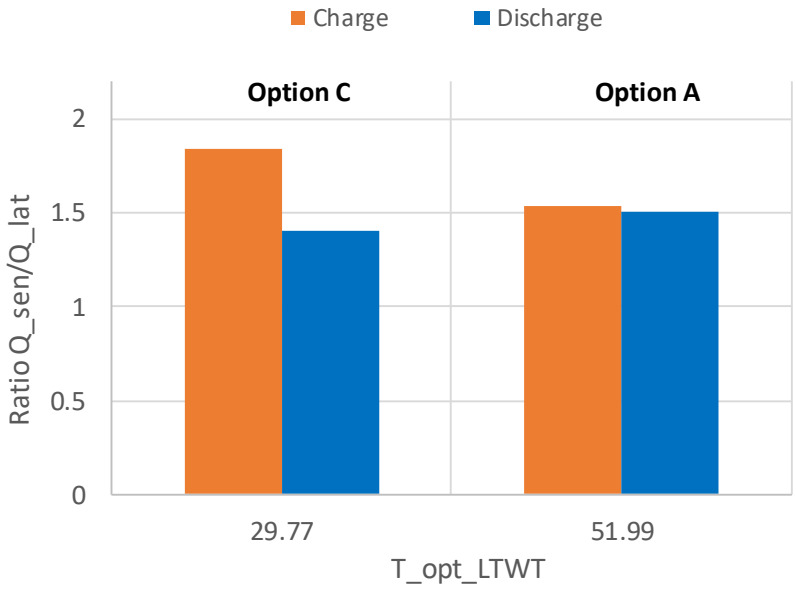

Figure 33. Ratio Q_sen/Q_lat for charge and discharge for options A and C

According to what has been presented so far, Option A is the best choice for the optimization of the parameter T_LTWT, as it has a better roundtrip efficiency and less excess heat. However, Option A does not guarantee liquid state of the refrigerant at the outlet of the preheater of the ORC. This can be a technical issue as if the refrigerant is at two-phase flow at the inlet of the evaporator there might be problems to distribute the fluid equally along the tubes. Then, Option C, which ensures saturated state at the outlet of the preheater, is the most feasible possibility regarding technical limitations of the equipment.

3.4. CASE OF STUDY

Currently, it is not easy to find a direct application for a CHEST system within the Spanish energy market. This is due to the fact that RES installed power in Spain is not large enough to cover the energy demand of the country. As an example, in 2018 there were 4.5 GW of installed capacity for solar photovoltaic was and 23.1 GW for wind energy, facing maximum values of energy demand of 40 GW [22]. So, the renewable electricity, when produced, is directly discharged in the electrical grid to cover as much part of the demand as possible and there is no electricity surplus available to be used to charge the CHEST system. However, analyzing the workings of the Spanish electricity system, it was found out that some of its characteristics may benefit the integration of the CHEST technology employing some wind power plants of the country.

3.4.1. The Spanish energy market and the possibility of integration of a CHEST system

The market operator is the independent organism in charge of establishing the exchanges of electric energy produced in the electricity market in Iberian Peninsula. Spain and Portugal operate in a single energy market, whose market operator is named *Operador de Mercado Ibérico* (OMI) and has two poles: the Spanish pole (OMIE) manages short-term markets (daily and intraday) and the Portuguese one (OMIP) is responsible for the futures market. In this section, the functioning of the daily market will be analyzed [23, 24].

The energy price per hour is decided by a price matching process: sale offers for each hour of the day are organized and plotted from lower to higher price and purchase offers are structured in decreasing order; then, the intersection of both curves is the final energy price for that hour. Knowing these prices, the OMIE establishes the based daily operating schedule, which is formed by the breakdown of the different sale and energy purchasing processes that are expected to occur. This process is done along one daily session (daily market) so as to adjust the estimated energy production and consumption to the reality. The daily market closes at 12.00h of the previous day, before the energy delivery. After that, there are a total of six intraday markets and one European Cross-Border Intraday market (XBID) that allow renegotiating the energy configuration for their corresponding operating hours [23, 25, 26].

By means of the daily market, the OMIE obtained the most economical solution for the energy dispatch for the following day, but it does not verify whether this result is technically feasible. The system operator (SO) is the entity responsible for checking that the based daily operating schedule obtained by OMIE is also physically possible, otherwise, the SO has some adjustment facilities in order to solve the technical problems that may appear and ensure the actual match between energy production and consumption at a national level. Among them, the technical constraints market is of special interest for this Master Thesis.

A technical constraint is defined as any circumstance, resulting from the state of the production and transport energy system, that is likely to affect the security, quality or reliability of supply and requires the modification of the scheduled production programs of the units of production [25, 27].

To solve these technical constraints the different programming units of the Spanish electrical grid make economic offers either to increase their production up to their maximum installed

power or to decrease it with respect to the production programmed in the based daily operating scheduled. The solving process is made in two stages. In the first one the modifications of the schedule that need to be done are identified and the solutions that are technically feasible are selected regardless of their price[18]. Secondly, the equilibrium between generation and consumption (unbalanced during Stage 1) needs to be established again. In this case, the economic criterion is determining. This process is done to solve the technical constraints found for the daily market, after this, technical constraints can be also readjusted for the result of the intraday market and at real time [25, 27].

Information regarding technical constraints can be consulted in the SO's website (www.esios.ree.es). On it, the hours a programming unit participated in the technical constraints market, as well as the difference between the actual energy generated and the one that was expected to be produced for each day of the year, can be seen. This difference can be positive if the programming unit offered to increase its production, or negative if it proposed to decrease it. Among the programming units that participate in this market, several wind power plants can be found which, mostly, make offers to decrease its scheduled production. Thus, those wind power plants are generating less electricity than the amount initially programmed; even though they were capable of generating more power, the grid cannot support it due to technical issues.

The proposal for this Section is to make a selection among the wind power plants participating in the technical constraints market and employ their hourly data of the energy reduction with respect to the based daily operating scheduled to drive a possible CHEST system integrated in the power plant. In other words, instead of stopping some of the turbines of the plant, they keep functioning as initially planned, but the power generated is not provided to the electrical grid, instead, it is used as input to the HT-HP of the CHEST system. Figure 34 depicts this idea, it can be noticed the grey areas that correspond to the energy available for charging the CHEST system.

[18] In case two options are technically equivalent, it will be selected the one that implies the lowest economic cost [25].

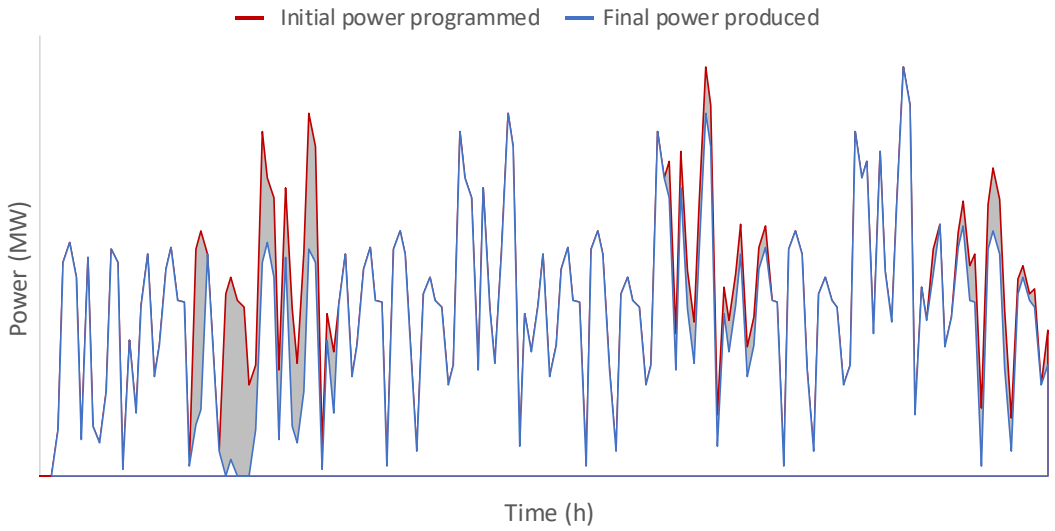

Figure 34. Initial power programmed for a power plant and actual power produced. Reductions (grey areas) with respect to the initial power are due to technical constraints.

Then, the TES tanks will be charged by means of the power reduction offered in the technical constraints market. Regarding the discharge of the CHEST system, this can be done at times of high price of the energy in the daily market. Also, the possibility of purchasing energy at low prices in the daily market in case there is no technical constraints or their value is below the nominal power of the HT-HP will be also consider.

3.4.2. Power plants under study

Two power plants are studied in this Section, as they were the best examples that meet the following criteria:

- Active participation in technical restrictions market during 2018: The interest of this study is focused on programming units that have regularly participated in the market at least half of the time of the year and that have offered reductions in their scheduled program.
- Type of technology: Onshore wind power plants. Wind energy is one of the most promising RES in Spain and it is already contributing in the technical restrictions market, so a better integration of them in the electrical grid is of special interest.
- Installed power of less than 50 MW: Actually, the most interesting for this study is to find wind power plants with an installed power as low as possible, so the integration of a CHEST system (of, for example, 1MW) would have more influence in the performance of the plant. Checking the wind power plants participating in the technical restrictions market, the median installed power is around 50MW [28], so the installed power of the plants selected were below this value.

Thus, considering the requirements aforementioned, the wind power plants selected were Puerto Escandón and Leboreiro. Table 16 gives a summary of the main characteristic of both plants:

Table 16. Characteristics of wind power plants selected for the case of study [29, 30].

Name	Puerto Escandón	Leboreiro
Programming unit code	EGMJALO	EEGPEL
Location	Teruel, Spain	Lugo, Spain
Year of commissioning	2008	2005
Operator	Molinos de Jalón S.A	Enel Greenpower
Wind turbine model	Gamesa G90/2000 (2000 kW)	Made AE-46/I (660 kW)
Number of wind turbines	13	32
Total installed power	26 MW	21.12 MW

As an example, Figure 35 and Figure 36 illustrate the technical restrictions profiles in January 2018 for the wind power plants selected. This represent the amount of power that can be potentially used for charging the CHEST system. It can be seen that the order of magnitude of the power in each case is different, then, the size of the CHEST system would be probably larger for Puerto Escandón than for Leboreiro.

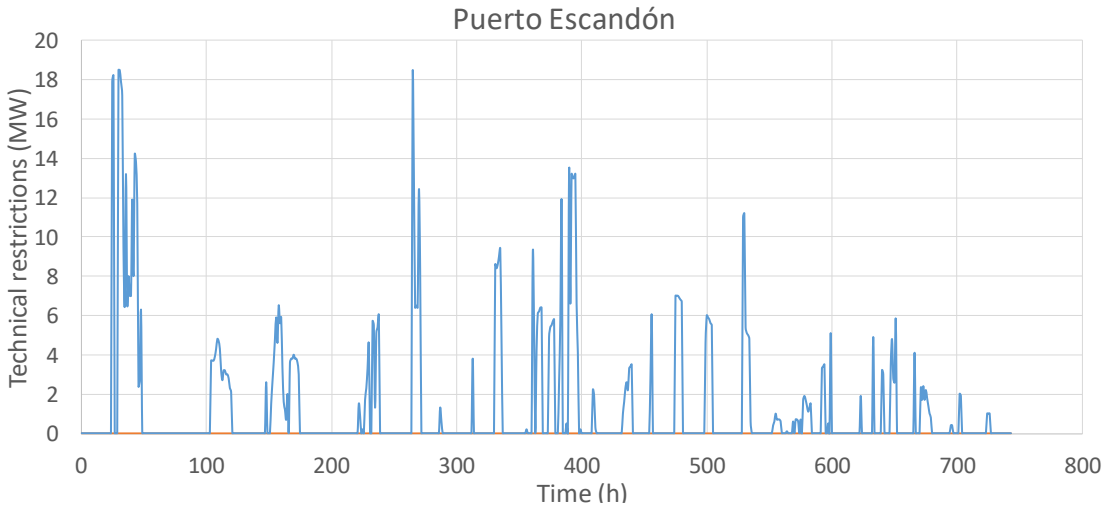

Figure 35. Technical restrictions profile for Puerto Escandón wind farm for January 2018

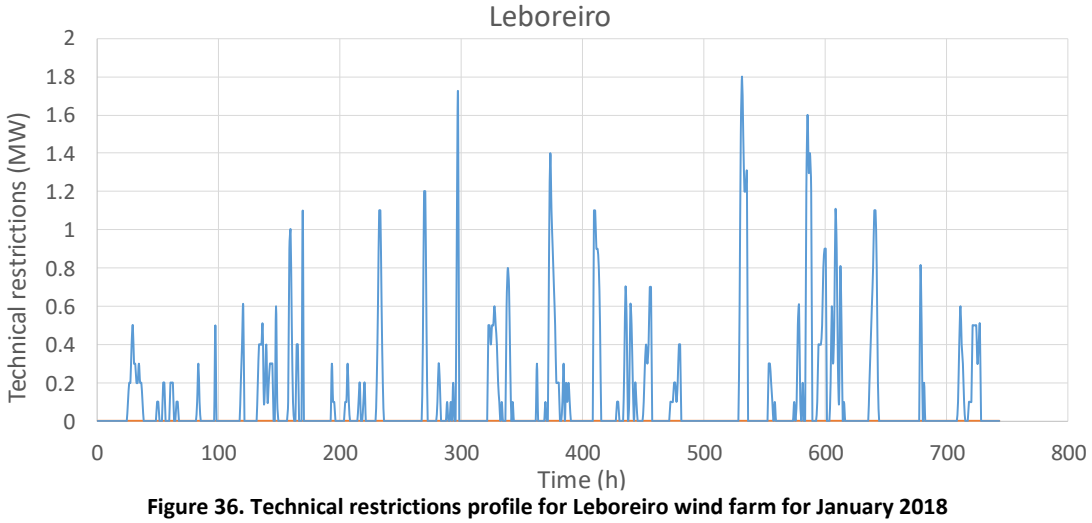

Figure 36. Technical restrictions profile for Leboreiro wind farm for January 2018

3.4.3. Modifications made in the TRNSYS-CHEST model

Some changes regarding the control of the power entering in the HT-HP or delivered by the ORC are implemented in the TRNSYS-CHEST model in order to assess the performance of the cases under study in this section. These changes are located in the input files utilized and in the *POWER CONTROL* calculator. Figure 37 shows the novelties introduced in the model:

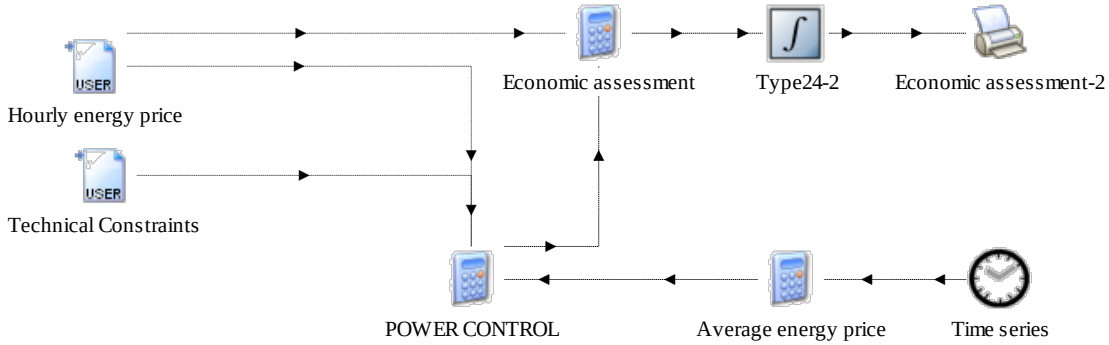

Figure 37. Changes made in the TRNSYS-CHEST model for the analysis of the Technical constraints

a) New inputs of the model

Below, the new inputs used in the model are explained. Information about energy prices or technical constraints profile is collected from SO's website [28]:

- Hourly energy price: In this file the energy prices (€/MWh) for each hour (**Energy_price_h**) of the year 2018 are defined.
- Technical constraints: The technical constraints profile in MW, as depicted in Figure 35 and Figure 36 , for the year 2018 is collected in this file under the variable name **Tech_Const**.
- Time series: This type takes into account the moment of the year that the simulation is in each timestep. This is used to obtain the month of the year for each timestep.
- Average energy price: In this calculator, the average value for the energy price for every month of the year (**Energy_price_month**) is saved.

This information is used in *POWER CONTROL* to compare the hourly price with the average price for that month and decide whether to sell or buy energy.

b) Charging strategy

As it was previously explained, in this occasion the CHEST system will be charged by means of the data related to the technical constraints. Then, regarding the parameter SF_P_el_in_HP (Eq.(6)), the variable P_el_surplus_RES is substituted by **Tech_Const**.

$$\boldsymbol{SF\_P\_el\_in\_HP = (Tech\_Const > P\_el\_in\_nom\_HP)} \qquad \textbf{(42)}$$

Also, as mentioned above, the possibility of buying energy at low prices to improve the performance of the system is introduced. To do that, a control variable (SF_Purchase_power) is introduced in *CONTROL CARDS.* This variable will be one in case this option is considered during

the simulation and zero otherwise. The purchasing criteria is evaluated in the variable Purchased_power_est:

$$\begin{aligned} \boldsymbol{Purchased\_power\_est} = (&Energy\_price\_h \\ &< Energy\_price\_month) * (1 - SF\_P\_el\_in\_HP) \\ &* (P\_el\_in\_nom\_HP - Tech\_Const) \\ &* SF\_Purchase\_power * (F\_ctrl\_char\_TES\_delayed \\ &= 1) \end{aligned} \quad \textbf{(43)}$$

According to this equation, power will be bought when the energy price for that hour is lower than the average price of the corresponding month, when the available power from the technical constrains is less than the nominal power of the HT-HP and if the option of purchase power is activated. The amount of power to be acquired is the difference between the power provided by the technical constraints and the nominal input power of the HT-HP, so it will work at full capacity. Finally, the last term of the equation (F_ctrl_char_TES_delayed=1) is introduced so as to avoid charging and discharging of the system at the same time, as in case tanks are full, the system will be discharged independently of the energy price (see next Section).

Then, the estimated power input for the HT-HP (previously, Eq. (8)) is now calculated considering this purchased power:

$$\begin{aligned} \boldsymbol{P\_el\_in\_est\_HP\_MW} &\\ &= Tech\_Const * (1 - SF\_P\_el\_in\_HP) \\ &+ P\_el\_in\_nom\_HP * SF\_P\_el\_in\_HP \\ &+ Purchased\_power\_est \end{aligned} \quad \textbf{(44)}$$

Finally, the actual power that has been purchased, considering TES sizing restriction, is:

$$\boldsymbol{Purchased\_power} = \boldsymbol{Purchased\_power\_est} * \boldsymbol{F\_ctrl\_char\_TES} \quad \textbf{(45)}$$

c) Discharging strategy

In this Section the discharge strategy has been changed and now the objective is to sell electricity at peak hours. Accordingly, there is no information about electrical demand to be covered, and calculations corresponding to bypassed power, surplus and deficit (Eqs. (3), (4) and (5), respectively) are no longer used. Moreover, the ORC's net output power will be fixed at its nominal power, so it will always be working at full load and the variable SF_P_el_net_ORC (Eq. (7)) is also deleted. Thus, the estimated net power output of the ORC (formerly, Eq. (9)) is calculated as:

$$\begin{aligned} \boldsymbol{P\_el\_net\_est\_ORC\_MW} = (&Tech\_Const \\ &= 0) * P\_el\_net\_nom\_ORC \\ &* [(F\_ctrl\_char\_TES\_delayed = 1) * (Energy\_price\_h \\ &> Energy\_price\_month) + (F\_ctrl\_char\_TES\_delayed \\ &= 0)] \end{aligned} \quad \textbf{(46)}$$

Then, usually, the ORC will be activated when there is no technical constraint and the energy price for that hour is higher than the average value for that month. The net output power of the ORC will always be the nominal one stated in *CONTROL CARDS.* Additionally, an extra condition

is set in case the TES systems were already charged in the previous timestep (F_ctrl_char_TES_delayed=0). When this happens, the ORC will start working regardless of the price of the energy, because it is interesting to have always some remaining space to store energy coming from technical constraints.

d) Economic assessment

Benefit and cost are calculated for this section so as to analyze the viability of a CHEST system for the cases under study. To do that, gross profit and cost are assessed:

$$\boldsymbol{gross\_energy\_profit} = Energy\_price\_h * P\_el\_net\_ORC \quad \textbf{(47)}$$

$$\boldsymbol{purchased\_energy\_cost} = Energy\_price\_h * Purchased\_power \quad \textbf{(48)}$$

These quantities are integrated to have the results for the complete simulation period and calculate the net profit as the difference between the gross profit obtained from energy selling and the cost of buying energy.

3.4.4. Integration of a CHEST system in the selected wind power plants.

Having done the corresponding changes in the TRNSYS-CHEST model, studies for the two wind power plants selected are performed. The simulations are done for the data of the year 2018 using a timestep of 1 h. Option C is selected for being the most technically feasible possibility and Mode 2 (T_w_in_evap_HP= 80 °C and T_w_in_cond_ORC= 10 °C) is selected for these cases.

The assessment of the external heat source needed for this Mode is out of the scope of this Thesis. As an example, solar thermal collectors can be used to heat up water up to 80°C. Also, within the CHESTER project, an installation located in Aalborg, Denmark, uses a pit storage of 1000000 m^3 to store waste heat coming from industries nearby that allows the interaction of a CHEST system with a DH network. Water stored can reach temperatures of 80°C. Thus, a similar system can be also a solution for the integration of the heat source [31].

For this Section parametric studies regarding the size of the equipment, under the conditions previously explained, are done. Then, the nominal power and the size of the TES system is assessed to obtain the optimum results from a technical and economic point of view. TES systems are always sized to allow a maximum discharge time of 6 hours.

In order to establish an order of magnitude for the sizing of the CHEST system in each case, the frequencies of the power values of the technical constraints is studied. In Figure 38 and Figure 39 the cumulative relative frequency of the power reduction by means of the technical constraints is represented for the two wind power plant under study. It can be seen that for Puerto Escandón, although maximum values are close to 20 MW, 95% of the occasions a technical constraint takes place, its value is below 10 MW. On the other hand, for Leboreiro, 95% of the power technical restrictions is lower than 1.5 MW even though sometimes values up to 5.5 MW are reached.

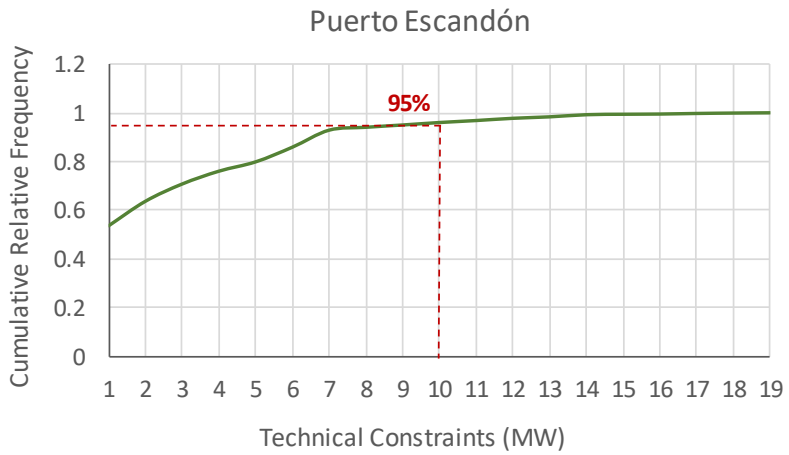

Figure 38. Cumulative Relative Frequency of the power of the technical constraints for Puerto Escandón.

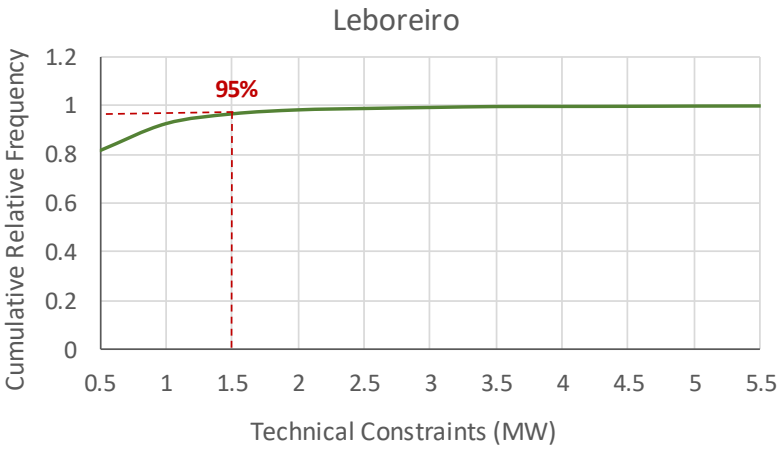

Figure 39. Cumulative Relative Frequency of the power of the technical constraints for Leboreiro.

Having this information, parametric studies are done increasing the size of the HT-HP and ORC from 1 to 10 MW for Puerto Escandón and from 0.25 to 1.5 MW for Leboreiro. Regarding the sizes of the TES systems, values for Option C in Table 15 are used for 1 MW and these are scaled linearly for the different sizes assessed. Moreover, for each study, the possibility of buying energy or not is analyzed. As mentioned before, energy is purchased at low prices when a technical restriction takes place to make the HT-HP work at full load. Table 17 shows the all combinations studied in this section.

Table 17. Parametric studies for Puerto Escandón and Leboreiro

PUERTO ESCANDÓN			LEBOREIRO		
CASE	**Nominal power (MW)**	**Purchase energy?**	**CASE**	**Nominal power (MW)**	**Purchase energy?**
1.1a	1	NO	**2.1a**	0.25	NO
1.1b	1	YES	**2.1b**	0.25	YES
1.2a	2.5	NO	**2.2a**	0.5	NO
1.2b	2.5	YES	**2.2b**	0.5	YES
1.3a	5	NO	**2.3a**	0.75	NO
1.3b	5	YES	**2.3b**	0.75	YES
1.4a	7.5	NO	**2.4a**	1	NO
1.4b	7.5	YES	**2.4b**	1	YES
1.5a	10	NO	**2.5a**	1.25	NO
1.5b	10	YES	**2.5b**	1.25	YES
-	-	-	**2.6a**	1.5	NO
-	-	-	**2.6b**	1.5	YES

a) Puerto Escandón simulation results

In this section, results of technical and economic aspects are presented for the wind power plant of Puerto Escandón, located in Teruel. Firstly, in Figure 40, the roundtrip efficiency is depicted along with the percentage of energy produced by the CHEST system with respect to the total energy generated by the power plant (produced by wind farm and CHEST system) during the year 2018, for all the cases of study. It is observed that both the efficiency and the percentage of energy production increases with the increase of the nominal power of CHEST.

In the runs which have the same nominal power, if energy is purchased (*.*b tests) the roundtrip efficiency decreases with respect to the occasions when no energy is bought (*.*a tests). This drop is more pronounced for high values of nominal power, as it goes from 17% in Case 1.1 to 33% in Case 1.5. However, even though these decreases are remarkable, the lowest roundtrip efficiency reached is 0.90 (Case 1.3b), so the values are acceptable even for the most adverse occasions. On the other hand, high values of roundtrip efficiency obtained in *.*a cases are consequence of the HT-HP working at partial load. When this happens, COP raises, as it was explained in Section 2.7.2, so TES systems are charged in a more efficient manner than if the HT-HP works at full load. Then, less electrical energy is necessary for the charging and better roundtrip efficiency is achieved.

Also, when energy is purchased the share of energy produced by CHEST increases considerably (e.g., it is 2.16 times higher in Case 1.5b than in Case 1.5a). This is due to the fact that by buying energy in the market the CHEST system charges faster, because HT-HP always works at full nominal power, so more charging-discharging cycles take place during the year, then, more energy is produced.

Thus, from a technical point of view, it appears to be more interesting the purchase of energy, as the number of cycles per year is higher and the roundtrip efficiency achieved is still reasonable, so more advantage is taken from the CHEST system.

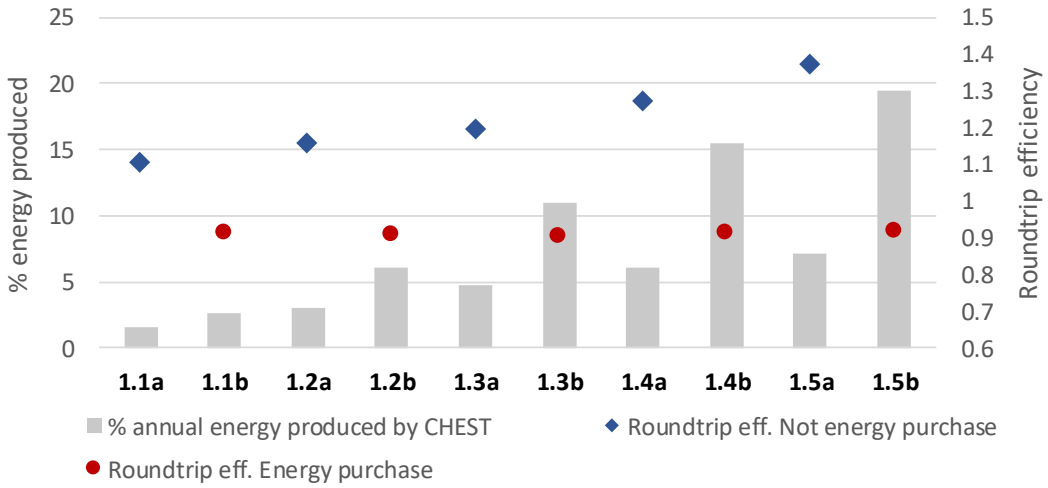

Figure 40. Technical performance for Puerto Escandón case

Focusing in the economical point of view, in Figure 41 the net profit and the benefit obtained per MWh produced (calculated as the net profit divided by the total energy produced by the ORC during the simulation) is represented for the different runs. It can be seen that for the cases with no purchase of energy the net profit obtained is higher, as the energy cost is equal to 0. It should be noticed that the cases with higher benefit are also the ones with less annually energy production (Figure 40), which makes that the benefit obtained per MWh produced is higher when no energy is purchased. These results indicate that the energy purchase may not be so interesting from an economical view, as the cost of energy production increases.

Moreover, no operational costs are studied so far, but they will increase with the increase of the working hours of the system. These results might indicate that a CHEST system working only some months of the year (the windiest or the ones with higher profiles of technical constraints) can be also an interesting possibility, as the system would work only at profitable periods, reducing operational costs. Finally, it should be mentioned that when the nominal power of the system increases the net profit also raises, but the unitary benefit per MWh produced starts to decrease (especially when energy is bought). Then, a compromise solution between high production and attractive prices should be found.

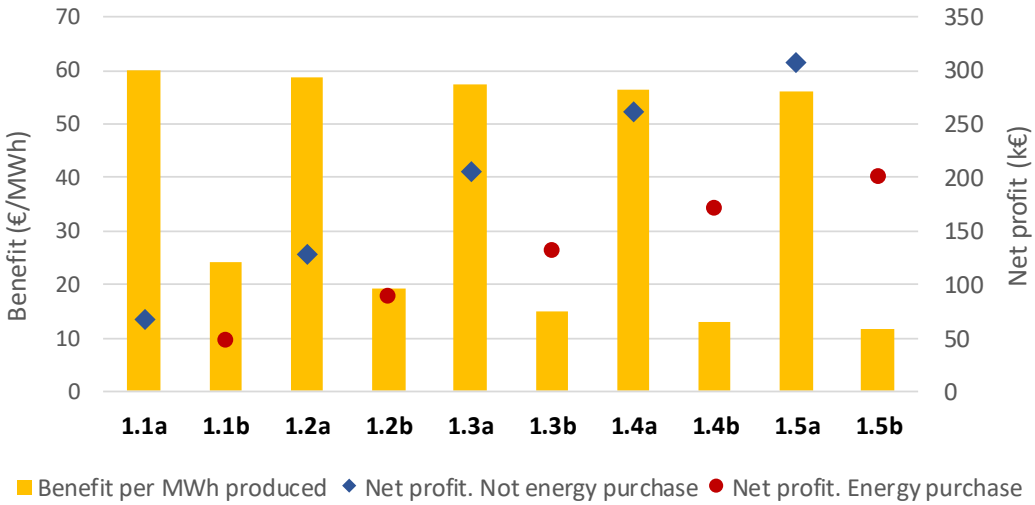

Figure 41. Economic performance for Puerto Escandón case

So far it seems that the bigger the system (inside the working range seen in Figure 38) the better, as it implies more energy production and, consequently, more net benefit. However, there are other economic aspects that have not been considered so far, such as the capital cost (CAPEX) or the payback period (PB) of the CHEST system. Up until now, no installation with similar characteristics has been built, thus, reliable data of its CAPEX cannot be obtained. In literature some references of cost per installed power have been found for PTES systems (600$/kW in [32]; between 350 and 750€/kW in [33] and 400£/kW in [34]). Based on this, a value of 550 €/kW with a margin of ±30% is established to develop a preliminary study and make an approximation of the simple payback period for each case of study. CAPEX is calculated as a linear relationship with the estimated power and no economies of scale are considered.

Making the assumptions mentioned above, CAPEX and PB are depicted in Figure 42. As expected, CAPEX is the same for the same installed power and PB periods are higher for cases of energy purchase. According to literature, the estimated lifetime of a PTES system is around 25-30 years [35], then, paybacks below 15-20 years are admissible. Results show that a CHEST system can be economically possible in this case for installed power below 7.5MW (Case 1.4).

As PB periods obtained are longer than 10 years, non-discount methods may be not accurate enough as they do not consider the effect of the inflation or the opportunity cost. To check this issue, the changes in the discounted payback were studied for one specific case (1.3a) varying the discount rate from 0.1% to 1%; the inflation rate from 1% to 5% and considering the ±30% deviation of the CAPEX. Results show a maximum PB value of 16.5 years when CAPEX is 30% higher than the value calculated and the two rates (discount and inflation) are set to 1%. On the other hand, the minimum PB is 8 years when CAPEX is 30% lower and inflation rate is above 3%. Thus, variations compared to the non-discount method are not significant, as the PBs obtained were 9.3 years for the most positive scenario and 17.4 for the most negative one.

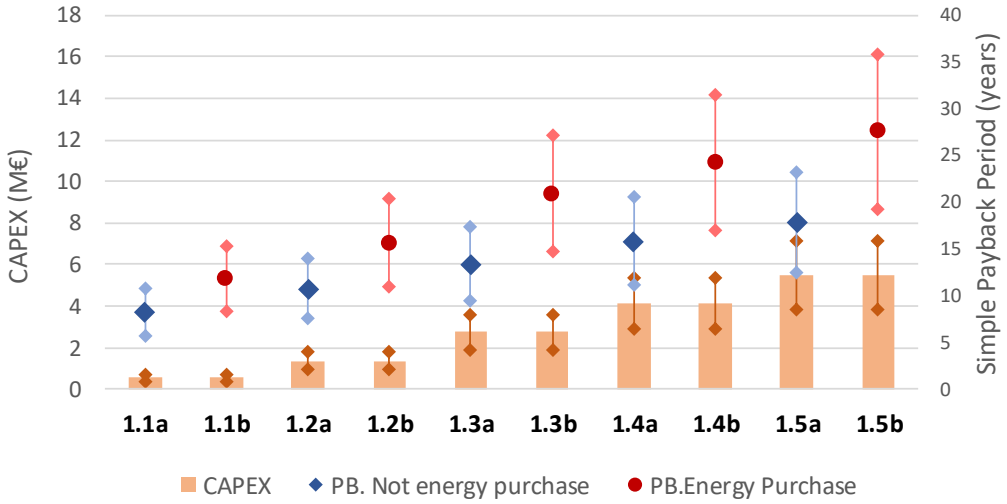

Figure 42. Capital cost (CAPEX) and payback (PB) period for Puerto Escandón case

Once all the techno-economic aspects for Puerto Escandón case have been assessed, it can be concluded that the most suitable solution is having a system with an installed power sufficiently high to have an impact in the total production of the power plant but without leading to high PB periods. Among the cases studied, Cases 1.3a and 1.4a seem to be the most promising ones. Also, purchasing of energy at low prices does not appears to be the best solution for increasing the functioning cycles of the CHEST.

b) Leboreiro simulation results

Results for Leboreiro wind power plant are presented in this section. Conclusions reached are very similar to the ones of the previous Section. From a technical point of view (Figure 43), results of roundtrip efficiency are similar to the ones obtained in Puerto Escandón case, but the percentage of energy produced by CHEST is lower in this occasion (the maximum value obtained in Leboreiro case is 4.38% compared to 20% reached in Puerto Escandón case). This is due to the fact that the installed power of both wind power plants are similar, however, the amount of power traded in the technical constraints market during the year 2018 is much lower in this case (as it was depicted in Figure 39) then, this power plant has less capacity of enhancement by the means proposed in this Master thesis.

Regarding economic aspects (Figure 44 and Figure 45), the net profit obtained and the CAPEX are one order of magnitude lower than in the previous study, which makes that results for benefit per MWh produced and PB periods are similar to Puerto Escandón case.

In this occasion, installed power up to 1.25 MW seems techno-economically feasible for cases where no energy is purchased. However, it should be noted that the improvement of the power plant is not really significant, so, considering the information collected for the year 2018, it might not be interesting, from a technical point of view, the implementation of a CHEST system in this case.

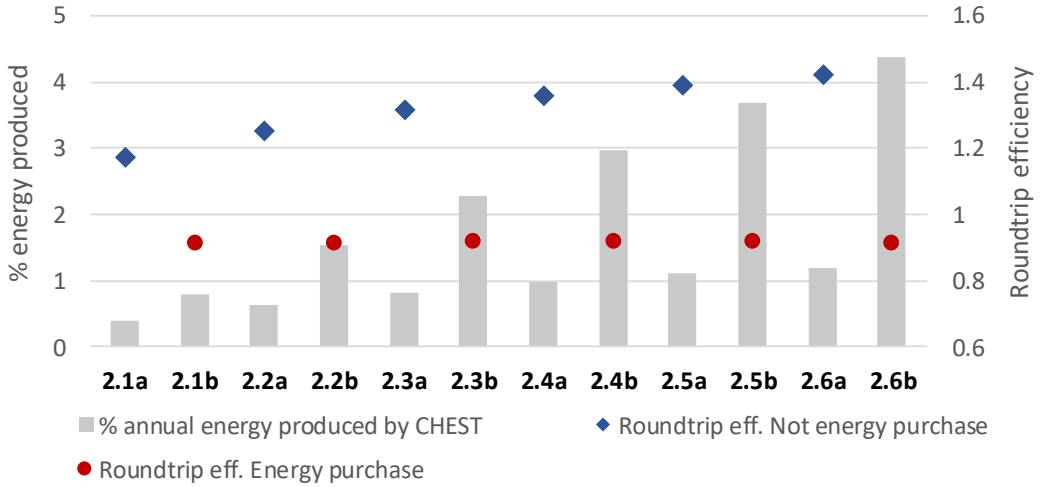

Figure 43. Technical performance for Leboreiro case

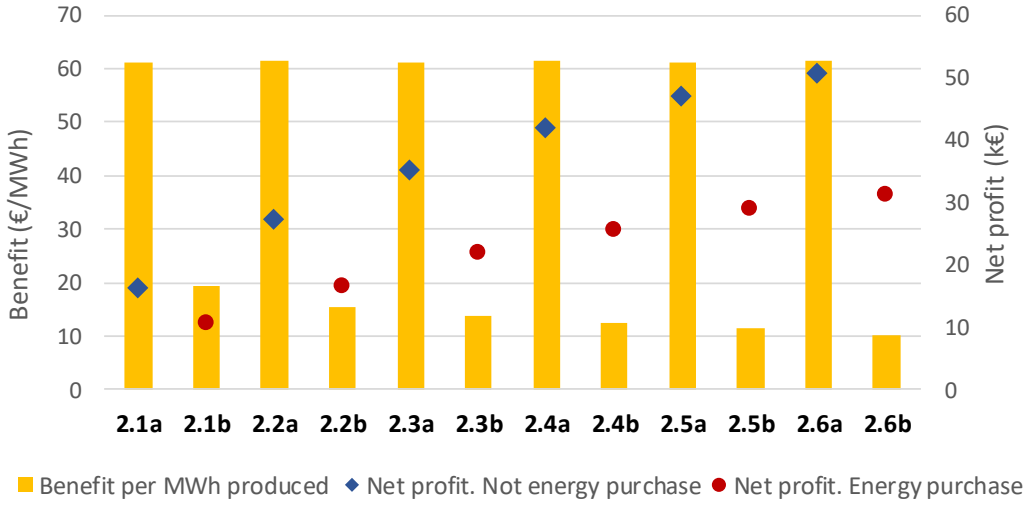

Figure 44. Economic performance for Leboreiro case

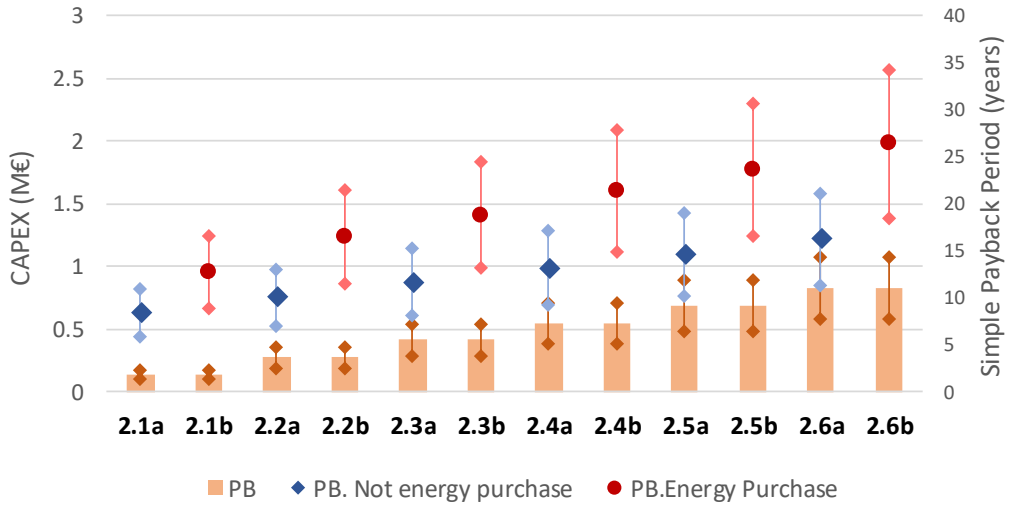

Figure 45. Capital cost (CAPEX) and payback (PB) period for Leboreiro case

4. CONCLUSIONS AND FUTURE WORK

4.1. CONCLUSIONS

This Master thesis intends to give a response to the problematic of intermittent and unpredictable behavior of RES, which hampers their integration in the current energy system. To do so, a review of the existing large-scale storage technologies was done and a solution by means of a CHEST technology is proposed.

Thus, a model of CHEST system was developed using the software TRNSYS. The main novelties of the proposed model (TRNSYS-CHEST model) compared to previous work done in the field are the assessment of the transient behavior of the system; the decoupling of the CHEST system (energy charged and discharged from TES is initially unknown, as it depends on the boundary conditions of the system); the detailed study of the TES systems, especially for the SHS system; and accounting for partial load conditions. TRNSYS-CHEST model allows, by controlling the temperatures of source and sink and the sizing parameters for the equipment and the TES systems, the assessment of the input power used by the HT-HP or net power provided by the ORC, the seasonal roundtrip efficiency for the period simulated as well as the evolution of the level of charge of the storage tanks, considering the heat which is stored in them or rejected. Also, three optimization strategies for the low-temperature water tank temperature (T_LTWT) were proposed.

Firstly, a verification study was performed to ensure the correct behavior of the model and solution consistency. Then, the comparison of the working modes proposed as well as the study of the optimization options are done so as to find the most suitable combination for a hypothetical case of electricity production. Results showed that Mode 2, with an inlet water temperature of 80 °C for the source and 10 °C for the sink, is the best option as it has one of the highest roundtrip efficiencies (0.99) without requiring too high values of source temperature. Regarding the optimization of the temperature of LTWT, Option A is found to be the most efficient one but presents some technical issues regarding the inlet of the ORC's evaporator. Then, Option C, which ensures saturated liquid at the inlet of the ORC's evaporator, reducing the technical complexity of the system, is selected. Option C also presents other advantages, as the optimum temperature for the LTWT is lower than the one obtained in Option A, which leads to lower energy losses to the environment; and, as the excess sensible heat that appears can be used for heating purposes, there is still room for improvement.

Finally, a possibility for the integration of a CHEST system in the current electrical Spanish grid is proposed for two different wind power plants. Electrical energy for charging is obtained from the energy reduction with respect to the based daily operating scheduled due to technical constraints and the energy discharged is sold in the market at peak times. Also, the possibility of buying energy at low prices to charge the system is studied. Results showed that by purchasing energy the contribution of the CHEST system to the power plant increases but its efficiency is reduced and the cost of each MWh produced increases. A parametric study varying

the sizes of the system is performed to find the most suitable scale for each case considering the CHEST's contribution to energy production and economic aspects like annual benefit, capital costs and payback period. Results showed that CHEST systems may be techno-economically possible as long as long shares of energy contribution can be achieved at reasonable payback periods. As an example, in Case 1.3a, which has a CHEST system that contributes to 5% to the annual energy production of the power plant, a CAPEX of 1.9 M€ and PB period of 9.4 years can be achieved for an optimistic scenario.

4.2. FUTURE WORK

The TRNSYS-CHEST model presented in the Master thesis is a first version that could still be improved by assessing more deeply some of its components. Among the next steps to be taken, there is the analysis of energy losses in SHS tanks, as, so far, the temperature of the HTWT has been considered as a fixed parameter. To do that new EES maps will have to be created with this temperature lowering from 133°C.

Also, other parasitical consumptions, such as the heating up of pipes and other components, can be included in the model. Moreover, the study of the PCM behavior inside the LHS tank, considering the thermomechanical properties of the material to determine in detail how the phase change process is happening, remains to be done. This will also allow the assessment of the energy losses to the ambient as well as the possibility of considering the PCM starting at ambient temperature for first charging processes. For this, a new TRNSYS type will have to be created, as TRNSYS libraries do not include PCM's tanks.

The integration of this model in other bigger energy system (DH networks, addition of industrial waste heat etc.), along with the development of more detailed control strategies for energy dispatch to determine its behavior in real applications is another interesting future step. Also, temperatures of source and sink have been introduced as fixed values, but data of temperature profiles can be obtained and assessed to have a more realistic performance.

Regarding the CHESTER project, the next step is the design of a laboratory-scale prototype to test the system. This will provide experimental data that will be used for the validation of the TRNSYS-CHEST model and also it will give a first approximation of the economic cost for an installation of its kind.

4.3. PUBLICATIONS

During the development of the Master thesis the author collaborated in the following publications with regard to the CHESTER project:

- Lindeman L, Sánchez-Canales V, O´Donoghue L, et al (2019) Thermodynamic analysis of a high temperature heat pump coupled with an organic Rankine cycle for energy storage. I Int Ing Termodinámica 1–12
- Sánchez-Canales V, Hassan AH, Corberán JM, et al (2019) Excess electricity storage via thermal energy storage. EUROTHERM Seminar #112 1–10

REFERENCES

1. European Commission (2017) Energy, transport and environment indicators 2017 edition
2. INTEGRACIÓN DE LAS ENERGÍAS RENOVABLES EN EL SISTEMA. https://www.eoi.es/blogs/martaluque/2013/11/20/integracion-de-las-energias-renovables-en-el-sistema/. Accessed 20 Sep 2018
3. J. Galindo El almacenamiento de energía incrementa la eficiencia de las renovables. https://ielektro.es/2017/11/16/almacenamiento-energia-renovables/. Accessed 20 Sep 2018
4. Argyrou MC, Christodoulides P, Kalogirou SA (2018) Energy storage for electricity generation and related processes: Technologies appraisal and grid scale applications. Renew Sustain Energy Rev 94:804–821. https://doi.org/10.1016/j.rser.2018.06.044
5. Jockenhöfer H, Steinmann WD, Bauer D (2018) Detailed numerical investigation of a pumped thermal energy storage with low temperature heat integration. Energy 145:665–676. https://doi.org/10.1016/j.energy.2017.12.087
6. CHESTER (Compressed Heat Energy STorage for Energy from Renewable sources) Project. https://www.chester-project.eu/. Accessed 14 Feb 2019
7. Steinmann WD (2017) Thermo-mechanical concepts for bulk energy storage. Renew Sustain Energy Rev 75:205–219. https://doi.org/10.1016/j.rser.2016.10.065
8. Thess A (2013) Thermodynamic efficiency of pumped heat electricity storage. Phys Rev Lett 111:1–5. https://doi.org/10.1103/PhysRevLett.111.110602
9. Guo J, Cai L, Chen J, Zhou Y (2016) Performance optimization and comparison of pumped thermal and pumped cryogenic electricity storage systems. Energy 106:260–269. https://doi.org/10.1016/j.energy.2016.03.053
10. Steinmann WD (2014) The CHEST (Compressed Heat Energy STorage) concept for facility scale thermo mechanical energy storage. Energy 69:543–552. https://doi.org/10.1016/j.energy.2014.03.049
11. Frate GF, Antonelli M, Desideri U (2017) A novel Pumped Thermal Electricity Storage (PTES) system with thermal integration. Appl Therm Eng 121:1051–1058. https://doi.org/10.1016/j.applthermaleng.2017.04.127
12. Lindeman L (2018) Thermodynamic Analysis of a High Temperature Heat Pump coupled with an Organic Rankine Cycle for Energy Storage. Universitat Politècnica de València
13. Klein S. (2018) Engineering Equation Solver; (Version V10.451), F-Chart Software
14. Thermal Energy System Specialists (2017) Trnsys 18. Getting Started. 1:49–50
15. Cecchinato L (2010) Part load efficiency of packaged air-cooled water chillers with inverter driven scroll compressors. Energy Convers Manag 51:1500–1509. https://doi.org/10.1016/j.enconman.2010.02.008
16. Comission E Ecodesign Directive
17. CETIAT (2010) Part-load performance behavior of On-Off and variable capacity heat pumps.
18. Danfoss (2015) The Turbocor Family of Compressors Model TT300, Danfoss TURBOCOR. Datasheet, www.turbocor.com, USA
19. Fahlén P (2012) Capacity control of heat pumps. Rehva 28–31
20. Thermal Energy System Specialists (2017) Trnsys 18. Mathematical Reference. 4
21. Estado actual de la energía termosolar (CSP) – HELIONOTICIAS.

http://helionoticias.es/estado-actual-de-la-energia-termosolar-csp/. Accessed 20 May 2019
22. Estadísticas del Sistema Eléctrico | Red Eléctrica de España. https://www.ree.es/es/estadisticas-del-sistema-electrico/3015/3001. Accessed 24 Apr 2019
23. (2014) Funcionamiento del Pool Eléctrico. http://mifacturadeluz.com/funcionamiento-del-pool-electrico/. Accessed 25 Apr 2019
24. omip. https://www.omip.pt/. Accessed 7 May 2019
25. Núm (2017) Boletín Oficial Del Estado. 690–695
26. Secretaría de Estado de Energía (2019) Resolución de 9 de mayo 2018
27. (2014) El Mercado de Restricciones Técnicas. http://mifacturadeluz.com/mercado-de-restricciones-tecnicas/. Accessed 25 Apr 2019
28. ESIOS electricidad · datos · transparencia. https://www.esios.ree.es/es. Accessed 30 Apr 2019
29. Puerto Escandón (España) - Parques eólicos - Acceso en línea - The Wind Power. https://www.thewindpower.net/windfarm_es_2253_puerto-escandon.php. Accessed 30 Apr 2019
30. Leboreiro (España) - Parques eólicos - Acceso en línea - The Wind Power. https://www.thewindpower.net/windfarm_es_1979_leboreiro.php. Accessed 30 Apr 2019
31. Federico Bava DS D2.1 Case studies : User Requirements and Boundary Conditions Definition. CHESTER. https://www.chester-project.eu/wp-content/uploads/2018/11/CHESTER_D2.1_Case-Studies_v5.0.pdf
32. Gallo AB, Simões-Moreira JR, Costa HKM, et al (2016) Energy storage in the energy transition context: A technology review. Renew Sustain Energy Rev 65:800–822. https://doi.org/10.1016/j.rser.2016.07.028
33. Smallbone A, Jülch V, Wardle R, Roskilly AP (2017) Levelised Cost of Storage for Pumped Heat Energy Storage in comparison with other energy storage technologies. Energy Convers Manag 152:221–228. https://doi.org/10.1016/j.enconman.2017.09.047
34. Proctor P (2014) Energy storage: a potential game changer and enabler for meeting our future energy needs?
35. Benato A, Stoppato A (2018) Pumped Thermal Electricity Storage: A technology overview. Therm Sci Eng Prog 6:301–315. https://doi.org/10.1016/j.tsep.2018.01.017

ANNEXES

ANNEX I: CLASSIFICATION OF VARIABLES (FIXED, DEPENDENT AND INDEPENDENT)

Component	Inputs/ outputs	Status	Value	Units
Compressor (HT-HP)	Overall efficiency	Fixed	0.752	-
	Isentropic efficiency	Fixed	0.8	-
	Electrical power input (P_{input_HP})	**Independent**	-	MW
	Refrigerant mass flow rate	Dependent	-	kg/s
Evaporator (HT-HP)	Source inlet temperature ($T_{w\_inlet\_evap}$)	**Independent**	-	C
	Source temperature difference (ΔT_{w_evap})	**Independent**	-	K
	Expected pinch point	Fixed	5	K
	Degree of superheat	Fixed	5	K
	Refrigerant-side pressure drop	Fixed	50	kPa
	Source mass flow rate	Dependent	-	kg/s
	Total capacity	Dependent	-	MW
Subcooler (SC) (HT-HP)	Water-side mass flow rate	Dependent	-	kg/s
	Expected pinch point	Fixed	5	K
	Refrigerant-side pressure drop	Fixed	5	kPa
	Refrigerant outlet temperature	Dependent	-	C
PCM (LHS) HT-HP side	Expected pinch point	Fixed	5	K
	Refrigerant-side pressure drop	Fixed	5	kPa
	Condensation heat capacity	Dependent	-	MW
PCM	PCM melting temperature	Fixed	133	C
Sensible Heat Storage (SHS)	Temperature of low-temperature water tank (T_{LTWT})	**Independent**	-	C
	Temperature of high-temperature water tank (T_{HTWT})	**Independent**	-	C
	Water specific heat	Fixed	4.2	kJ/kgK
	Subcooling heat capacity	Dependent	-	MW
	Preheating heat capacity	Dependent	-	MW
PCM (LHS) ORC side	Expected pinch point	Fixed	5	K
	Degree of superheat	Fixed	5	K
	Refrigerant-side pressure drop	Fixed	50	kPa
	Evaporation heat capacity	Dependent	-	MW
ORC Expander	Isentropic efficiency	Fixed	0.88	-
	Mechanical efficiency	Fixed	0.99	-
	Electrical efficiency	Fixed	0.98	-
	Refrigerant mass flow rate	Dependent	-	kg/s
	Output net electrical power (P_{output_ORC})	**Independent**	-	MW
ORC Pump	Isentropic efficiency	Fixed	0.8	-
	Mechanical efficiency	Fixed	0.99	-
	Electrical efficiency	Fixed	0.95	-
	Input net electrical power	Dependent	-	MW

Component	Inputs/ outputs	Status	Value	Units
ORC Condenser	Sink inlet temperature ($T_{w\_inlet\_cond}$)	**Independent**	-	C
	Sink temperature difference (ΔT_{w_cond})	**Independent**	-	C
	Expected pinch point	Fixed	5	K
	Refrigerant-side pressure drop	Fixed	25	kPa
	Sink mass flow rate	Dependent	-	kg/s
	Total capacity	Dependent	-	MW
ORC Preheater (PH)	Water-side mass flow rate	Dependent	-	kg/s
	Expected pinch point	Fixed	6.5	K
	Refrigerant-side pressure drop	Fixed	5	kPa
	Refrigerant outlet temperature	Dependent	-	C

ANNEX II: HT-HP PERFORMANCE MAP

DTw_evap$_{HP}$ [K]	T_LTWT [C]	T_w_evap$_{HP}$ [C]	m_w$_{SC}$ [kg/s]	Q_SHS$_{HP}$ [MW]	Q_LHS$_{HP}$ [MW]	Q_tot$_{HP}$ [MW]	COP$_{HP}$ [-]
2	**25**	**40**	5.441905	2.471	1.33	3.801	3.801
2	**25**	**55**	6.79442	3.085	1.628	4.713	4.713
2	**25**	**70**	8.658625	3.931	2.058	5.989	5.989
2	**25**	**85**	11.434908	5.192	2.718	7.91	7.91
2	**25**	**100**	16.062555	7.293	3.824	11.117	11.12
2	**55**	**40**	5.781686	1.9	1.33	3.23	3.23
2	**55**	**55**	7.218649	2.372	1.628	4	4
2	**55**	**70**	9.19925	3.023	2.058	5.081	5.081
2	**55**	**85**	12.148878	3.993	2.718	6.711	6.711
2	**55**	**100**	17.065464	5.608	3.824	9.433	9.433
2	**70**	**40**	6.009629	1.598	1.33	2.928	2.928
2	**70**	**55**	7.503245	1.995	1.628	3.623	3.623
2	**70**	**70**	9.561932	2.542	2.058	4.6	4.6
2	**70**	**85**	12.627848	3.357	2.718	6.075	6.075
2	**70**	**100**	17.738272	4.716	3.824	8.54	8.54
2	**85**	**40**	6.309859	1.281	1.33	2.611	2.611
2	**85**	**55**	7.878092	1.599	1.628	3.227	3.227
2	**85**	**70**	10.039627	2.038	2.058	4.096	4.096
2	**85**	**85**	13.258711	2.691	2.718	5.409	5.409
2	**85**	**100**	18.624442	3.78	3.824	7.604	7.604
2	**100**	**40**	6.747659	0.9437	1.33	2.274	2.274
2	**100**	**55**	8.424702	1.178	1.628	2.806	2.806
2	**100**	**70**	10.736212	1.502	2.058	3.56	3.56
2	**100**	**85**	14.178647	1.983	2.718	4.701	4.701
2	**100**	**100**	19.91667	2.785	3.824	6.61	6.61
4	**25**	**40**	5.285623	2.4	1.297	3.697	3.697
4	**25**	**55**	6.591102	2.992	1.582	4.575	4.575
4	**25**	**70**	8.370195	3.8	1.991	5.791	5.791
4	**25**	**85**	10.988076	4.989	2.611	7.599	7.599
4	**25**	**100**	15.267191	6.932	3.635	10.566	10.57
4	**55**	**40**	5.615645	1.846	1.297	3.143	3.143
4	**55**	**55**	7.002635	2.301	1.582	3.884	3.884
4	**55**	**70**	8.892811	2.923	1.991	4.914	4.914
4	**55**	**85**	11.674147	3.837	2.611	6.447	6.447
4	**55**	**100**	16.220439	5.331	3.635	8.965	8.965
4	**70**	**40**	5.837042	1.552	1.297	2.849	2.849
4	**70**	**55**	7.278715	1.935	1.582	3.517	3.517

DTw_evap$_{HP}$ [K]	T_LTWT [C]	T_w_evap$_{HP}$ [C]	m_w$_{SC}$ [kg/s]	Q_SHS$_{HP}$ [MW]	Q_LHS$_{HP}$ [MW]	Q_tot$_{HP}$ [MW]	COP$_{HP}$ [-]
4	**70**	**70**	9.243411	2.458	1.991	4.449	4.449
4	**70**	**85**	12.134401	3.226	2.611	5.837	5.837
4	**70**	**100**	16.859932	4.483	3.635	8.117	8.117
4	**85**	**40**	6.12865	1.244	1.297	2.541	2.541
4	**85**	**55**	7.642345	1.551	1.582	3.133	3.133
4	**85**	**70**	9.705194	1.97	1.991	3.961	3.961
4	**85**	**85**	12.740612	2.586	2.611	5.196	5.196
4	**85**	**100**	17.702221	3.593	3.635	7.227	7.227
4	**100**	**40**	6.553877	0.9166	1.297	2.214	2.214
4	**100**	**55**	8.172598	1.143	1.582	2.725	2.725
4	**100**	**70**	10.378574	1.452	1.991	3.443	3.443
4	**100**	**85**	13.6246	1.905	2.611	4.516	4.516
4	**100**	**100**	18.930463	2.648	3.635	6.282	6.282
6	**25**	**40**	5.135719	2.332	1.266	3.598	3.598
6	**25**	**55**	6.394384	2.903	1.538	4.441	4.441
6	**25**	**70**	8.094793	3.675	1.927	5.602	5.602
6	**25**	**85**	10.571133	4.799	2.512	7.311	7.311
6	**25**	**100**	14.547446	6.605	3.462	10.066	10.07
6	**55**	**40**	5.456382	1.793	1.266	3.06	3.06
6	**55**	**55**	6.793635	2.233	1.538	3.77	3.77
6	**55**	**70**	8.600214	2.826	1.927	4.754	4.754
6	**55**	**85**	11.231171	3.691	2.512	6.203	6.203
6	**55**	**100**	15.455756	5.079	3.462	8.541	8.541
6	**70**	**40**	5.6715	1.508	1.266	2.774	2.774
6	**70**	**55**	7.061475	1.877	1.538	3.415	3.415
6	**70**	**70**	8.939278	2.377	1.927	4.304	4.304
6	**70**	**85**	11.67396	3.104	2.512	5.615	5.615
6	**70**	**100**	16.0651	4.271	3.462	7.733	7.733
6	**85**	**40**	5.954838	1.209	1.266	2.475	2.475
6	**85**	**55**	7.414253	1.505	1.538	3.042	3.042
6	**85**	**70**	9.385867	1.905	1.927	3.832	3.832
6	**85**	**85**	12.257169	2.488	2.512	4.999	4.999
6	**85**	**100**	16.867682	3.423	3.462	6.885	6.885
6	**100**	**40**	6.368005	0.8906	1.266	2.157	2.157
6	**100**	**55**	7.928679	1.109	1.538	2.646	2.646
6	**100**	**70**	10.037091	1.404	1.927	3.331	3.331
6	**100**	**85**	13.107614	1.833	2.512	4.345	4.345
6	**100**	**100**	18.038021	2.523	3.462	5.984	5.984

ANNEX III: ORC PERFORMANCE MAP FOR OPTIONS A & B

DTw_cond$_{ORC}$ [K]	T_opt$_{LTWT}$ [C]	T_w_cond$_{ORC}$ [C]	m_w$_{PH}$ [kg/s]	Q_SHS$_{ORC}$ [MW]	Q_LHS$_{ORC}$ [MW]	Q_cond$_{ORC}$ [MW]	η_{ORC} [-]
2	**40**	**10**	9.3121	3.6442	2.32182	4.92915	0.1676
2	**40**	**20**	9.6547	3.77825	2.77458	5.5151	0.1526
2	**40**	**35**	-	-	-	-	-
2	**40**	**40**	-	-	-	-	-
2	**40**	**60**	-	-	-	-	-
2	**55**	**10**	11.2647	3.70208	2.26394	4.92915	0.1676
2	**55**	**20**	11.9056	3.9127	2.64014	5.5151	0.1526
2	**55**	**35**	12.8102	4.20998	3.48063	6.65126	0.13
2	**55**	**40**	12.8493	4.22286	3.94367	7.12654	0.1225
2	**55**	**60**	-	-	-	-	-
2	**70**	**10**	14.1219	3.75454	2.21147	4.92915	0.1676
2	**70**	**20**	14.9338	3.9704	2.58243	5.5151	0.1526
2	**70**	**35**	16.3737	4.35323	3.33739	6.65126	0.13
2	**70**	**40**	16.9181	4.49797	3.66856	7.12654	0.1225
2	**70**	**60**	-	-	-	-	-
2	**85**	**10**	18.9256	3.84109	2.12492	4.92915	0.1676
2	**85**	**20**	20.0157	4.06233	2.49051	5.5151	0.1526
2	**85**	**35**	21.9496	4.45484	3.23578	6.65126	0.13
2	**85**	**40**	22.683	4.60367	3.56286	7.12654	0.1225
2	**85**	**60**	26.2513	5.32789	5.54449	9.82912	0.09198
2	**100**	**10**	28.618	4.00242	1.96359	4.92915	0.1676
2	**100**	**20**	30.1859	4.2217	2.33113	5.5151	0.1526
2	**100**	**35**	33.2387	4.64866	3.04196	6.65126	0.13
2	**100**	**40**	34.2472	4.7897	3.37684	7.12654	0.1225
2	**100**	**60**	39.709	5.55357	5.3188	9.82912	0.09198
5	**40**	**10**	9.4304	3.69047	2.44059	5.09394	0.1631
5	**40**	**20**	9.6947	3.79392	2.9568	5.71269	0.1481
5	**40**	**35**	-	-	-	-	-
5	**40**	**40**	-	-	-	-	-
5	**40**	**60**	-	-	-	-	-
5	**55**	**10**	11.4483	3.76242	2.36864	5.09394	0.1631
5	**55**	**20**	12.1056	3.97842	2.7723	5.71269	0.1481
5	**55**	**35**	12.8784	4.23241	3.73462	6.92729	0.1255
5	**55**	**40**	12.2245	4.0175	4.4604	7.43749	0.118
5	**55**	**60**	-	-	-	-	-
5	**70**	**10**	14.3533	3.81608	2.31498	5.09394	0.1631
5	**70**	**20**	15.1991	4.04095	2.70978	5.71269	0.1481
5	**70**	**35**	16.6914	4.4377	3.52932	6.92729	0.1255
5	**70**	**40**	17.2454	4.58498	3.89292	7.43749	0.118
5	**70**	**60**	-	-	-	-	-
5	**85**	**10**	19.2364	3.90416	2.2269	5.09394	0.1631
5	**85**	**20**	20.372	4.13463	2.61609	5.71269	0.1481
5	**85**	**35**	22.3766	4.54149	3.42553	6.92729	0.1255
5	**85**	**40**	23.145	4.69743	3.78046	7.43749	0.118
5	**85**	**60**	26.8603	5.45149	5.98969	10.39732	0.0874
5	**100**	**10**	29.1796	4.08248	2.04858	5.09394	0.1631
5	**100**	**20**	30.7275	4.29744	2.45328	5.71269	0.1481
5	**100**	**35**	33.78	4.72435	3.24267	6.92729	0.1255
5	**100**	**40**	35.0037	4.8955	3.5824	7.43749	0.118
5	**100**	**60**	40.6831	5.6898	5.75138	10.39732	0.0874
10	**40**	**10**	9.6033	3.75815	2.66664	5.38723	0.1556
10	**40**	**20**	9.3957	3.67689	3.43592	6.07426	0.1406

DTw_cond$_{ORC}$ [K]	T_opt$_{LTWT}$ [C]	T_w_cond$_{ORC}$ [C]	m_w$_{PH}$ [kg/s]	Q_SHS$_{ORC}$ [MW]	Q_LHS$_{ORC}$ [MW]	Q_cond$_{ORC}$ [MW]	η_{ORC} [-]
10	**40**	**35**	-	-	-	-	-
10	**40**	**40**	-	-	-	-	-
10	**40**	**60**	-	-	-	-	-
10	**55**	**10**	11.7714	3.8686	2.55619	5.38723	0.1556
10	**55**	**20**	12.4309	4.08533	3.02748	6.07426	0.1406
10	**55**	**35**	12.2245	4.0175	4.4604	7.43749	0.118
10	**55**	**40**	-	-	-	-	-
10	**55**	**60**	-	-	-	-	-
10	**70**	**10**	14.7609	3.92443	2.50036	5.38723	0.1556
10	**70**	**20**	15.6555	4.16494	2.94788	6.07426	0.1406
10	**70**	**35**	17.2454	4.58498	3.89292	7.43749	0.118
10	**70**	**40**	17.7655	4.72327	4.34009	8.02222	0.1103
10	**70**	**60**	-	-	-	-	-
10	**85**	**10**	19.7835	4.01521	2.40959	5.38723	0.1566
10	**85**	**20**	20.9983	4.26175	2.85106	6.07426	0.1406
10	**85**	**35**	23.145	4.69743	3.78046	7.43749	0.118
10	**85**	**40**	23.9791	4.86674	4.19662	8.02222	0.1103
10	**85**	**60**	27.6866	5.6192	6.93782	11.51204	0.07964
10	**100**	**10**	29.8493	4.17462	2.25017	5.38723	0.1556
10	**100**	**20**	31.6803	4.43069	2.68212	6.07426	0.1406
10	**100**	**35**	34.9523	4.88831	3.58959	7.43749	0.118
10	**100**	**40**	36.2267	5.06654	3.99682	8.02222	0.1103
10	**100**	**60**	42.4853	5.94186	6.61517	11.51204	0.07964

ANNEX IV: ORC PERFORMANCE MAP FOR OPTION C

DTw_cond$_{ORC}$ [K]	T_w_cond$_{ORC}$ [C]	m_w$_{PH}$ [kg/s]	T_opt$_{LTWT}$ [C]	Q_SHS$_{ORC}$ [MW]	Q_LHS$_{ORC}$ [MW]
2	**10**	7.9489	27.9467	3.51101	2.455
2	**20**	9.1891	36.9075	3.71478	2.83806
2	**35**	11.7006	50.2665	4.07689	3.61372
2	**40**	12.796	54.8291	4.21449	3.95205
2	**60**	19.3815	73.2809	4.88646	5.98591
5	**10**	8.2952	30.6851	3.56908	2.56197
5	**20**	9.614	39.5253	3.78141	2.96931
5	**35**	12.3362	53.0076	4.157	3.81003
5	**40**	13.5233	57.5306	4.30124	4.17666
5	**60**	20.8352	76.1053	5.0063	6.43488
10	**10**	8.9151	35.0996	3.67136	2.75343
10	**20**	10.4068	44.0003	3.89865	3.21417
10	**35**	13.5233	57.5306	4.30124	4.17666
10	**40**	14.9113	62.0934	4.45803	4.60533
10	**60**	23.7303	80.8666	5.228	7.32902